UNIVERSIDADE DE LISBOA
FACULDADE DE CIÊNCIAS
DEPARTAMENTO DE BIOLOGIA

Functional analysis of Chestnut and *Phytophthora* genes involved in plant-pathogen interaction

Eduardo Marcelo Rodrigues Francisco

Mestrado em Biologia Molecular e Genética

Dissertação orientada por:
Susana Maria Traquete Serrazina
Patrícia Morais Fernandes

2025

Agradecimentos

Agradeço à minha orientadora Doutora Susana Serrazina, por todo o apoio que me prestou ao longo do desenvolvimento desta tese, especialmente pela maneira como me motivou e pela sua enorme disponibilidade, e ainda pela influência positiva que foi para mim a nível profissional e pessoal. Agradeço também à minha coorientadora, Doutora Patrícia Fernandes, que, apesar da distância que nos separa e das diferenças do fuso horário, esteve sempre disponível para me responder a dúvidas, e ainda me deu feedback altamente detalhado e atento aos pormenores, fundamental para a escrita da minha tese.

Quero também agradecer à Doutora Rita Costa, à Doutora Helena Machado, e à Doutora Patrícia Conde, por todo o trabalho por detrás dos ensaios de inoculação feitos no INIAV, e à Doutora Elena Corredoira e à sua equipa da Misión Biológica de Galicia pelo material biológico que nos forneceram.

Gostaria ainda de agradecer ao meu colega Gonçalo Candeias, pela orientação extra que me deu durante a unidade curricular de Iniciação ao Laboratório em Biologia Molecular e Genética, cuja experiência positiva me levou a escolher este tema para a minha tese de mestrado.

Por fim, agradeço à minha família, por me apoiarem incondicionalmente ao longo de todo o meu percurso académico, através de altos e baixos, e tornarem possível a conclusão desta tese de mestrado.

Part of the results from this thesis are included in the following publication: Susana Serrazina, María Teresa Martínez, Silvia Valladares, Lucía Del Castillo, Marcelo Francisco, Marta Berrocal-Lobo, Eduardo Piñas, Pablo Piñeiro, Rui Malhó, Rita Costa, Elena Corredoira. Overexpression of Ginkbilobin-2 homologous domain gene to enhance the tolerance to *Phytophthora cinnamomi* in plants of European chestnut, *BMC Genomics* **27**, 155 (2026). https://doi.org/10.1186/s12864-025-12485-x

Some results have also been included in the following poster: Marcelo Francisco, María Teresa Martínez, Patrícia Conde, Helena Machado, Rui Malhó, Patrícia Fernandes, Rita Lourenço Costa, Elena Corredoira, Susana Serrazina. Functional analysis of Chestnut and *Phytophthora cinnamomi* genes involved in plant-pathogen interaction. The poster was presented 4 times in 2 national events and 2 international events:

- VI International Conference of the Portuguese Society of Genetics, ITQB NOVA, Oeiras, June 5th, 2025
- V Simpósio Nacional da Castanha, Sabugal, July 3rd, 2025
- BioISI Day '25, FCUL, Lisbon, October 2nd, 2025
- CIÊNCIAS Research & Innovation Day, FCUL, Lisbon, October 22nd, 2025

Work supported by UID/04046/2025 - Biosystems and Integrative Sciences Institute Centre grant from FCT, Portugal.

Abstract

Ink disease, caused by the oomycete *Phytophthora cinnamomi* Rands, is a form of root rot that affects many woody plants worldwide, including chestnut trees. This pathogen has characteristics, such as long-lasting and chemical-resistant oospores, which make it considerably hard to control. Both the European (*Castanea sativa* Mill.) and the American [*Castanea dentata* (Marshall) Borkh.] chestnut species are susceptible to *P. cinnamomi*, having been historically affected by this oomycete. In contrast, the Asian chestnut species *Castanea crenata* Sieb. and Zucc. is resistant. The expression of the putative resistance gene *Cast_Gnk2-like* in this species might be one of the factors contributing to defense. Taking advantage of recently published data regarding the functional validation of *Cast_Gnk2-like* as a relevant defense factor and *P. cinnamomi* transcriptome in resistant and susceptible chestnut species throughout the infection process, the goals of this work are: 1) assess *Cast_Gnk2-like* overexpression from transformed *C. sativa* embryo clumps; 2) analyze the effect of *Cast_Gnk2-like* overexpression of transformed *C. dentata* on *P. cinnamomi* gene expression during the infection process; 3) analyze *P. cinnamomi* proteins using in silico tools to complement our understanding of their function and properties. We found that 3 out of 6 different transformed *C. sativa* lines had high enough significant overexpression and were selected for plant regeneration and further studies. Due to limitations of the study, no conclusions could be taken from the *C. dentata* inoculation assays, but in silico analysis results revealed many insights regarding the properties of the selected *P. cinnamomi* proteins.

Keywords: *Castanea*; *Cast_Gnk2-like*; host-pathogen interaction; oomycete; qPCR

Resumo

A doença da tinta, causada pelo oomiceto hemibiotrófico *Phytophthora cinnamomi* Rands, é um tipo de podridão radicular que afeta várias espécies de árvores a nível mundial, incluindo os castanheiros. Este agente patogénico propaga-se em regiões com precipitação abundante através de zoósporos que seguem sinais químicos de raízes de potenciais hospedeiros. Para além disso, forma estruturas, tais como clamidósporos ou oósporos duradouros e resistentes a químicos, que dificultam consideravelmente o seu controlo. Os mecanismos de combate à *P. cinnamomi* consistem na aplicação de fosfito e metalaxil, e métodos biológicos são escassos. A *P. cinnamomi* infeta o sistema radicular, avança pelos tecidos vasculares e compromete a absorção de nutrientes e água, eventualmente levando à morte da planta. Esta progressão varia entre hospedeiros suscetíveis e resistentes e algumas plantas podem não exibir sintomas por vários anos. Tanto o castanheiro europeu (*Castanea sativa* Mill.) como o castanheiro americano [*Castanea dentata* (Marshall) Borkh.] são suscetíveis a infeções por *P. cinnamomi*, tendo sido historicamente afetados por este oomiceto. A produção de castanha na Europa diminuiu bastante a partir dos anos 60 devido à doença da tinta, e esta doença também afetou severamente populações de *C. dentata* no sul da sua área de distribuição. Contrastando com este cenário, a espécie de castanheiro asiática *Castanea crenata* Sieb. and Zucc. é resistente e utilizada em programas de melhoramento de espécies suscetíveis a *P. cinnamomi*. A expressão do gene putativo de resistência *Cast_Gnk2-like* em *C. crenata* pode ser um dos fatores que contribuem para a sua defesa. A proteína Cast_Gnk2-like é homóloga à proteína Ginkbilobin-2 de *Ginkgo biloba* Linnaeus, que tem propriedades antifúngicas e é capaz de se ligar a resíduos de manose presentes na parede celular de hifas. A sobrexpressão da *Cast_Gnk2-like* em espécies de *Quercus* suscetíveis resulta num aumento da tolerância a *P. cinnamomi*, e a proteína isolada é capaz de abrandar o seu crescimento *in vitro.* Nesta parte do projeto do grupo, a validação de *Cast_Gnk2-like* em castanheiros suscetíveis (*C. sativa* e *C. dentata*) está a decorrer. Por outro lado, estudos anteriores mostraram diferenças no transcritoma de *P. cinnamomi* durante a infeção de *C. crenata* e *C. sativa*. Entre os genes de *P. cinnamomi* com expressão diferencial, encontravam-se vários efetores, tais como elicitinas e proteínas Nep-1-like (NLP), capazes de provocar morte celular no hospedeiro, e proteínas avirulence (Avr), que modulam a defesa do hospedeiro. Várias proteínas envolvidas na degradação da parede celular do hospedeiro e proteínas envolvidas na resposta ao stress celular também exibiram expressão diferencial. Aproveitando os dados nos dois estudos, os objetivos deste trabalho são: 1) avaliar a sobrexpressão de *Cast_Gnk2-like* em embriões somáticos de *C. sativa* via qPCR; 2) analisar a sobrexpressão de *Cast_Gnk2-like* em plântulas transgénicas de *C. dentata* e a expressão génica de 4 efetores (*Pc_ELI-1B*, *Pc_ELL*, *Pc_NPP1* e *Pc_Avr1b-1*), 2 enzimas que degradam a parede celular (*Pc_PG* e *Pc_Pel*) e 2 proteínas envolvidas na resposta ao stress (*Pc_KatG* e *Pc_GST*), totalizando 8 genes de *P. cinnamomi*, durante o processo de infeção destas plantas; 3) analisar proteínas de *P. cinnamomi* utilizando ferramentas *in silico* para aumentar a nossa compreensão das suas funções e propriedades. Os embriões de *C. sativa* (das linhas transformadas e não transformadas), obtidos de trabalhos anteriores, foram processados para se extrair o seu RNA, que foi quantificado, sujeito a um processo de eliminação de DNA genómico e convertido em cDNA. Este cDNA foi utilizado nas reações de qPCR, nas quais se quantificou a expressão do gene *Cast_Gnk2-like*, utilizando os genes *Actin* e *Elongation factor 1 alpha* como genes de referência. Após o cálculo da expressão relativa e a análise estatística, determinou-se que a linha transformada de *C. sativa* CL-3-GIN-1 expressava o gene *Cast_Gnk2-like* 38 vezes mais que a linha não transformada CL3, e as linhas CL-9-GIN-1 e CL-9-GIN-11 expressavam o gene 51 e 27 vezes mais que a linha não transformada CL9, respetivamente. Apesar do elevado erro padrão, estas linhas apresentaram sobrexpressão de *Cast_Gnk2-like* e foram selecionadas para regeneração de

plântulas e validação do gene. Para o segundo objetivo do trabalho, plântulas de *C. dentata* com 2 meses (das linhas transformadas de *C. dentata*, da linha não transformada de *C. dentata* Ellis #1, suscetível, e da linha não transformada de *C. crenata* CC14, resistente) foram inoculadas com *P. cinnamomi*. As plantas foram divididas em três tempos de recolha das raízes: 2, 24 e 48 horas após a inoculação. Estes tempos foram escolhidos porque representam a infeção desde a penetração das hifas de *P. cinnamomi* nas raízes até à sobrexpressão da *Cast_Gnk2-like* por parte do hospedeiro, que ocorre às 48 h de acordo com trabalhos prévios. Após a recolha, as raízes foram processadas para a extração de RNA, seguida da quantificação e conversão em cDNA, o qual foi utilizado para reações de qPCR. Neste caso, para além do gene *Cast_Gnk2-like*, analisou-se a expressão dos 8 genes de interesse de *P. cinnamomi*. Para normalização, utilizou-se o gene *40S ribosomal protein S3a*. Foi também incluída nas reações de qPCR uma amostra obtida a partir de micélio de *P. cinnamomi*, crescido em meio líquido, como controlo. No segundo objetivo, não foi possível calcular a expressão relativa de genes de *P. cinnamomi* nas amostras de raízes de castanheiro, bem como de *Cast_Gnk2-like*, devido a limitações na quantidade de material vegetal e, consequentemente, do patógeno. Devido a estas limitações, não se puderam tirar conclusões dos ensaios de inoculação de *C. dentata*, mas foi possível obter pistas para melhorar o ensaio de inoculação. Na análise *in silico*, utilizaram-se programas informáticos capazes de prever características de proteínas com base nas suas sequências de aminoácidos, tais como a localização subcelular, o ponto isoelétrico, locais de fosforilação e locais de glicosilação. As sequências de aminoácidos também foram utilizadas para prever domínios conservados, recorrendo a ferramentas do InterPro e do NCBI, e a estrutura tridimensional das proteínas, utilizando o AlphaFold Server 3.0. Os resultados da análise *in silico* revelaram informações interessantes relativas às características das proteínas de *P. cinnamomi* selecionadas. Todas as proteínas em estudo incluíam um péptido sinal, exceto a Pc_GST. As elicitinas Pc_ELI-1B e Pc_ELL diferiam num aminoácido chave para a sua função, e a Pc_ELL continha uma região intrinsecamente desordenada, o que pode indicar funções e localizações diferentes. A análise de resíduos conservados indicou que a Pc_NPP1 pertence a uma subclasse não citotóxica de NLPs de oomicetos, portanto, é possível que não induza morte celular no hospedeiro. A proteína Pc_Avr1b-1 contém uma região intrinsecamente desordenada, mas não contém a sequência RxLR, crucial para a função das proteínas Avr. A Pc_PG tem uma região intrinsecamente desordenada que pode influenciar a sua função catalítica, e a Pc_Pel, embora anotada como uma pectate lyase, tem características típicas de uma pectin lyase. A Pc_KatG, sendo secretada, para além da sua função de combate ao stress no patógeno, pode ter alguma influência na infeção. A Pc_GST contém um domínio extra que não está presente noutras GST, cuja função poderá estar relacionada com a ligação a substratos exógenos potencialmente nocivos. No geral, os resultados neste estudo são importantes para os projetos de investigação em curso, pois permitiram a seleção de linhagens transformadas com um gene putativo de resistência à *P. cinnamomi*, bem como uma melhor compreensão dos papéis das proteínas de *P. cinnamomi* selecionadas. Ainda com base nestes resultados, são propostas otimizações técnicas a futuros ensaios de inoculação de plântulas jovens de *C. dentata*, tais como o aumento da quantidade de inóculo e o uso de mais plântulas, para que seja possível analisar a expressão génica com sucesso.

Palavras-chave: *Castanea*; *Cast_Gnk2-like*; interação hospedeiro-patógeno; oomiceto; qPCR

Index

List of Figures

List of Tables

List of Supplementary Materials

Supplementary Figures

Supplementary Tables

List of Abbreviations

Avr: Avirulence
bp: Base pair
CaMV35S: Constitutive 35S promoter of the cauliflower mosaic virus
Cast_Gnk2-like: Ginkbilobin-2-like
CRRSPs: CYSTEINE-RICH RECEPTOR-LIKE SECRETED PROTEINs
Ct: Threshold cycle
CWDEs: Cell wall-degrading enzymes
DUF26: Domain of unknown function 26
EF-1α: Elongation factor 1 alpha
ET: Ethylene
ETI: Effector-triggered immunity
GNK2: Ginkbilobin-2
GSTs: Glutathione-S-transferases
HR: Hypersensitive response
IDR: Intrinsically disordered region
JA: Jasmonic acid
KatGs: Catalase-peroxidases
NLPs: Nep-1-like proteins
NLRs: Nucleotide-binding site leucine-rich repeat proteins
PAMPs: Pathogen-associated molecular patterns
PDA: Potato Dextrose Agar
PDB: Potato Dextrose Broth
PGs: Polygalacturonases
pI: Isoelectric point
pLDDT: Predicted local distance difference test
PRRs: Pathogen recognition receptors
PTI: Pattern-triggered immunity
PTMs: Post-translational modifications
PTS: Peroxisome targeting signal
qPCR: Quantitative PCR
RLKs: Receptor-like kinases
RLPs: Receptor-like proteins
ROS: Reactive oxygen species
RT: Reverse transcriptase
SA: Salicylic acid

1. Introduction

Phytophthora cinnamomi Rands, the causal agent of ink disease, is a hemibiotrophic oomycete capable of infecting the roots of a wide variety of plant species, including avocado, holm oak, cork oak and chestnut (Hardham & Blackman, 2018). This negatively affects economically important crops, such as avocado trees, leading to an annual loss of US$40 million in California alone (Hardham & Blackman, 2018). Additionally, in combination with other factors, *P. cinnamomi* plays a significant role in oak decline, a disease that affects *Quercus suber* L. and *Quercus ilex* L. trees, in Mediterranean territories (de Sampaio e Paiva Camilo-Alves et al., 2013). Originating from Southeast Asia, this phytopathogen is currently widely distributed (Fig. 1), being present in territories such as Australia, America, and Europe, with some projections pointing towards a potential expansion of its distribution in the future due to climate change (Burgess et al., 2017). The introduction of *P. cinnamomi* in new territories has led to ecosystem damage, as seen in the Two Peoples Bay Nature Reserve, in Australia (Hart et al., 2024). Therefore, its potential economic and environmental impacts should not be underestimated.

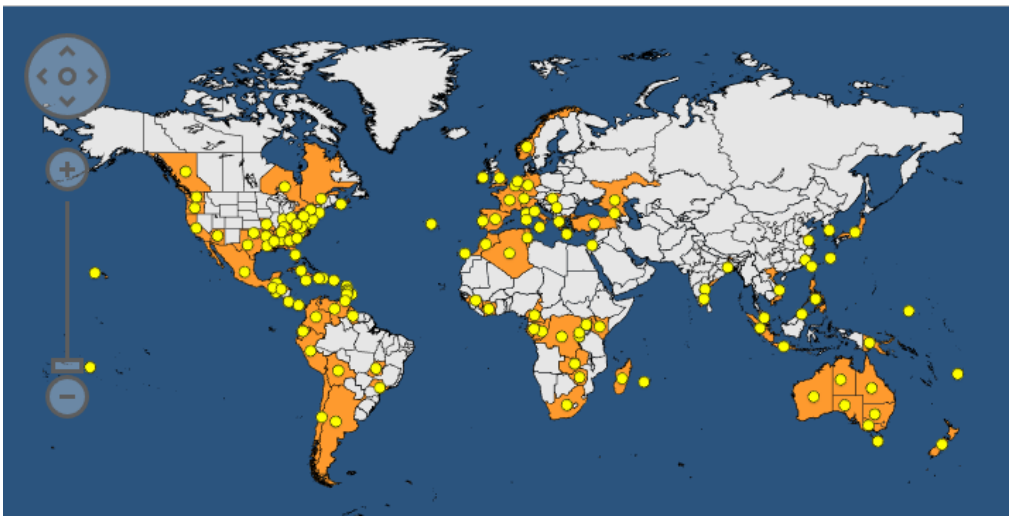

Figure 1: Map of *P. cinnamomi* distribution in the world, retrieved from the EPPO Global Database website (https://gd.eppo.int/taxon/PHYTCN/distribution). Last updated on the 7th of August, 2025. Yellow circles indicate territories where *P. cinnamomi* is currently present.

Taking into consideration *P. cinnamomi*'s destructive effect on crops and ecosystems, control measures are necessary. Protection of crops from *P. cinnamomi* is mostly done via chemical control measures, which are limited to the application of metalaxyl and phosphite (Hardham & Blackman, 2018). Phosphite can disrupt hyphal growth and promote plant defenses, while metalaxyl prevents normal RNA polymerase function, but there are many reported cases of acquired resistance to at least one of these compounds in many different *Phytophthora* species (Bhatt & Sharma, 2020; Hardham & Blackman, 2018; Kongtragoul et al., 2021). Biological control methods are scarce, although Bosso et al. (2016) indicates that the presence of the fungi *Scopulariopsis brumptii* Salvanet-Duval and *Byssochlamys nivea* Westling can reduce *P. cinnamomi* growth in vitro and promote chestnut tree survival in long-term exposure to infected soil. Furthermore, applying mulch to the soil also seems to inhibit *P. cinnamomi* growth and activity (Downer et al., 2001; Richter et al., 2011). Elevated levels of exogenous cellulase produced by microorganisms thriving in the mulch can damage *P. cinnamomi*'s cell wall, making it susceptible to degradation due to its cellulose content (Downer et al., 2001; Hardham & Blackman, 2018). Nonetheless, the low variety of solutions to such a widespread and impactful pathogen is very concerning.

1.1. *Phytophthora cinnamomi* reproduction and host infection

Generally, *P. cinnamomi* thrives in territories with persistent precipitation or flooding, as the wet soil favors propagation of asexual biflagellate zoospores, the main infection propagule (Hardham & Blackman, 2018; Kasteel et al., 2023). Zoospores are produced by sporangia, whose development begins when there is low nutrient availability (Hardham & Blackman, 2018). Initially multinucleate, a decrease in temperature will trigger the division of the sporangia into multiple uninucleate zoospores, which are released through hydrostatic pressure (Hardham & Blackman, 2018). These zoospores are motile and capable of following chemotactic signals from root exudates and other metabolites released by potential hosts, including those associated with flooding-induced anaerobiosis, such as ethanol (Badri & Vivanco, 2009; Cahill, 1994; Hardham & Blackman, 2018; Kasteel et al., 2023). This means that not only is *P. cinnamomi* propagated more easily during rainy seasons, but it might also benefit from the stress induced by the soil flooding on nearby plants, targeting the roots more efficiently.

Additionally, *P. cinnamomi* also has alternative, more resilient propagation methods. This species forms asexual chlamydospores specialized in short-term survival between rainy events (Jung et al., 2013). *P. cinnamomi* can also generate sexual oospores, which, due to the thickness and composition of their walls, along with the ability to become dormant, can withstand drought and remain viable in soil for long periods of time (Jung et al., 2013). However, some research suggests that the resilience of these structures is mostly due to being sheltered within the root material where they are formed (Gyeltshen et al., 2021).

Once *P. cinnamomi* zoospores reach the roots, they encyst, secrete adhesive proteins to attach to the surface, and germinate hyphae (Hardham & Blackman, 2018). These penetrate and grow through the root tissue by secreting cell wall-degrading enzymes (CWDEs), which destabilize the cell wall of the host by digesting specific compounds, such as cellulose, hemicellulose, and pectins (Hardham & Blackman, 2018). Hyphae growth continues within the roots, both inter- and intracellularly, through the fusion of exosomes and secretion of membrane and wall material (Hardham & Blackman, 2018; Redondo et al., 2015; Ruiz Gómez et al., 2015). Once they reach the central vascular bundle, the hyphae obstruct the xylem flow and cause water stress to the host plant (Hardham & Blackman, 2018; Ruiz Gómez et al., 2015). In hosts such as *Q. ilex*, mucilage deposits can occur in response to infection, as well as the de-esterification of plant cell walls, resulting in gaps between the stele and the vascular cortex and further reducing the water intake by the host roots (Ruiz Gómez et al., 2015). Throughout the infection, *P. cinnamomi* causes necrosis of fine feeder roots and the rest of the root system (Hardham & Blackman, 2018; McConnell & Balci, 2015; Oßwald et al., 2014). Symptoms of the infection can be observed in the aerial parts of the plant, starting with chlorosis and wilting, and progressing into dieback of branches, defoliation and, eventually, host death (Fernandes et al., 2022). This progression can happen very quickly, but the infection may also be asymptomatic for many years (Hardham & Blackman, 2018).

P. cinnamomi is a hemibiotroph, meaning it has two distinct infection phases: a biotrophic one, in which it requires living host cells for nourishment and growth, followed by a necrotrophic one, in which it causes the death of infected cells and obtains nutrients from them (Crone et al., 2013; Hardham & Blackman, 2018; Liao et al., 2022). During the biotrophic phase, *P. cinnamomi* may form haustorial-like structures, specialized hyphae that grow into the apoplast and become enveloped by the host membrane (the extrahaustorial membrane) (Judelson & Ah-Fong, 2019; Redondo et al., 2015). If present, haustoria formation benefits pathogen survival until the necrotrophic stage, as it is thought to be involved in nutrient uptake and effector delivery (Judelson & Ah-Fong, 2019). In the necrotrophic stage, those survival mechanisms are no longer maintained, and hypersensitive response (HR) mediated cell death is favored by the pathogen through its interactions with the host (Midgley et al.,

2024). The processes regulating the maintenance of each stage of *P. cinnamomi* infection, as in some lesser-studied *Phytophthora* species, are still not fully understood (Midgley et al., 2022).

1.2. *Phytophthora cinnamomi*, chestnut trees and *Cast_Gnk2-like*

Chestnut trees belong to the genus *Castanea* in the Fagaceae family (Fernandes et al., 2022). Native to eastern Asia, they have since spread and across Europe and North America, diverging into multiple species, four of them having great ecological and economic importance: the European chestnut (*C. sativa* Mill.), the American chestnut [*C. dentata* (Marshall) Borkh.], the Chinese chestnut (*C. mollissima* Blume), and the Japanese chestnut (*C. crenata* Sieb. and Zucc.) (Fernandes et al., 2022; Mellano et al., 2012). While European and Asian species have historically been cultivated for nut and timber production, *C. dentata* was valued for being a keystone species in North American forests (Anagnostakis, 1987; Fernandes et al., 2022).

In the past, both *C. sativa* and *C. dentata* populations have been severely affected by *P. cinnamomi*. Alongside chestnut blight (caused by *Cryphonectria parasitica* (Murr.) Barr.), it was one of the contributing factors of the functional extinction of *C. dentata* forests in the United States (Anagnostakis, 1987, 2012; Fernandes et al., 2022). In Europe, ink disease has been reported since the 19th century, with epidemics throughout that time period, negatively impacting *C. sativa* cultivars, which led to a downward trend of nut production from 1961 to 2015 (*FAOSTAT*, 2024; Pimentel, 1947 as cited by Robin et al., 2006). In contrast, Asian species, such as *C. crenata*, are resistant to *P. cinnamomi* infection and are used in breeding programs with susceptible species to enhance cultivar resistance (Fernandes et al., 2022).

In *Ginkgo biloba* Linnaeus, another Asian plant species, seeds secrete a protein known as Ginkbilobin-2 (GNK2), which seems to have antifungal properties, due to the ability to bind to D-mannose and D-glucose residues in the hyphae, inhibiting growth (Miyakawa et al., 2007, 2014). GNK2 includes a domain of unknown function 26 (DUF26), which is characterized by the presence of a specific cysteine-rich repeat (C-X_8-C-X_2-C), belonging to the category of CYSTEINE-RICH RECEPTOR-LIKE SECRETED PROTEINs (CRRSPs) (Vaattovaara et al., 2019). Although the biochemical function is not yet fully described, this domain seems to be associated with responses to biotic stressors, since not only it is the element that binds to hyphae, but may also play a role in other pathogen stress responses (Lv et al., 2023; Miyakawa et al., 2007, 2014).

In *Castanea* spp., there is a homolog to Ginkbilobin-2, known as Ginkbilobin-2-like (*Cast_Gnk2-like*), and its basal expression levels are much higher in *C. crenata* than in its European counterpart (Santos et al., 2017). Upon inoculation with *P. cinnamomi*, the gene has higher expression in *C. crenata* and *C. sativa* × *C. crenata* hybrid genotypes relative to *C. sativa*, suggesting it might play a role in ink disease resistance, especially considering that the cell walls of *P. cinnamomi* hyphae also contain mannose residues (Bartnicki-Garcia, 1966; Santos et al., 2017). Consequently, the potential of this gene to improve resistance to *P. cinnamomi* in European and American chestnut trees, as well as other susceptible Fagaceae species, is currently being studied (Serrazina et al., 2024b, Symposium review).

The *Cast_Gnk2-like* nucleotide sequence was obtained in a transcriptome analysis of *C. crenata* roots infected with *P. cinnamomi* (Serrazina et al., 2015). Analysis of the encoded protein sequence revealed a signal peptide, meaning the protein could be located in the apoplast (Colavolpe et al., 2023). The apoplast functions as an important interface for pathogenic oomycetes, since it is where proteases and secondary metabolites inhibit pathogen growth and immune receptors detect pathogen-associated molecular patterns (PAMPs), as well as the release location of some effectors (Lo Presti et al., 2015; Rocafort et al., 2020).

Cast_Gnk2-like has also been shown to be capable of significantly reducing the growth of *P. cinnamomi* in vitro (Colavolpe et al., 2023). Furthermore, previous gene functional analysis studies done on both *Q. ilex* and *Q. suber*, other susceptible Fagaceae, showed that overexpression of the gene points to an improvement of the tolerance to *P. cinnamomi* (Serrazina et al., 2022; Serrazina et al., 2024b; Serrazina et al., 2024a). There is also ongoing work regarding the overexpression of the gene in susceptible chestnuts for functional validation. Three *C. dentata* lines transformed with the *Cast_Gnk2-like* gene have already been obtained (McGuigan et al., 2020). Analysis of *Cast_Gnk2-like* expression in transformed plantlets from the three selected lines showed that it was overexpressed in root and collar tissue (Gonçalo Candeias, 2024). For *C. sativa*, six transformed embryo lines have been obtained, but data regarding the conversion to plantlets and *Cast_Gnk2-like* expression hasn't been published yet (Serrazina et al., 2024b; Serrazina et al., 2025).

Despite the promising results obtained so far, *Cast_Gnk2-like* is one of the genes with a promising role in plant defense against *P. cinnamomi*, as the infection process involves modulation of many other genes, both from the host and the parasite.

1.3. *Phytophthora cinnamomi* transcriptome in host-pathogen interactions

Plant responses to infection can be very complex, involving multiple defense-signaling pathways, such as the jasmonic acid (JA), salicylic acid (SA) and ethylene (ET) pathways, which can interact with each other (Koornneef & Pieterse, 2008). Biotrophic pathogens are usually more affected by SA-mediated defense mechanisms, while the JA and ET responses seem more effective on necrotrophs (Koornneef & Pieterse, 2008). Generally, pathogen detection can occur in two ways: one of them is through the recognition of PAMPs by pathogen recognition receptors (PRRs), which leads to pattern-triggered immunity (PTI) response (Ngou et al., 2022). Some examples of PRRs include receptor-like kinases (RLKs) and receptor-like proteins (RLPs) (Han, 2019). Pathogens have adapted to PAMP detection by secreting effectors, virulence proteins capable of inhibiting this first layer of defense (Ngou et al., 2022). Additionally, haustoria formation can prevent PRRs from detecting PAMPs, thereby inhibiting PTI, and can also cause host cells to reorganize organelles in a way that facilitates the activity of effectors that affect transcription (Judelson & Ah-Fong, 2019). The other mechanism of pathogen detection is the recognition of some of the effectors by intracellular host receptors called nucleotide-binding site leucine-rich repeat proteins (NLRs), which activate the effector-triggered immunity (ETI) mechanism once bound to the effector, leading to localized cell death (Han, 2019; Ngou et al., 2022; X. Yu et al., 2024). However, PTI and ETI are not entirely separate and have interconnected pathways, even synergizing at times, in order to provide more efficient and effective immune responses (X. Yu et al., 2024). In some instances, for example, PAMP recognition can play a positive role in NLR function, and ETI activation can boost the PTI response (Ngou et al., 2021).

While these interactions are well studied for other phytopathogens, in the case of *P. cinnamomi* and its hosts, there is a lack of information detailing how they interact during infection. Some exceptions are relatively well studied, such as the interaction with *Persea americana* Mill. (Backer et al., 2022; Reeksting et al., 2014). However, evidence suggests that *P. cinnamomi* can express different genes according to the host it is infecting, which could contribute to its wide host range (Shands et al., 2024). This means that data relative to the infection process in other hosts might not be sufficient to understand how *P. cinnamomi* behaves when infecting chestnuts. A recent article (Fernandes et al., 2024) has shed light on how this complex process could unfold during *P. cinnamomi*-*Castanea* spp. interactions. More specifically, it revealed many changes that occur in the transcriptome of *P. cinnamomi* between different infection timepoints in both *C. sativa* and *C. crenata* roots, as well as the transcriptome of both hosts. At 48 and 72 h post-infection, there were many

differentially expressed *P. cinnamomi* genes when comparing the pathogen gene expression between both host species, including some effectors. Additionally, in both chestnut species, many *P. cinnamomi* transcripts were downregulated at 72 h post-infection when compared to the 48 h mark. The number of downregulated *P. cinnamomi* genes was greater in *C. sativa* than in *C. crenata*, and included many effectors and nutrient transporters.

Some of these genes could play a role in the transition from biotrophy to necrotrophy. For example, according to Fernandes et al. (2024), the transcript *necrosis inducing-like protein NPP1 type* (Genbank XM_067936805.1) is more expressed by *P. cinnamomi* in *C. sativa* roots at 48 h post-inoculation than when infecting *C. crenata* roots at the same timepoint. NPP1 is the name of a specific type of conserved protein domain, which is present in Nep-1-like proteins (NLPs), a class of proteins capable of inducing cell death in many plants (Gijzen & Nürnberger, 2006). NLPs are very common across plant pathogens, including those of the *Phytophthora* genus, and their overexpression could indicate a shift from the biotrophic to the necrotrophic phase. Similar patterns were also observed for other effectors in Fernandes et al. (2024) such as elicitins. Proteins of the elicitin class can induce cell death when recognized as PAMPs, triggering the hypersensitive response of the host (Sabnam et al., 2023). In these cases, they tend to be downregulated during the biotrophic phase, but, in some interactions, they can benefit the early stages of infection, as they help absorb sterols from the host membrane (which *Phytophthora* spp. cannot produce) and improve virulence and hyphae propagation (Hardham & Blackman, 2018; Horta et al., 2008, 2010). This dual function of elicitins may be regulated by the expression of other genes, as, for example, in *Phytophthora infestans* (Mont.) de Bary, another oomycete with a biotrophic phase, there is one study that shows other effectors can inhibit elicitin-induced cell death (Bos et al., 2006). Elicitins can be distinguished between acidic (α) and basic (β) elicitins, with the latter being more capable of inducing host cell death than the acidic ones (Nespoulous et al., 1992). In *P. cinnamomi,* these are represented by α-cinnamomins and β-cinnamomins, which play different roles during *Q. suber* infection, as β-cinnamomin tends to act in the early stages of infection, contributing significantly to the oomycete's ability to propagate inside the host, while α-cinnamomins have a gradual increase in their expression and play a lesser role in virulence (Horta et al., 2008).

Some *RxLR* transcripts were downregulated at 72 h post-infection compared to the 48 h timepoint in both chestnut species, being more expressed in *C. crenata* than in *C. sativa* at both timepoints (Fernandes et al., 2024). RxLR proteins are pathogen effectors characterized by the presence of the amino acid sequence Arg-X-Leu-Arg (S. Wang et al., 2023). This motif plays a role in the transport of this effector into the cytoplasm of host cells (Dou et al., 2008; Hardham & Blackman, 2018). These proteins can affect the host via different modes of action, such as inhibiting transcription of defense-related genes or disrupting phosphorylation of proteins involved in pathogen recognition (S. Wang et al., 2023). Through these mechanisms, RxLR proteins can suppress host-mediated cell death, a vital ability for phytopathogenic oomycetes that require a biotrophic stage of infection (Jing et al., 2016; S. Wang et al., 2023; Yin et al., 2022).

Besides effectors, there were also other types of protein with differential expression, such as CWDEs. For example, pectate lyases and polygalacturonases (PGs) are usually associated with the early stages of infection, since they help degrade the host's cell wall (Hardham & Blackman, 2018; Hugouvieux-Cotte-Pattat, 2016; Jia et al., 2009). In (Fernandes et al., 2024), their expression was also, for most genes, higher at the 48 h mark than the 72 h one for both *C. sativa* and *C. crenata* infections. These types of enzymes act by degrading pectic components of the middle lamella, weakening the cohesion between cells and making other cell wall polymers more susceptible to degradation by enzymes such as cellulases and hemicellulases. This represents a key process in cell-wall degradation (D'Ovidio et al., 2004) .

Some genes allow us to infer how much stress the pathogen is being subjected to, with catalases as a prime example. Catalases are enzymes that reduce the effects of oxidative stress by converting hydrogen peroxide into water and oxygen (Sepasi Tehrani & Moosavi-Movahedi, 2018). Catalases can be divided into three groups: true catalases, catalase-peroxidases (which resulted from gene duplication of ancestral peroxidase genes), and heme-independent catalases (Zámocký & Koller, 1999). Catalase-peroxidases (KatGs) share high sequence homology with heme peroxidases, which can be further divided into three classes: bacterial peroxidases (class I), fungal peroxidases (class II), and plant secreted peroxidases (class III) (Welinder, 1992). Plants can increase the concentration of reactive oxygen species (ROS) in the first stages of infection, inhibiting the pathogen and activating other defense mechanisms (Ali et al., 2018). In response to this, species of the *Phytophthora* genus can upregulate catalase expression, increasing their survivability (Blackman & Hardham, 2008). In (Fernandes et al., 2024), the transcript *Catalase/peroxidase HPI* was downregulated at 72 h post-infection in *C. sativa* roots, compared to the 48 h timepoint. Glutathione-S-transferases (GSTs) are another group of proteins involved in defense against stress, and they are found across many taxa, including the *Phytophthora* genus (Bryant et al., 2006; Marrs, 1996; Morel et al., 2009; Strange et al., 2001). GSTs generally act by inactivating toxic compounds (especially hydrophobic ones) or reducing the effects of oxidative stress via detoxification of lipid peroxides, by conjugating these compounds with glutathione (Bryant et al., 2006; Morel et al., 2009). While effectors interact with host proteins and CWDEs with the host cell wall, GSTs perform their function in the *P. cinnamomi* cytosol, organelles, or cell membrane, and KatGs may be secreted or also act intracellularly (Frova, 2006; Zamocky et al., 2009).

Fernandes et al. (2024) analyzed the expression of many genes from all of these aforementioned classes and others, delivering a solid framework for analyzing the progression of *P. cinnamomi* infection in both susceptible and resistant chestnut species. These findings will support inoculation studies in order to understand the influence of introducing the putative resistance gene *Cast_Gnk2-like* in susceptible Fagaceae, an important step in the ongoing effort to protect these crops from *P. cinnamomi* (Serrazina et al., 2024b).

1.4. Objectives of this work

Chestnut trees are an important source of food and valuable wood, and many other economically important species of trees are also susceptible to *P. cinnamomi*. Research into this interaction could therefore help mitigate the global impact of this oomycete, by contributing to a better understanding of the infection mechanisms, which will in turn support the development of a wider variety of accessible control strategies. This would help protect a culturally and economically important crop in Portugal, contribute to the preservation (and potential reintroduction) of the American chestnut and assist in the protection of other susceptible crops to *P. cinnamomi*, such as *Q. suber*.

Therefore, in order to better understand the potential of *Cast_Gnk2-like* as a resistance gene against *P. cinnamomi,* there are three main goals for this work: 1) quantifying *Cast_Gnk2-like* overexpression on transformed *C. sativa* embryogenic lines, which will be of use for gene functional analysis studies in the future; 2) analyzing *P. cinnamomi* gene expression during root infection in transformed *C. dentata* hosts, as well as the potential effects of *Cast_Gnk2-like* overexpression; 3) using in silico tools to analyze a selection of *P. cinnamomi* genes and the role they play in the infection process, in order to better interpret the results from the second goal.

2. Materials & Methods

2.1. Assessment of *Cast_Gnk2-like* expression in *C. sativa* embryo material

2.1.1. Harvesting of transformed *Castanea sativa* embryos

C. sativa embryogenic lines (in the form of multiple embryo clumps; Supplementary Fig. S1) were delivered to us, from Dr. Elena Corredoira (Misión Biológica de Galicia, Santiago de Compostela), corresponding to six transformed lines (CL-3-GIN-1, CL-3-GIN-3, CL-9-GIN-1, CL-9-GIN-4, CL-9-GIN-11 and CL-9-GIN-12) from two different genotypes, along with the respective non-transformed clumps (CL-3-WT and CL-9-WT). The transformants were previously obtained by cloning the *Cast_Gnk2-like* gene into a pK7WG2D plant transformation vector and transferring it into *Agrobacterium tumefaciens* strain EHA105 (Serrazina et al., 2024b). All six transformed lines used are estimated to have one copy of the *Cast_Gnk2-like* gene driven by the constitutive 35S promoter of the cauliflower mosaic virus (CaMV35S).

Once delivered, clumps from the same genotype were divided into three biological replicates and transferred to 2 ml Eppendorf tubes, weighed, flash-frozen in liquid nitrogen, and stored at -80ºC to later be used for RNA extractions. Each biological replicate contained approximately 0,1 g of embryogenic material from the clumps, with the remaining material being stored separately as backup.

2.1.2. RNA extraction and DNAse treatment

After grinding with a mortar and pestle in liquid nitrogen, the collected material was used for RNA extraction. For *C. sativa* samples, the extraction protocol was based on Chang et al. (1993) and Gambino et al. (2008), with the final RNA pellet being eluted in 30µl of DEPC-treated water. To remove genomic DNA contamination, the RNA samples were treated with Ambion® TURBO DNA-free™ kit (ThermoFisher Scientific), according to the manufacturer's instructions.

The extracted RNA in the samples was quantified and checked for contaminants with a NanoDrop™ One Microvolume UV-Vis Spectrophotometer (Thermo Fisher Scientific), using RNase-free water for the blanks. Electrophoresis was performed to confirm RNA integrity. A 1% agarose gel was prepared with 1x TAE buffer. Green Safe Premium (NZYTech) was used as the intercalating agent, and the 1 kb Plus DNA Ladder (NEB) was added to one of the wells as a control. The concentration of the RNA was measured a second time after the DNAse reaction, to correct for potential RNA loss during the process. Another electrophoresis was also performed to re-evaluate RNA integrity and verify that previously identified bands corresponding to genomic DNA were no longer present.

2.1.3. Reverse Transcriptase reaction and preparation of cDNA for qPCR

The cDNA was synthesized using the RevertAid H Minus First Strand cDNA Synthesis Kit (ThermoFisher Scientific). Before the reverse transcription, the quantity of all samples was normalized to the sample with the lowest amount of RNA (CL-3-WT-1), with 3383 ng of total RNA. So, 3000 ng of RNA from each sample was used, with the final reaction volume of 40 µl. Following the instructions of the kit, 500 ng of Oligo$(dT)_{23}$ primers were added to each reaction. A Biometra TOne PCR thermocycler was used as an incubator for the reverse transcription.

From each cDNA sample, 3 µl were used to make a pool of all the samples. This cDNA pool was used to make serial dilutions, from 1:10 to $1:10^4$, which were used as standards for the qPCR

standard curve. An additional 3 µl from each sample was also used to prepare the respective unknown samples for qPCR, with 69 µl of DEPC-treated water being added as an intermediate step, and then used to prepare a 1:10 dilution, which was used in the qPCR reactions.

2.1.4. *Cast_Gnk2-like* expression analysis

qPCR was performed on a CFX96 qPCR thermocycler (Bio-Rad), using 7,5 µl of the NZYSupreme qPCR Green Master Mix (2x) ROX Plus (NZYtech), 4 µl of cDNA (1.2 ng), 2,9 µl of nuclease-free water, and 0,3 µl of each primer (final concentration of 0,2 µM) per reaction. Cycling conditions included an initial denaturation step at 95ºC for 3 minutes, followed by 40 cycles of denaturation at 95ºC for 15 s and annealing for 30 s at specific temperatures for each primer pair (Table 1), ending with a melting curve analysis step (from 60ºC to 95ºC, in increments of 0,5ºC, for 5 s each). Besides *Cast_Gnk2-like*, the gene of interest, the relative expression of two reference genes, *Elongation factor 1 alpha* (*EF-1α*) and *Actin*, was also measured via qPCR. These reference genes were selected because the Ct values obtained in test plates were more stable. Two technical replicates were done per sample, and the qPCR plate was done twice, totaling 4 technical replicates per sample.

The *Cast_Gnk2-like* gene was amplified with the primers that were used in Serrazina et al. (2022) designed from *C. crenata*. The primers for the reference genes *EF-1α* and *Actin* were designed for *C. dentata* (Dakota Matthews, personal communication, October 2024), but since the coding sequences are very similar between members of the *Castanea* genus, they are expected to amplify the target genes on *C. sativa* as well.

The resulting data were analyzed according to the method described in (Hellemans et al., 2007) to calculate the relative gene expression in each transformed line compared to the controls, using the geometric average of the values of reference genes for normalization of gene expression. Statistical significance analysis was performed on SPSS software (version 29), using the Kruskal-Wallis test followed by post hoc pairwise comparisons (Dunn's test) among all biological groups originating from the same line (CL-3-WT or CL-9-WT), after confirming their values did not follow a normal distribution.

Table 1: List of primers used for *Castanea* spp. qPCR assays; bp: base pair. *EF-1α* and *Actin* serve as normalization for *Cast_Gnk2-like* expression. All primers had been designed prior to this study.

Gene	Primers	Amplicon length	Annealing temperature
Cast_Gnk2-like	Fwd: 5' GGGGACCTAAAGCTTGACTCA 3' Rev: 5' CATCGCAACAGTTGGGAAGTT 3'	129 bp	60ºC
EF-1α	Fwd: 5' CGGTTACTGAGTACTAGCCTTG 3' Rev: 5' CTGCCGAAGACCTTATTGAAAG 3'	84 bp	60ºC
Actin	Fwd: 5' CCTTGCTGGTCGTGATCTC 3' Rev: 5' GTCTCAAGTTCCTGCTCATAGTC 3'	150 bp	62ºC

2.2. Analysis of *P. cinnamomi* gene expression in the context of *C. dentata* infection

2.2.1. *Castanea dentata* inoculation with *Phytophthora cinnamomi* and root harvesting

C. dentata plants were grown from previously obtained transformed embryo lines (McGuigan et al., 2020). Shoot micropropagation started at FCUL and then transferred to Instituto Nacional de Investigação Agrária e Veterinária (INIAV, Oeiras) to induce root formation. Five different lines were used: a susceptible *C. dentata* line (Ellis #1), 3 transformed *C. dentata* lines (PF-B4GK10, PF-B4GK31, and PF-B4GK32) (McGuigan et al., 2020), and a *C. crenata* line (CC14), a control for *P.*

cinnamomi resistance. The transformed lines had previously been obtained by isolating the *Cast_Gnk2-like* gene from infected *C. crenata* roots, cloning it into a plant transformation vector, and inserting it in Ellis #1 embryo clumps, using *A. tumefaciens* AGL-1 strain as described in McGuigan et al. (2020).

Before proceeding with the gene expression analysis, some changes were made from the original plans. From the initial three transformed lines, PF-B4GK10 was removed from this study because it has the lowest non-significant overexpression of *Cast_Gnk2-like* relative to Ellis #1 (Gonçalo Candeias, 2024). This data comes from an ongoing study to assess *Cast_Gnk2-like* in these transformed plantlets, both in the roots and in the stem base (Serrazina et al., 2024b). The PF_B4GK31 line has higher overexpression than PF-B4GK10, but it was still not statistically significant. However, PF-B4GK32, the line with the most significant overexpression, tends to form small roots, rendering low amounts of material for RNA extraction. For this reason, it was decided that the PF-B4GK31 line would also be included in the *P. cinnamomi* inoculation assay, in order to have sufficient root material for pathogen gene expression profiling, despite lacking statistically significant overexpression in root tissue.

Three months after root formation, *C. dentata* plantlets (Fig. 2) were subjected to *P. cinnamomi* [PH107 strain; (Bairrão et al., 2021)] inoculation at INIAV (Supplementary Fig. S2). Multiple plants from each line were divided into three groups. In the first group, root tissue was collected at 2 h after inoculation; in the second one, at 24 h; and in the last one at 48 h. Additionally, the groups were divided into two treatments: inoculated plants and mock-inoculated control plants. The final number of plants per group varied between one and four. The timepoints chosen were based on those used for (Fernandes et al., 2024). However, since this study is focused on the effect of *Cast_Gnk2-like* expression, which peaks at 48 h post-infection (Fernandes et al., 2024; Santos et al., 2017), they were adapted.

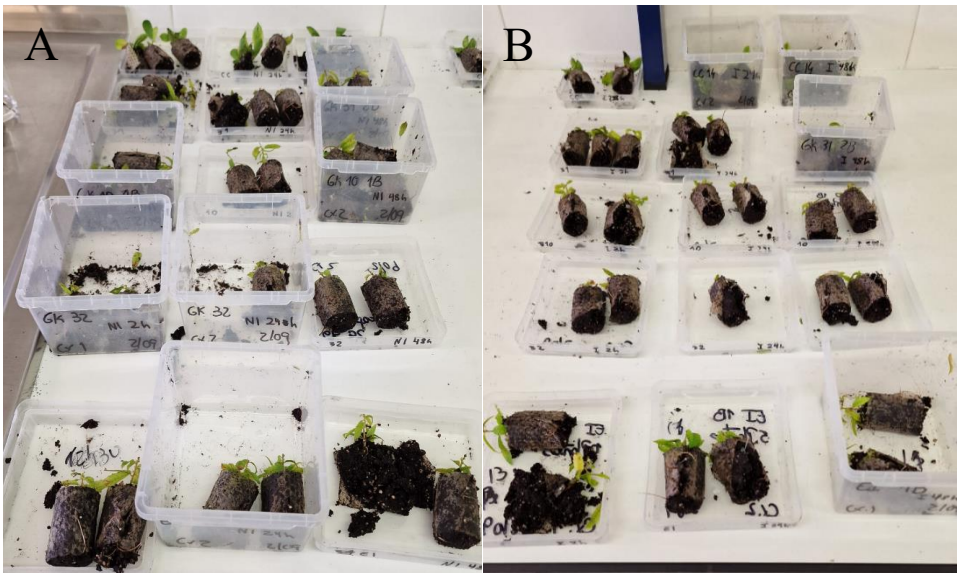

Figure 2: *C. dentata* plantlets in paper pots used in the *P. cinnamomi* infection assay. A: control plants. B: Inoculated plants. Each row corresponds to a different line, from top to bottom: CC14, PF-B4GK31, PF-B4GK10, PF-B4GK32 and Ellis #1. Each column corresponds to a different time point for root collection, from left to right: 2 h, 24 h and 48 h post-inoculation. A: mock inoculated plants; B: plants inoculated with *P. cinnamomi*.

The inoculation method consisted of pinning 1,0 x 0,5 cm Potato Dextrose Agar (PDA) blocks with *P. cinnamomi* mycelium over one root of the plant (Supplementary Fig. S3). The control plants received a mock treatment, where sterile PDA blocks were pinned instead. All plants were kept at room temperature and laboratory illumination during the experiment. Roots from the same line, time-point, and treatment were weighed together, taking into account the number of plants per group, and

stored at -80ºC. Some roots were collected into separate 2 ml tubes with sterile distilled water and used to confirm if *P. cinnamomi* successfully infected the *C. dentata* roots, via a reisolation assay. These roots were surface sterilized in a 1,5% bleach solution for 15 seconds and rinsed in distilled water. Then, they were left at 20ºC for at least 4 days in a petri dish containing a modified P_5ARPH selective medium: 17g/L cornmeal agar, 5 mg/L natamycin, 250 mg/L ampicillin, 10 mg/L rifampicin, 100 mg/L pentachloronitrobenzene, and 25 mg/L hymexazol (Jeffers, 1986).

In order to have a control for *P. cinnamomi*, liquid cultures of the PH107 strain were prepared from a culture of the oomycete in PDA. They were left growing in an Erlenmeyer flask with 20 ml of potato dextrose broth (PDB) medium, in the dark, at a temperature of 22-24ºC, for 11 days, until the mycelium covered most of the bottom of the flask. Then, the mycelium was collected from three different cultures, and approximately 0,2g of each was used as a biological replicate. Each replicate was ground into powder with liquid nitrogen and quartz sand. Although 3 biological replicates were prepared, only one of them was used.

2.2.2. RNA extraction

The RNA extraction protocol used for *C. dentata* samples was based on Le Provost et al. (2007), with a final elution volume of 10 µl. For *P. cinnamomi* mycelium control samples, RNA was extracted using the RNeasy® Plant Mini Kit (Qiagen), following the manufacturer's instructions, with a final elution volume of 30 µl. RNA quantification and integrity assessment were performed as previously described in section 1.2. The RNA samples were not subjected to a separate DNAse treatment, since the reverse transcriptase kit used included a DNAse reaction step.

2.2.3. Reverse Transcriptase reaction and preparation of cDNA for qPCR

For the conversion of *C. dentata* and *P. cinnamomi* RNA into cDNA, the QuantiTect® Reverse Transcription kit (Qiagen) was used. A total of 1000ng of RNA was used per reaction. This protocol includes a genomic DNA elimination step, in which 2 µl of gDNA Wipeout Buffer (7x) was added to the sample RNA and a variable volume of nuclease-free water, with the final volume of 14µL. Subsequently, the Quantiscript Reverse Transcriptase, Quantiscript RT Buffer (5x) and RT primer mix are added accordingly, with a final reaction volume of 20µL. Additionally, to confirm that no detectable genomic DNA was present at the end of the reaction, a qPCR reaction was performed using RNA collected after the genomic DNA elimination step. The standards were prepared as previously described in section 1.3. For the unknown samples, because the initial amount of total RNA was as low as 1000ng, 3 µl from each were diluted in 69 µl of DEPC-treated water and were used directly for qPCR preparation with no further dilutions.

2.2.4. *Cast_Gnk2-like* and *P. cinnamomi* gene expression analysis

The preparation of the qPCR was done as described in section 1.4, the only difference being the use of iTaq Universal SYBR Green Supermix (BioRad), and a higher amount of cDNA (approximately 2ng) per unknown sample reaction. For *C. dentata*, in addition to *Cast_Gnk2-like, Actin,* and *EF-1α*, the relative expression of a selection of *P. cinnamomi* genes was also analyzed (Introduction and Table 2). These include 4 effectors, 2 CWDE's and 2 stress-related genes, which were selected from Fernandes et al. (2024). The selection was done based on two factors: the predicted function and the differential expression levels. The predicted function of these genes was related to different aspects of the infection process (cell wall degradation, manipulation of host physiology and protection from host defenses), and the expression levels where different when comparing the 48 h and

72 h timepoints of infection and when comparing *C. crenata* and *C. sativa* at the same time points of infection (Fernandes et al., 2024). Therefore, these were adequate genes to assess the impact of *Cast_Gnk2-like* overexpression.

The gene *40S ribosomal protein S3a* (IUM83_18029) was used as a reference gene for *P. cinnamomi* (Shands et al., 2024). The list of primer sequences is available in Table 3. The qPCR reactions and cycling protocol were the same indicated in section 2.1.4.

Table 2: *Phytophthora cinnamomi* genes selected for in silico analysis and gene expression analysis via qPCR. The Gene column refers to the locus tag of the genes on NCBI. The Transcript ID column refers to the ID of the mRNA sequence, and the Protein ID refers to the ID of the amino acid sequence. All genes have a PROVISIONAL RefSeq status as of November 2025. The abbreviations in the last column, given in the present study, are not registered yet.

Gene	Transcript ID	GenBank ID	General function	Annotation	Abbreviation	Protein length (a.a.)
IUM83_06732	XM_067930962.1	KAG6610698.1	Effectors	basic elicitin	*Pc_ELI-1B*	98
IUM83_06738	XM_067930968.1	KAG6610502.1		Elicitin-like protein	*Pc_ELL*	181
IUM83_12198	XM_067936805.1	KAG6623126.1		necrosis inducing-like protein NPP1 type	*Pc_NPP1*	251
IUM83_03646	XM_067927665.1	KAG6616076.1		Avr1b-1 Avirulence-like protein	*Pc_Avr1b-1*	559
IUM83_15875	XM_067940718.1	KAG6611156.1	Cell wall degrading enzymes	Pectate lyase	*Pc_Pel*	365
IUM83_03849	XM_067927881.1	KAG6616035.1		putative polygalacturonase	*Pc_PG*	414
IUM83_04478	XM_067928562.1	KAG6613468.1	Stress response	Catalase/peroxidase HPI	*Pc_KatG*	687
IUM83_00365	XM_067924129.1	KAG6609417.1		putative glutathione S-transferase	*Pc_GST*	454

Table 3: List of primers used for amplification of *P. cinnamomi* genes in the qPCR assay; bp: base pair. *40S ribosomal protein S3a* is the reference gene.

Gene	Primers	Amplicon length	Annealing temperature
Pc_ELI-1B (IUM83_06731)	Fwd: 5' ATGAACTTCACCGCTCTGC 3' Rev: 5' AAGGACGACTCGGACAGGATA 3'	131 bp	58,5ºC
Pc_ELL (IUM83_06738)	Fwd: 5' GCTATGTGCAAGGTGGACGC 3' Rev: 5' TCGTGGGGATGGTCAGGTC 3'	88 bp	62ºC
Pc_NPP1 (IUM83_12198)	Fwd: 5' ACCTCAACAAAGTGTCCCCC 3' Rev: 5' CAGCTCCGATAGAGAGACGC 3'	96 bp	60ºC
Pc_Avr1b-1 (IUM83_03646)	Fwd: 5' GAGGTACCGACGCCAATGAA 3' Rev: 5'CTGTCGACCGTCACCTTCTC 3'	187 bp	60ºC
Pc_PeL (IUM83_15875)	Fwd: 5' GTGATCATGGGCAAGGGTCT 3' Rev: 5' GGTCGTCAAGAACAAGTGG 3'	96 bp	58,5ºC
Pc_PG (IUM83_03849)	Fwd: 5' CAGCAGCAAGACCCAACCC 3' Rev: 5' CTTCTTGTAGGTGCCCGTGA 3'	117 bp	60ºC
Pc_KatG (IUM83_04478)	Fwd: 5' GGTGCAGCTGTTCGCTTCG 3' Rev: 5' AGTGGTCGGCCTTCATAACCTTG 3'	83 bp	62ºC
Pc_GST (IUM83_00365)	Fwd: 5' GGCTTGCGTTGTTCATTGGT 3' Rev: 5' GCATGTCGGTAGTCGGGTAG 3'	195 bp	60ºC
40S ribosomal protein S3a (IUM83_18029)	Fwd: 5' CTGTTCTGCATCGCCTTCAC 3' Rev: 5' GCGGATGTACACGTTCTGGA 3'	231 bp	60ºC

All *P. cinnamomi* primer sequences (Table 3), except those for the reference gene, were designed using the PrimerSelect software (version 11.1.0, DNASTAR) and the NCBI Primer Blast

tool (Ye et al., 2012). For the *P. cinnamomi* reference gene, the primer pair from Shands et al. (2024) was used. For *Pc_PG*, possible non-specific amplicons have a length much greater than the conventional limit of 200 base pairs for qPCR reactions, and for *Pc_KatG* the only non-specific amplification occurs on another catalase gene, with a very similar expression profile according to Fernandes et al. (2024). For the chestnut genes, the same primers indicated for *C. sativa* (Table 1) were used. The resulting data were analyzed according to the method described in (Hellemans et al., 2007) to calculate the gene expression in each transformed line compared to the controls, using the geometric average of the values of reference genes for normalization of gene expression.

2.3. In silico analysis of *Phytophthora cinnamomi* genes

In silico analysis of the selected *P. cinnamomi* genes (Table 2) was done with bioinformatic tools mostly focused on the amino acid sequence. The main purpose was the analysis of the function of the encoded protein

Signal IP 6.0 was used to predict the presence of signal peptides, while DeepLoc2.1 and Euk-mPLoc 2.0 were used to predict the subcellular location, including potential secretion into the extracellular medium (Chou & Shen, 2007, 2008, 2010; Ødum et al., 2024; Shen & Chou, 2006; Teufel et al., 2022). Clustalw 2.1 (Sievers & Higgins, 2021) was used to show alignments between proteins when necessary (accessed from https://www.genome.jp/tools-bin/clustalw, Bioinformatics Center, Institute for Chemical Research, Kyoto University, Uji, Kyoto 611-0011, Japan).

Expasy's Compute pI/Mw tool and DictyOGlyc 1.1(trained on *Dictyostelium discoideum* proteins) were used to infer some physical and chemical properties of the proteins that could influence their function, including the molecular weight, the isoelectric point and O-glycosilation sites (Gasteiger, 2003; Gupta et al., 1999). Additionally, NetPhos 3.1 was employed to predict phosphorylation sites on serine, threonine and tyrosine residues, and NetNGlyc 1.0 was used to predict N-glycosylation sites (Blom et al., 1999; Gupta & Brunak, 2002).

NCBI CD Database and the InterProScan search were used to predict functional areas of the proteins, such as conserved domains and active sites, while classifying them into families (Jones et al., 2014; Marchler-Bauer et al., 2011; Marchler-Bauer & Bryant, 2004).

For assessing the 3D structure of the proteins, AlphaFold Server, a versatile AI tool capable of predicting protein structure, ligand interactions, and chemical modifications, was used (Abramson et al., 2024). For visualization of those predicted structures and image treatment, the web app Mol* Viewer was used (Sehnal et al., 2021).

3. Results & Discussion

3.1. *C. sativa* embryos gene expression

The RNA isolation yield was variable (Supplementary Table S1), with post-DNAse treatment concentrations ranging between 100 and 400 ng/µl. No signs of degradation were detected on gel electrophoresis, as the bands corresponding to ribosomal RNA were well distinguished (Supplementary Fig. S4).

After retrieving sufficient amounts of RNA per sample and confirming the absence of degradation, the qPCR results showed the amplification efficiency for the primers used was 79,6% for *Cast_Gnk2-like*, 84% for *EF-1α*, and 80% for *Actin*. The standard curves obtained were considered sufficient for gene expression analysis in the context of this study, as notable differences between transformed and non-transformed lines were expected. *Cast_Gnk2-like* expression in transformed lines was normalized to the expression level of reference genes and compared to their respective wild-type

lines (Fig. 3). The results show higher levels of expression in all transformed lines [as expected, given the constitutive CaMV35S promoter (Amack & Antunes, 2020)], most notably in CL-3-GIN-1, CL-9-GIN-1 and CL-9-GIN-11 (38-, 51- and 27-fold more than their wild-type counterpart, respectively). Due to their high fold change values and statistical significance, these transformed lines are adequate candidates with *Cast_Gnk2-like* overexpression for further gene expression studies.

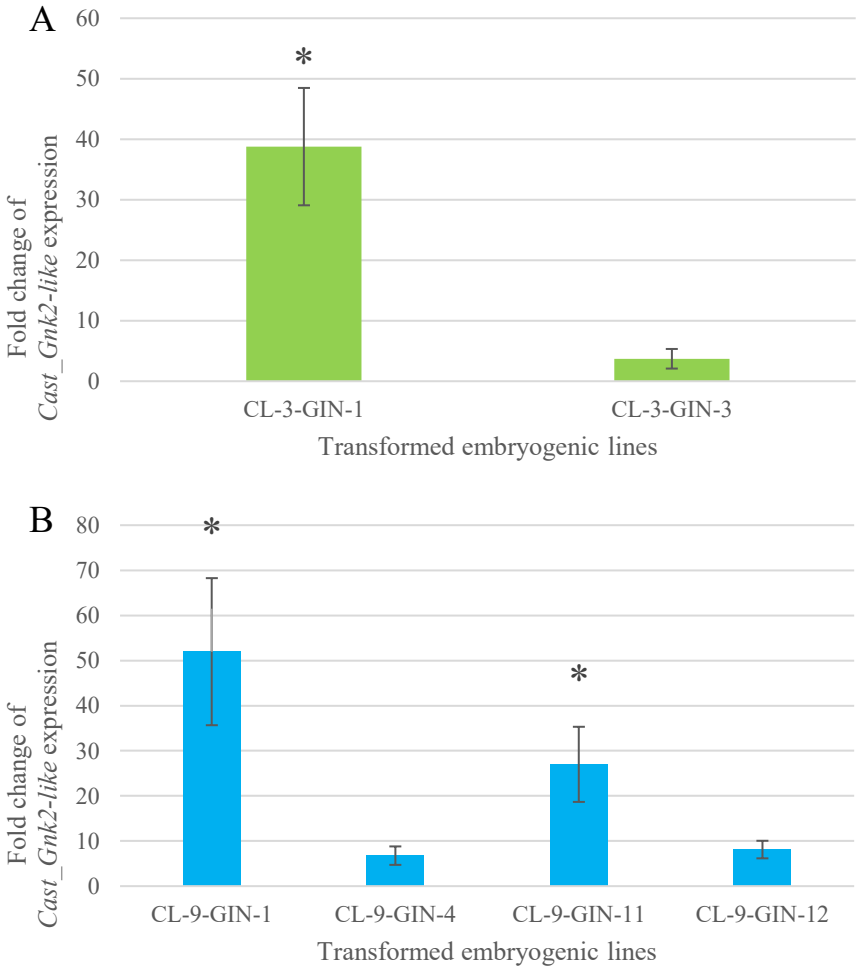

Figure 3: Fold change of *Cast_Gnk2-like* expression among transformed embryo lines, relative to the respective wild-type lines. A: Transformed lines originating from the CL-3-WT genotype; B: Transformed lines originating from the CL-9-WT genotype. Vertical bars correspond to the mean ± standard error of the fold change values (n=3). Asterisk indicates that the p value obtained when comparing the transformed lines and the respective wild-type lines using the Kruskal-Wallis post hoc test is lower than 0,05, meaning the overexpression compared to the wild-type line is statistically significant. The full output of the statistical tests is in the Supplementary Fig. S5

It is worth noting, however, that there was a high degree of variability among biological replicates throughout all lines (with relatively high standard error values). Many environmental factors can lead to different phenotypes in biological samples, including the life cycle stage, the time of the day/year and even the potential differences in nutrient availability (Bustin, 2010). Although most of these factors were kept in control, multiple embryo clumps were used per line, some with signs of necrosis or cell differentiation. While these tissues were usually discarded, there could still have been some overall variation in those clumps. Since each biological replicate consisted of more than one embryo clump, the likelihood of a stochastic error was low. Nonetheless, it is still possible that the proportion of metabolically active clumps was different in each replicate, influencing the expression of *Cast_Gnk2-like* and showing higher Ct values in qPCR. The culture conditions of the *C. sativa* embryos could also have contributed to differences within the same transgenic line, resulting in what

is known as somaclonal variation (Krishna et al., 2016; Sarmast, 2016). This variation consists of mutations that arise during micropropagation of cell cultures, although pre-existing mutations in somatic cells also play a role (Sato et al., 2011). ROS accumulation in culture, culture time, growth regulators and other factors can contribute to genetic variation, by causing mutations, changes in DNA methylation or disruption of the cell cycle (Krishna et al., 2016). Perhaps, such changes could occur in a way that affects the expression *Cast_Gnk2-like* or the reference genes, skewing the Ct values of some samples and affecting the calculated fold change.

Similarly, the difference in expression exhibited between different transformed lines is also to be expected, as *Agrobacterium* mediated transformation events can have different results depending on the number of copies of the transgene and the regions of the genome in which they were inserted (Gelvin, 2003). The inserted *Cast_Gnk2-like* copy number was estimated to be one for every line, and all inserts included the same constitutive promoter (Serrazina et al., 2024b). Therefore, the most likely cause of transgenic line variability is the insertion location of *Cast_Gnk2-like*, as there is no information regarding where the gene was inserted in each transformed line. If a transgene is inserted in a transcriptionally less active region of the genome, its expression could be negatively affected (Gelvin, 2003). When comparing the present expression results to those of Gonçalo Candeias (2024), the variability between lines seems to be within the expected.

In that same work, the standard error values for the root tissue of *C. dentata* lines were also proportionally similar to those obtained in *C. sativa*. In comparison, *Q. suber* exhibited relatively lower standard error values, meaning that something inherent to the *Castanea* genus could also play a role in higher variability among biological replicates. Despite the relatively heterogeneous biological replicates of the *C. sativa* embryo lines, we can still conclude from this data that the most promising transformed lines for plant regeneration and further studies regarding the influence of *Cast_Gnk2-like* on resistance to *P. cinnamomi* upon infection are CL-9-GIN-1, CL-3-GIN-1, and CL-9-GIN-11, as they have the highest *Cast_Gnk2-like* expression values and are the only ones with significant overexpression. Additional expression studies, perhaps with a higher number of replicates and better selection of embryo clump tissue, could be necessary to more accurately confirm the fold change value of each of the three selected lines.

3.2. *C. dentata* inoculation assay and *P. cinnamomi* gene expression results

Upon root collection, all samples were weighed (Table 4). The fresh weight of samples from PF-B4GK32 and Ellis #1 lines was very low compared to other lines, risking insufficient RNA yield and consequent insufficient amounts of cDNA for the relative expression study. Indeed, one of the PF-B4GK32 samples, at 24 h post-inoculation, was excluded from the experiment for that reason. For the Ellis #1 line samples, a control for susceptibility to *P. cinnamomi* and the background genotype of the transformed lines, the RNA yield was still above the minimum threshold for RT reactions (the lowest concentration was 117,06 ng/µL).Although variable, the fresh root weight for samples of the CC14 and PF-B4GK31 genotypes was never a limiting factor for the experiment.

Table 4: Fresh weight of collected root material of each sample after the inoculation assay and the respective RNA yield. The name of the sample includes the genotype, the collection timepoint, and whether it was inoculated (inoc) or not (mock). "Pc PDB" refers to control *P. cinnamomi* mycelium samples prepared from liquid cultures. GK 31 and GK 32 represent the PF-B4GK31 and PF-B4GK32 lines, respectively. The table also includes the A260/A280 and the A260/A230 absorbance ratios obtained when quantifying the RNA of each sample.

Sample	Fresh weight (g)	RNA concentration (ng/µL)	Total RNA yield (ng)	A260/A280	A260/A230
CC14 2h mock	0,1830	817,556	8175,560	2,125	2,156
GK 31 2h mock	0,2100	895,564	8955,640	2,124	2,203
GK 32 2h mock	0,1090	726,025	7260,250	2,091	2,080
Ellis #1 2h mock	0,0574	117,060	1170,600	2,008	2,052
CC14 24h mock	0,1701	332,756	3327,560	1,905	1,572
GK 31 24h mock	0,1285	609,444	6094,440	2,074	1,968
GK 32 24h mock	0,0631	494,682	4946,820	2,037	1,875
Ellis #1 24h mock	0,1220	210,817	2108,170	1,870	1,404
CC14 48h mock	0,1862	467,141	4671,410	2,099	2,107
GK 31 48h mock	0,0971	290,466	2904,660	1,930	1,573
GK 32 48h mock	0,0730	341,884	3418,840	1,861	1,273
Ellis #1 48h mock	0,0804	760,576	7605,760	2,063	2,069
CC14 2h inoc	0,1009	263,027	2630,270	2,069	2,229
GK 31 2h inoc	0,1166	979,415	9794,150	2,136	2,153
GK 32 2h inoc	0,0180	158,645	1586,450	2,018	2,150
Ellis #1 2h inoc	0,0690	365,970	3659,700	2,071	1,962
CC14 24h inoc	0,0682	676,652	6766,520	2,102	2,244
GK 31 24h inoc	0,1033	1207,775	12077,750	2,092	1,923
GK 32 24h inoc	0,0112	26,530	265,300	1,895	1,874
Ellis #1 24h inoc	0,0847	838,682	8386,820	2,136	0,985
CC14 48h inoc	0,1726	1470,768	14707,680	2,125	2,085
GK 31-1 48h inoc	0,1535	1787,754	17877,540	2,159	1,167
GK 32 48h inoc	0,0365	253,152	2531,520	2,112	1,575
Ellis #1 48h inoc	0,1270	337,248	3372,480	2,088	1,010
Pc PDB 4	0,1916	1099,843	32995,290	2,222	2,490

The *P. cinnamomi* reisolation assay results (Supplementary Fig. S4) confirmed that the pathogen had infected the roots in most groups. *P. cinnamomi* was not detected in any line at the 2 h timepoint, but such results were expected, since the hyphae growing inside the roots would be very small and possibly still in the root epidermis, perhaps leaving it vulnerable to the bleach treatment. For the remaining timepoints, *P. cinnamomi* was reisolated successfully from all lines except one. In CC14, at 48 h, there was no *P. cinnamomi* growth, meaning there is a lack of certainty on whether those roots were infected. Given the positive results in other groups, it seems likely that *P. cinnamomi* was active during the inoculation assay, but perhaps the roots that were selected for this test from CC14 were not infected yet, so it wasn't detected.

Because of the low cumulative fresh weight of some samples in each time point and treatment combination, it was not possible to have biological replicates for all samples, so only one replicate was used for each sample. Additionally, the high amounts of metabolites that are present in woody plants,

such as polysaccharides and polyphenols (Le Provost et al., 2007), in combination with the low weight, limited the RNA yield. Still, gel electrophoresis showed no signs of RNA degradation (Supplementary Fig. S7). When preparing the reverse transcription, RNA samples had to be normalized to 1000 ng due to the low yield in some lines, impacting downstream processes. After testing the RNA, no genomic DNA was detected (Supplementary Fig. S8).

Multiple qPCR tests showed that the analysis of *P. cinnamomi* gene expression would not be possible in this assay. Early tests showed us that amplification of most genes was hard to detect, to which less diluted cDNA samples were prepared. After testing the primers of the genes of interest, even using the lowest dilution factor (1:10, so there would be enough cDNA for all genes), there was no amplification or very low amplification (Ct>35) in all samples tested, except in the *P. cinnamomi* mycelium samples and the cDNA pool which included mycelium cDNA (Table 5). Even when there was amplification in unknown samples, the high Ct values did not allow for safe calculations of the fold change. A qPCR run made with all samples using the primers for the *P. cinnamomi* reference gene *40s ribosomal protein S3a* showed that it could only be detected in four *C. dentata* root samples, with Ct values between 33 and 40 (Supplementary Table S2). Melting curve data is available in Supplementary Fig. S9.

Table 5: Ct values of the primer tests for all *P. cinnamomi* genes except the reference gene. N/A: no amplification detected. Pool -1 and Pool -3 were standards. NTC is the negative control. Melting curve data is available in the Supplementary Fig. S10.

Sample	*Pc_Avr1b-1*	*Pc_ELI-1B*	*Pc_KatG*	*Pc_ELL*	*Pc_GST*	*Pc_NPP1*	*Pc_Pel*	*Pc_PG*
Pool -1	29,76	24,01	22,43	25,43	27,21	33,3	N/A	34,68
Pool -3	N/A	33,85	31,39	32,92	34,17	N/A	N/A	N/A
Mycelium	27,17	19,89	19,47	21,98	24,49	30,69	38,02	33,2
CC14	N/A	N/A	N/A	N/A	N/A	N/A	N/A	N/A
Ellis #1	N/A	N/A	36,32	N/A	N/A	N/A	N/A	N/A
PF-B4GK31	N/A	N/A	N/A	N/A	N/A	N/A	N/A	N/A
PF-B4GK32	N/A	N/A	N/A	N/A	35,12	N/A	N/A	N/A
NTC	N/A	N/A	N/A	N/A	N/A	N/A	N/A	N/A

Amplification of *P. cinnamomi* genes in mycelium samples and the lack of amplification in root samples probably indicates a low amount of *P. cinnamomi* inoculum in the *C. dentata* roots. Since there was only one small area of contact between the hyphae and the root system, it is possible that not all roots contained hyphae. Despite the successful re-isolation of *P. cinnamomi*, in certain groups it was only detected in some of the roots used for that control (Supplementary Fig. S6). So, it is likely that, similarly, not all the roots collected for RNA extraction in each group contained *P. cinnamomi* hyphae. This means the amount of hyphae relative to the amount of root material could have been below the required level, hence why the *P. cinnamomi* genes could not be detected.

There were similar drawbacks in the amplification of *Castanea* genes as well. In 10 samples, the expression of the reference gene *Actin* was never detected or had Ct values above 35 (Supplementary Table S3). To exclude the hypothesis of dilution errors in those samples, new pools were prepared and diluted, separated samples were also diluted, and qPCR experiments were repeated for all genes. Despite the amplification efficiency being similar to previous experiments, those same samples still exhibited Cts higher than 35 or no amplification occurred (Supplementary Table S4). So, the most likely hypothesis for this lack of amplification is that something went wrong during the reverse transcription, perhaps due to operator error during protocol execution or because of poor RNA

quality and contaminants. In many of the samples where *Actin* expression wasn't detected, RNA absorbance ratios were not ideal (Table 4 & Supplementary Table S4).

The fact that the plant reference gene was not detected in some samples severely limited *Cast_Gnk2-like* expression analysis. Despite that, since there was *Cast_Gnk2-like* amplification in all samples (Supplementary Table S5), the fold change of its expression could still be calculated for the 2 h timepoint in all lines, the 24 h timepoint in PF-B4GK31, and the 48 h timepoint in the PF-B4GK31 and Ellis #1 lines (Fig. 4). The only line where all three timepoints could be analyzed was PF-B4GK31, in which the expression of *Cast_Gnk2-like* in infected roots was calculated to be over double compared to the mock treatment in the first two timepoints, then sharply declines by the 48 h mark. In the remaining lines, *Cast_Gnk2-like* was less expressed at the 2 h timepoint. In Ellis #1, there was downregulation at 48 h post infection relative to the control. However, given the lack of biological replicates and the missing timepoints, in addition to the lack of data from the *P. cinnamomi* gene expression, it is difficult to take meaningful conclusions from this assay. The gene expression data is severely incomplete and a correlation with the different stages of infection is not possible. Perhaps with a bigger sample size from additional inoculation assays, allowing for biological replicates, and maybe alternative methods that guaranteed all of the roots collected were inoculated with *P. cinnamomi* hyphae, the outcome of this work would have been different and allowed for a deeper analysis of the infection process.

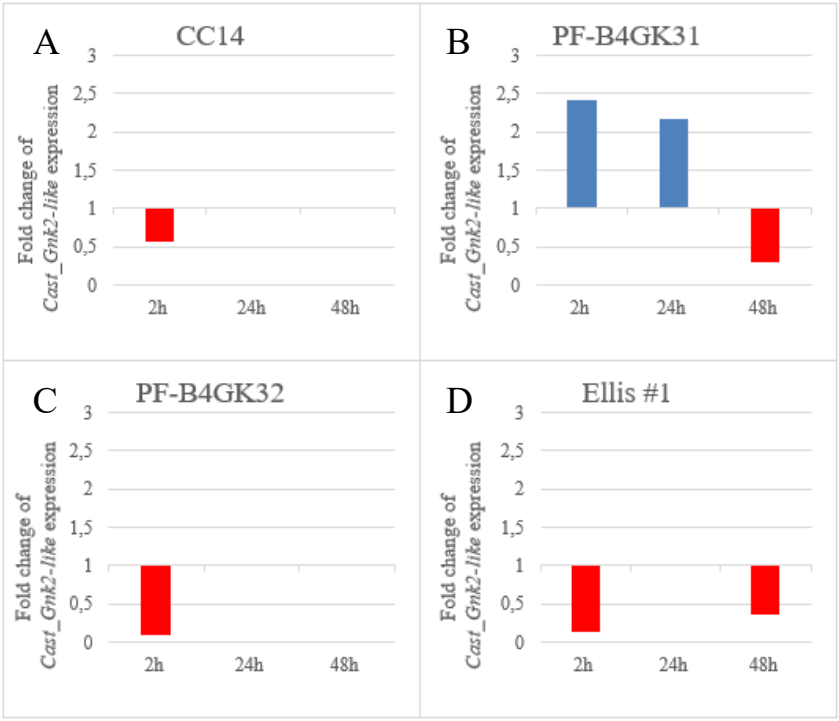

Figure 4: Relative *Cast_Gnk2-like* expression in each line and timepoint combination. Fold change of expression is calculated in relation to the mock treatment counterpart of each inoculated sample. Red: downregulation. Blue: upregulation. A: Fold change of CC14 samples; B: Fold change of PF-B4GK31 samples; C: Fold change of PF-B4GK32 samples; D: Fold change of Ellis #1. GK31 and GK32 represent the PF-B4GK31 and PF-B4GK32 lines, respectively. Missing bars correspond to samples that had no amplification of the *Actin* reference gene, meaning normalization of *Cast_Gnk2-like* expression was not possible.

Future inoculation assays could benefit from some changes in order to more easily detect *P. cinnamomi* gene expression. Using additional plants, increasing the amount of collected root tissue, and inoculating a greater root surface area could increase the amount of hyphae to analyze, resulting in greater *P. cinnamomi* RNA yield. A greater number of plants could also have the added benefit of allowing multiple biological replicates for each group. Additionally, a different inoculation method

capable of infecting the roots of every plant more evenly could result in more hyphae and *P. cinnamomi* RNA yield per group. Perhaps using *P. cinnamomi* zoospores instead of mycelium, using a protocol similar to that described in Del Castillo-González et al. (2024), could yield better results. If these adjustments result in greater RNA yield, they could also allow for an additional purification step, reducing the interference of secondary metabolites in downstream processes and further facilitating the detection of *P. cinnamomi* gene expression. In fact, the extraction protocol used originally included a purification step, using a commercial RNA extraction kit with spin column silica-based technology (Le Provost et al., 2007). It was decided that it would not be included, as we verified from initial extraction tests with different protocols that some RNA is usually lost during the purification process. Perhaps potential contaminants from plant metabolites would have been greatly reduced if the purification step had been performed. It is possible that, consequently, contaminants were present in some samples, negatively affecting reverse transcriptase activity. This may have reduced the cDNA yield from each sample, offering a possible explanation for the high Ct values in some samples. Additionally, since the reverse transcription had to be normalized to low concentrations, the resulting cDNA could not be too diluted, otherwise, the concentration could be too low to detect the target genes. However, this meant the concentration of contaminants in the qPCR reactions would also be greater, potentially contributing to higher Ct values or a higher proportion of undetected amplifications. These adjustments to the experiment design would likely contribute to more interpretable results.

3.3. Predicted characteristics of *P. cinnamomi* proteins

The *P. cinnamomi* genes under study were selected from Fernandes et al. (2024) as highly interesting in the context of infection due to the characteristics of their classes stated in the introduction, and the changes in expression in resistant and susceptible hosts, especially between the 48 h and 72 h timepoints. The amino acid sequences of their codified proteins were analyzed with different bioinformatics tools, and by comparing the data obtained with pre-existing research on those genes, we may better understand the roles they play in *P. cinnamomi*'s infection strategy. Additionally, the in silico analysis of these proteins would have assisted the interpretation of gene expression results from the inoculated *C. dentata* root material.

One important characteristic for this analysis is the location of the protein. The prediction of the subcellular localization obtained from two different models indicated that most of the *P. cinnamomi* proteins in the study are secreted, except for Pc_GST, which seems to be limited to the cytosol (Supplementary Tables S6 & S7). Aligning with these results, the SignalP 6.0 predictions indicate that all proteins except Pc_GST have a signal peptide (Table 6). The presence of signal peptides in these proteins complies with their proposed functions, as these putative effectors and CWDEs were expected to be secreted in order to interact with the host.

Table 6: Signal peptide predictions from Signal IP 6.0. Sec/SPI is a type of signal peptide, cleaved by SPase I. Signal peptide likelihood refers to the probability of that sequence being a signal peptide. N/A means that there is no cleavage site or associated probability, as no signal peptide was recognized.

Gene	Annotation	Prediction	Signal peptide Likelihood	Cleavage site	Probability
Pc_ELI-1B	basic elicitin	Signal Peptide (Sec/SPI)	0,9998	between pos. 20 and 21.	0,976194
Pc_ELL	Elicitin-like protein	Signal Peptide (Sec/SPI)	0,9997	between pos. 20 and 21	0,976097
Pc_NPP1	necrosis inducing-like protein NPP1 type	Signal Peptide (Sec/SPI)	0,9997	between pos. 19 and 20.	0,977916
Pc_Avr1b-1	Avr1b-1 Avirulence-like protein	Signal Peptide (Sec/SPI)	0,9998	between pos. 21 and 22	0,974944
Pc_Pel	Pectate lyase	Signal Peptide (Sec/SPI)	0,9998	between pos. 21 and 22	0,977886
Pc_PG	putative polygalacturonase	Signal Peptide (Sec/SPI)	0,9997	between pos. 20 and 21	0,978185
Pc_KatG	Catalase/peroxidase HPI	Signal Peptide (Sec/SPI)	0,9998	between pos. 21 and 22	0,969477
Pc_GST	putative glutathione S-transferase	Other	0	N/A	N/A

The predictions from "pI Mw" tool (Table 7) gave us some insights on the isoelectric point and the molecular weight. The isoelectric point (pI) of a protein is the pH at which it is neutrally charged, potentially decreasing its solubility and leading to aggregation (Bhatia & Dahiya, 2015; R. R. Burgess, 2009). The molecular weight is the sum of the atomic masses of all atoms in a certain molecule, as a protein for example (National Cancer Institute, 2011). Together, these properties can influence the function of proteins. For example, a study analyzing the effect of the pI in protein transport in the context of fungal infection in barley leaves suggests that a pI between 6,0 and 8,4 favors translocation of host proteins into the extrahaustorial membrane, although protein size also influences the process (Smigielski et al., 2019). However, it is not clear if it also plays a role in effector protein transport from the pathogen to the host. Smigielski et al. (2019) also pointed out that approximately 60% of the *Blumeria graminis* effectors analyzed had pIs outside of the optimal range, but there seemed to be no selection for specific pI values.

Table 7: Isoelectric point and molecular weight predictions of Expasy's Compute pI/Mw tool. For the proteins that were predicted to be secreted according to SignalP 6.0, the putative signal peptide was removed from the sequence before being submitted for calculation of isoelectric point and molecular weight values.

Gene	Annotation	Theoretical isoelectric point	Theoretical molecular weight (Da)
Pc_ELI-1B	basic elicitin	7,45	10293,8
Pc_ELL	Elicitin-like protein	4,05	15905,65
Pc_NPP1	necrosis inducing-like protein NPP1 type	8,28	24975,81
Pc_Avr1b-1	Avr1b-1 Avirulence-like protein	4,12	56007,41
Pc_Pel	Pectate lyase	7,14	36391,28
Pc_PG	putative polygalacturonase	8,78	41682,69
Pc_KatG	Catalase/peroxidase HPI	4,81	72077,54
Pc_GST	putative glutathione S-transferase	5,22	50528,03

The analysis of potential post-translational modifications (PTMs) was also required to understand protein function. For example, when a protein is phosphorylated, the additional phosphate groups can affect its structure and function by enabling new interactions between amino acid residues (Seok, 2021). Glycosylation is another type of PTM which affects the protein function, including the activity of some pathogen effectors (Lin et al., 2020). It can be divided into N-glycosylation, which is more conserved, and O-glycosylation, which varies depending on the kingdom (Strasser et al., 2021). N-glycosylation generally consists of the addition of N-acetylglucosamine and mannose chains in specific asparagine residues, with the possibility of other sugars being included at the end of the chain (Rayon et al., 1998). In fungi and protists, O-glycosylation usually occurs in serine or threonine residues, although there are some rare exceptions, and mostly consists of mannose chains, although some species can also use other sugars (Goto, 2007; West & Kim, 2019). The results from NetPhos 3.1 give us a list of potential phosphorylation sites of the proteins. It analyses the likelihood of phosphorylation of serine, threonine and tyrosine residues from the following kinases: ATM, CKI, CKII, CaM-II, DNAPK, EGFR, GSK3, INSR, PKA, PKB, PKC, PKG, RSK, SRC, cdc2, cdk5 and p38MAPK. DictyOGlyc 1.1 and NetNGlyc 1.0 analysis showed potential glycosylation sites of the proteins, further contributing to a better understanding of their function. The full list of phosphorylation and glycosylation sites, along with the corresponding graphs, is available in the supplementary material section (Supplementary Fig. S11-S13).

InterProScan detected the presence of a signal peptide in all proteins except Pc_GST, confirming the results obtained by SignalP 6.0. Another common domain detected in some proteins was the intrinsically disordered region (IDR) domain, which was present in Pc_ELL, Pc_Avr1b-1 and Pc_PG. IDRs are segments of a protein that do not have a defined tertiary structure because they don't contain enough hydrophobic residues for co-operative folding (Babu, 2016). They can play a role in binding, as they fold and acquire a structure based on their interaction with potential substrates, resulting in weak and easily reversible associations with specific targets (Babu, 2016). These regions are also commonly subjected to PTMs, which affect their binding capacity and, as a consequence, allow these proteins to be easily regulated (Babu, 2016). Thanks to these properties, proteins that contain IDRs are suitable for functions related to signaling cascades or transcription regulation, both very important for proper cell functioning in general (Dunker et al., 2015; Liu et al., 2006).

Lastly, AlphaFold 3.0 allowed us to get predictions of the structures of the *P. cinnamomi* proteins under study (Supplementary Fig. S14). The release of this tool made a great impact in the field of life sciences, especially molecular biology. Identifying and studying the structure of a single protein could take years, and now, this AI-powered tool is capable of delivering accurate predictions in a matter of minutes. Despite being a great assistance to many in this area of research, this tool has some limitations, and traditional methods are still necessary to confirm the structure of analyzed proteins.

By analyzing the previous predictions alongside the next in silico results, and comparing them to homologous proteins in databases, we could get a more detailed understanding of the putative function of each protein. It is worth noting that the signal peptides, which are cleaved from the proteins in vivo, were not included in the structure data input.

3.3.1. Elicitins Pc_ELI-1B and Pc_ELL

Overall, both Pc_ELI-1B and Pc_ELL were predicted to have the same domains, with the only difference being the presence of an IDR at the C-terminus of the latter (Fig. 5). Also, the lack of a C-terminal domain in Pc_ELI-1B indicates that it belongs to the ELI-1 clade of elicitin proteins (Jiang et al., 2006). Additionally, the sequences of the elicitin domains have differences, which can be seen in their alignment (Fig. 6), notably in the 13th position. The 13th amino acid is known to play an important

role in elicitin function, more specifically in the induction of necrosis, and it differs between basic and acidic elicitins, with the former having a lysine in that position and the latter a valine (Nespoulous et al., 1992). The presence of valine instead of lysine in that position can also negatively affect sterol binding capabilities (Plešková et al., 2011). Interestingly, Pc_ELL has a threonine in that position, which could have some implications in how the protein functions. The main difference regarding the amino acid in the 13th position is the polarity and charge: valine is hydrophobic and uncharged, while lysine is hydrophilic and positively charged, which might make it more likely to be exposed and interact with its targets (Chandani Kamble et al., 2021; L. M. Yu, 1995). Since threonine is a polar but uncharged amino acid, Pc_ELL might function more similarly to a basic elicitin, with one of the most important residues being hydrophilic (Chandani Kamble et al., 2021). However, other residues might also play a role in elicitin interactions, so the effect of the threonine in the 13th position might be limited or overshadowed by other factors (Nespoulous et al., 1992).

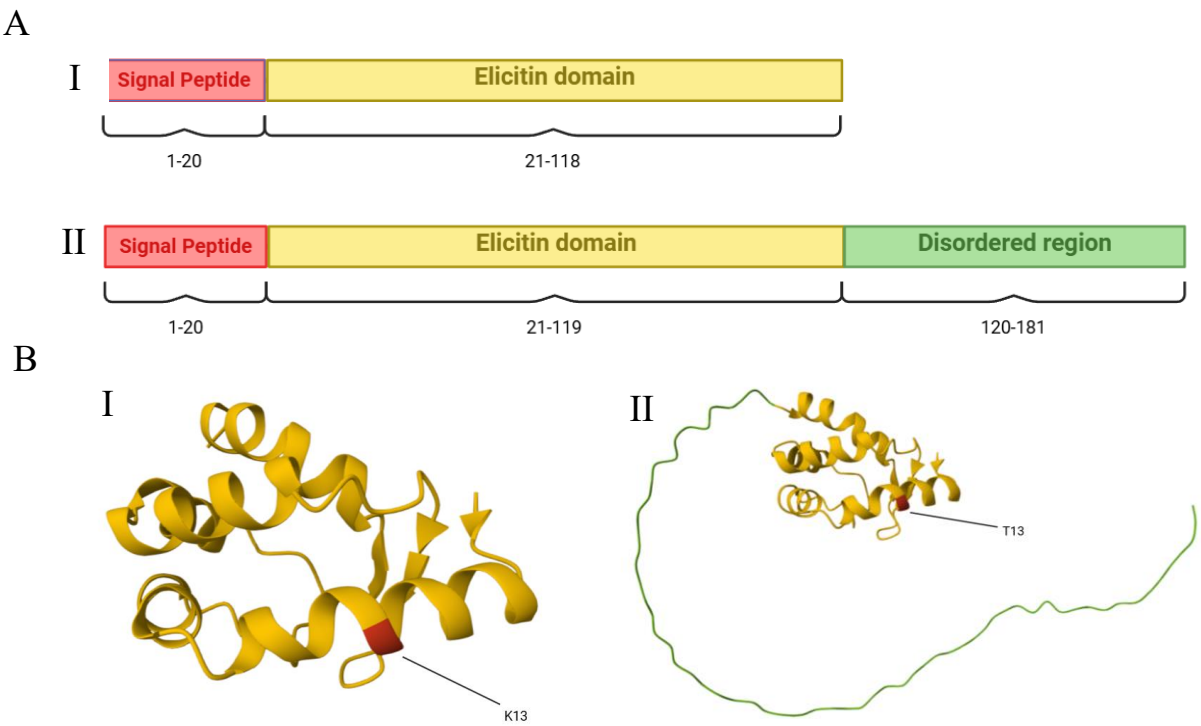

Figure 5: Structure of the Pc_ELI-1B and Pc_ELL proteins. A: Schematic representation of the domains and other features of the amino acid sequences of Pc_ELI-1B (I) and Pc_ELL (II) predicted by InterPro's domain search tool. Made in BioRender. Red: signal peptide; Green: intrinsically disordered regions (IDRs); Yellow: elicitin domains; B: AlphaFold Server 3.0 tridimensional structure prediction for Pc_ELI-1B (I) and Pc_ELL (II), with the 13th amino acid highlighted in red (K13: Lysine in the 13th position; T13: Threonine in the 13th position).

According to Jiang et al. (2006), when elicitins have many glycosylation sites in the C-terminal region, they tend to be associated with the cell wall or linked to the cell membrane, while those lacking that region are simply secreted. Given that Pc_ELL has a C-terminus domain but no predicted glycosylation sites, it is uncertain where it would be located after secretion, while Pc_ELI-1B is probably free in the apoplast. Additionally, it has been reported that RLPs can play a role in elicitin detection and reduce infection success (Du et al., 2015). Given that Cast_Gnk2-like has two cysteine-rich domains, common in RLPs and RLKs, and is likely secreted into the apoplast, it can be hypothesized that Cast_Gnk2-like interacts with Pc_ELI-1B and Pc_ELL. If this interaction does occur and triggers host defenses, it could be a contributing factor to the higher resistance to *P. cinnamomi* infection that species with higher *Cast_Gnk2-like* expression exhibit, like *C. crenata*

(Serrazina et al., 2024b). Because of their potential for both avirulence and virulence, elicitins seem to have an impact on *P. cinnamomi*-host compatibility, depending on whether they are recognized or not, respectively (Colas et al., 2001). Therefore, elicitins Pc_ELI-1B and Pc_ELL could be key components of the capacity of *P. cinnamomi* to successfully infect *C. dentata* and *C. sativa*, and studying them could open new possibilities for tackling the susceptibility of these species.

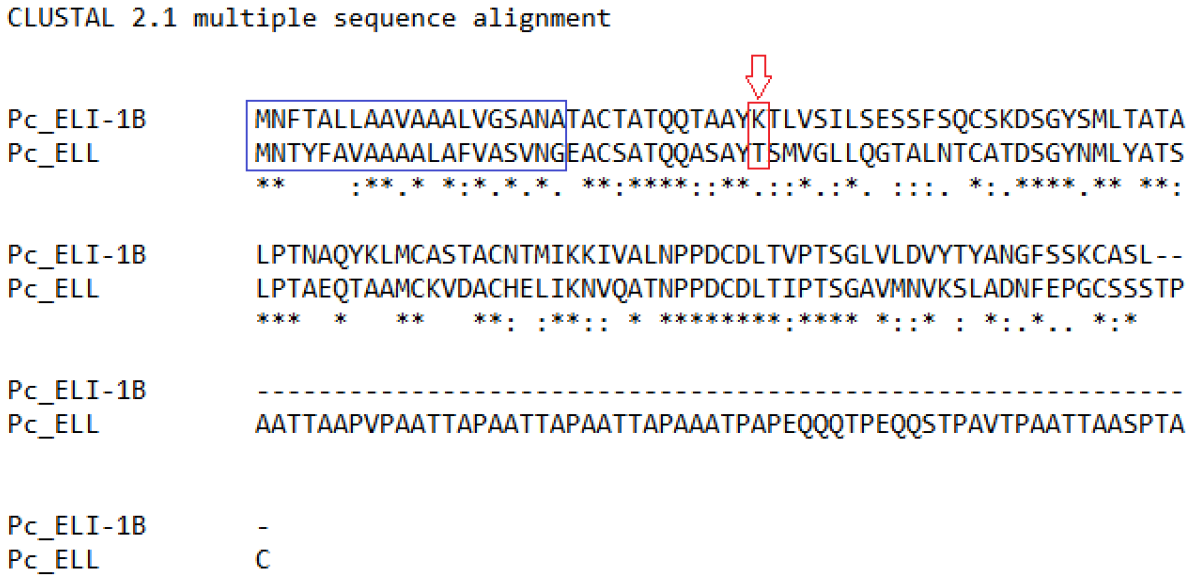

Figure 6: Amino acid sequence alignment of Pc_ELI-1B and Pc_ELL performed using Clustalw. The signal peptides are indicated in the blue box and the 13th residue is indicated by the red arrow and box.

3.3.2. Pc_NPP1 may have less necrotic activity than other NLPs

Pc_NPP1 was predicted to have a NPP1 domain, which is in accordance with its annotation (Fig. 7). The NPP1 domain is present in all NLPs, and these can be divided into three types, depending on the number of conserved cysteines (Gijzen & Nürnberger, 2006; Oome & Van Den Ackerveken, 2014). There is also a central conserved hepta-peptide motif (GHRHDWE), common to all types (Oome & Van Den Ackerveken, 2014). The cysteine residues and the heptapeptide play a role in the ability of NLPs to induce cell death during infection (Gijzen & Nürnberger, 2006). *Phytophthora* NLPs belong to type 1, which have two conserved cysteine residues before the central conserved region (Gijzen & Nürnberger, 2006). A *P. cinnamomi* NPP1 protein has been previously analyzed, and its gene expression peaked at the later timepoints of *C. sativa* infection, when the roots exhibited the most necrosis (Martins et al., 2019). Pc_NPP1 has a similar protein length and molecular weight to the NPP1 protein analysed in Martins et al. (2019) (Tables 2 & 7). However, when aligning both sequences, there are differences between them, as the percent identity was relatively low (35.38%, Supplementary Fig. S15) and the heptapeptide from Pc_NPP1 is quite different from the consensus sequence, but both have the same conserved cysteine residues (Fig. 8). Oomycete NPP1 proteins with poor conservation of the heptapeptide can be classified together in the type 1a subgroup, which usually only conserves three out of seven peptides: R102, H103, and W105, (Oome & Van Den Ackerveken, 2014). The residues H101, D104, and E106, which are not conserved in type 1a, play a major role in the necrotic activity of the protein (Oome & Van Den Ackerveken, 2014; Ottmann et al., 2009). In Pc_NPP1, besides the three peptides commonly conserved in type 1a, only residue D104 is conserved. This information suggests that the activity of Pc_NPP1 might differ from that of the NPP1 effector described in Martins et al. (2019) and other *Phytophthora* NLPs. The obligate biotrophic oomycete

Hyaloperonospora arabidopsidis contains many noncytotoxic NLPs in its genome, suggesting some importance for biotrophy (Cabral et al., 2012). Most of those lacked full conservation of the heptapeptide, so, it could be hypothesized that, similarly, Pc_NPP1 has relatively low necrotic activity and may play a role in the biotrophic phase of infection. More research would be necessary to understand how it differs from other NLPs and its role in *Castanea* spp infection.

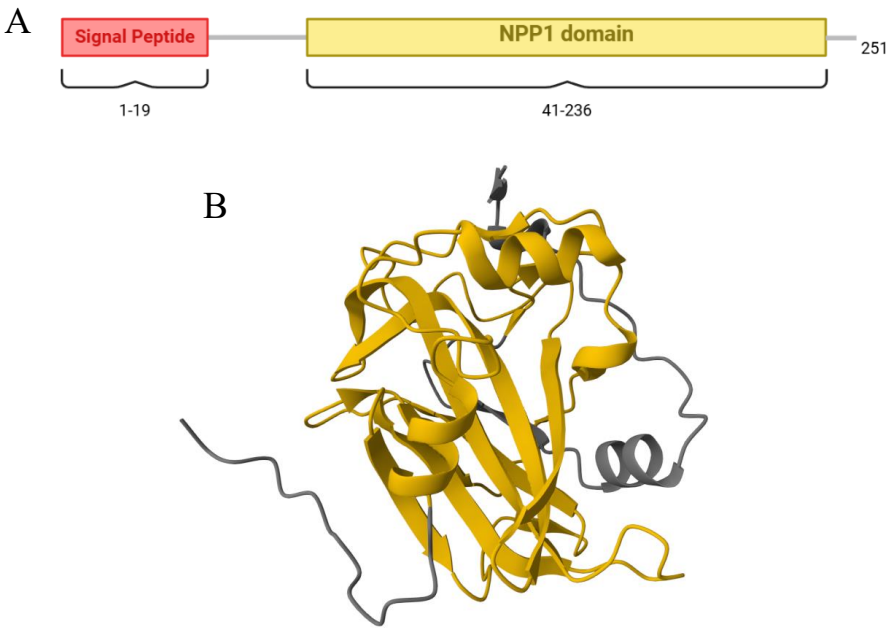

Figure 7: Structure of the Pc_NPP1 protein. A: Schematic representation of the conserved domains of the amino acid sequence predicted by InterPro's domain search tool. Made in BioRender. Red: signal peptide; Yellow: NPP1 domain. B: AlphaFold Server 3.0 tridimensional structure prediction for Pc_NPP1, with the NPP1 domain highlighted in yellow.

```
CLUSTAL 2.1 multiple sequence alignment


Pc_NPP1          -MNFLLLFVAFVTLLKMAAASSIDLNKVSPIAQPTPSTSAQKTAIRFKPRLSIG------
CAL47421.1       MVSAVLDSRFNVALWIFQRHPKYDVVDALRRCQHRCWEFVDPHPPRMQRQLSSTNLSFHI
                  :. :*     *:*  :   .. *: ..   .*      .:  . *:: :**


Pc_NPP1          AGGCVSFPAVNSAGETSSGLSEEYKGSIGCLNAPLGSQVYGRAAWYKSKFAIVYAWYFPK
CAL47421.1       TDGCHPYPAVQADGSVSGGLEWSGADDGDCKGSAWGSQVYARSAWYNNKYAIMYAWYFPK
                 :.** .:***:: *..*.**. .  .. .* .:. *****.*:***:.*:**:*******


Pc_NPP1          G-----FYNAYPTRRHDWASAVVWTNNPDSPSPKISGLSLSTADWQYETQAPATSGISDG
CAL47421.1       GKGRQHVHKLHSGHRHEWEFAVVWVDQPSADHSNLLGVSMSFG-PSFHKEAPVQPEHVVG
                 *     .:: :. :**:*  ****.::*.:  .:: *:*:* .  .:..:**. .    *


Pc_NPP1          TTPKLSHELQVDCGDAYLTTTDATGDFQPLIMWEQLPAAARTALNTTDFGN------AKV
CAL47421.1       SSIKLDSYSTFWGAKQGLRVTTDIGTTQDLIQWEQLTDAARASLTETNFDIDEAVVPVEM
                 :: **.    .  ..  * .*   *  * ** ****. ***::*. *:*.       .::


Pc_NPP1          PISDANFKKKLQDAWPFSGQTTRNSCREG
CAL47421.1       PLKDDVFQLKLNSTYPF------------
                 *:.*  *: **:.::**
```

Figure 8: Sequence alignment of Pc_NPP1 and the NPP1 protein described in Martins et al (2019) (CAL47421.1). The conserved cysteine residues are represented by the green box and arrows, and the conserved heptapeptide is in the red box. The signal peptide of Pc_NPP1 is represented by the blue box.

3.3.3. Pc_Avr1b-1 lacks the RxLR motif

InterPro's Domain Search and the NCBI CD database did not find any corresponding conserved domains for Pc_Avr1b-1 (Fig. 7). However, the predicted IDR region might play an important role in its function. Oomycete avirulence proteins (Avr) are a type of RxLR effector, which can affect host mechanisms through the interaction with cytoplasmic proteins or via transcription regulation (Catanzariti et al., 2007; S. Wang et al., 2023). Since IDRs can be involved in both processes (Babu, 2016; Dunker et al., 2015), it could be a key structure for the effector function of Pc_Avr1b-1. Also, when searching for homologues in NCBI, most of the top hits were uncharacterized proteins and Avr proteins from various *Phytophthora* species (Supplementary Fig. S16). These results are similar to the analysis from Joubert et al. (2021), which highlighted the closest homologue for each of the studied putative RxLR effectors in *P. cinnamomi*, most of them being annotated as "hypothetical proteins".

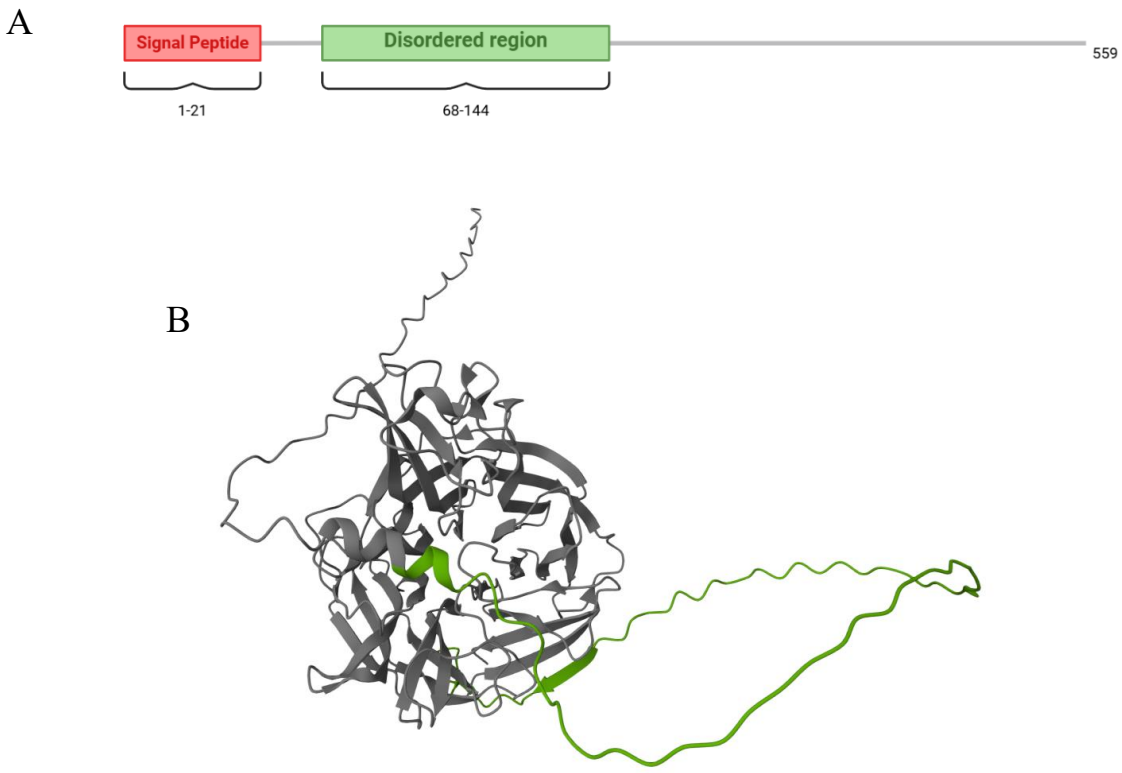

Figure 9: Structure of the Pc_Avr1b-1 protein. A: Schematic representation of the domains and other features of the amino acid sequence predicted by InterPro's domain search tool. Made in BioRender. Red: signal peptide; Green: intrinsically disordered regions (IDRs); B: AlphaFold Server 3.0 tridimensional structure prediction for Pc_Avr1b-1, with the IDR domain highlighted in green.

However, the amino acid sequence of Pc_Avr1b-1, unexpectedly, seems to lack the RxLR motif, as it was not detected by either domain search tools used. This could mean that Pc_Avr1b-1 is not an RxLR effector, contrary to what its initial annotation would suggest. Additionally, according to (Dou et al., 2008), the RxLR motif is necessary for transport of *Phytophthora sojae* (M.J.Kaufmann & J.W.Gerdemann) effector Avr1b into the host cell. Therefore, unless there is a different signaling sequence, Pc_Avr1b-1 is most likely not translocated into the host cytosol. Regardless, the presence of an IDR may indicate some uncharacterized function in the infection process, such as interacting with host proteins in the apoplast. The abundance of predicted phosphorylation sites throughout the protein,

as well as the few glycosylation sites (Supplementary Figs. S12 and S13), align with this possibility, as PTMs can sometimes be necessary for effector function (Lin et al., 2020; Tahir et al., 2019). Protein function studies done on Pc_Avr1b-1 are required to verify its location after secretion and what interactions it may be involved in.

3.3.4. Pc_PG contains a disordered region and Pc_Pel may be a pectin lyase

According to the InterPro domain search tool analysis, both CWDEs under study are predicted to be involved in the degradation of pectin of the host. Pc_PG has a predicted Glycosyl hydrolase family 28 domain from the 101st to the 400th amino acid (Fig. 9). The InterPro predictions are in accordance with the initial annotation for both CWDEs. Glycoside hydrolases are enzymes that degrade polysaccharides, and are divided into many families by their sequence structure (Bojarová-Fialová & Křen, 2007; Bourne & Henrissat, 2001). PGs are included in the Glycosyde hydrolase family 28, and hydrolyse homogalacturonan, a polymer of d-galacturonic acid and the main component of pectin (Nakamura & Iwai, 2019; Yadav et al., 2009). As for Pc_Pel, it contains a Pectin lyase fold domain (Fig. 9), although it was annotated as a pectate lyase (Engelbrecht et al., 2021). Pectate and pectin lyases have similar functions, as both degrade pectic acid by β-transelimination rather than hydrolysis, generating unsaturated oligogalacturonates (Yadav et al., 2009). They also have high structure similarity despite low sequence similarity (Mayans et al., 1997; Yadav et al., 2009). The main differences between pectate and pectin lyases include: 1) variations substrate specificity and mode of action; and 2) Ca^{2+} ions are required for pectate lyase activity, while the same does not seem to apply for pectin lyases (Zheng et al., 2021).

This means that both Pc_PG and Pc_Pel may break down pectin in different ways, promoting the degradation of the cell wall. Since pectin can also have carboxyl groups esterified with methanol, the activity of a pectin esterase could also be necessary for Pc_PG and Pc_Pel to be able to degrade pectin (Yadav et al., 2009). However, this may depend on the species, as some pectinases, such as the Pectin Lyase A from *Aspergillus niger* van Tieghem, only degrade esterified pectin (Van Alebeek et al., 2002; Yadav et al., 2009).

The prediction results for Pc_PG go into further detail, as its active site was predicted to be located between amino acids 268 and 281. Pc_PG has all the conserved residues seen in *Phytophthora* PGs (highlighted in Supplementary Fig. S17), including those that affect substrate binding (Götesson et al., 2002; Pagès et al., 2000). Also, Pc_PG contains a D(P/Q)TQQQ repeat similar to those found in some PGs reported in Götesson et al. (2002) (Supplementary Fig. S17). Another interesting prediction is the presence of an IDR between the signal peptide and the glycosyl hydrolase domain of Pc_PG. The presence of an IDR near the N-terminus of Pc_PG could mean this protein interacts with others in the extracellular space, perhaps even interacting with host proteins. CWDE activity might be influenced by the presence of these domains. For example, in some multimodular lignin-degrading enzymes, glycosylated IDR domains can promote binding to cellulose (Payne et al., 2013). Despite the single potential glycosylation site above the threshold in the IDR of Pc_PG (Supplementary Figs. S12 & S13), there are many potential phosphorylation sites which may contribute to this function (Supplementary Fig. S11), so it is possible for that region to improve the cell wall degrading activity of Pc_PG. Alternatively, it is possible for that region to be absent from the processed Pc_PG protein. There are PG proteins from plants that, besides the signal peptide, include a prosequence of around 50 amino acids, highly charged, which is also cleaved and is not in the final structure (DellaPenna & Bennett, 1988). However, this seems unlikely, since it was suggested that PcPG7 maintains the N-terminal domain (Götesson et al., 2002).

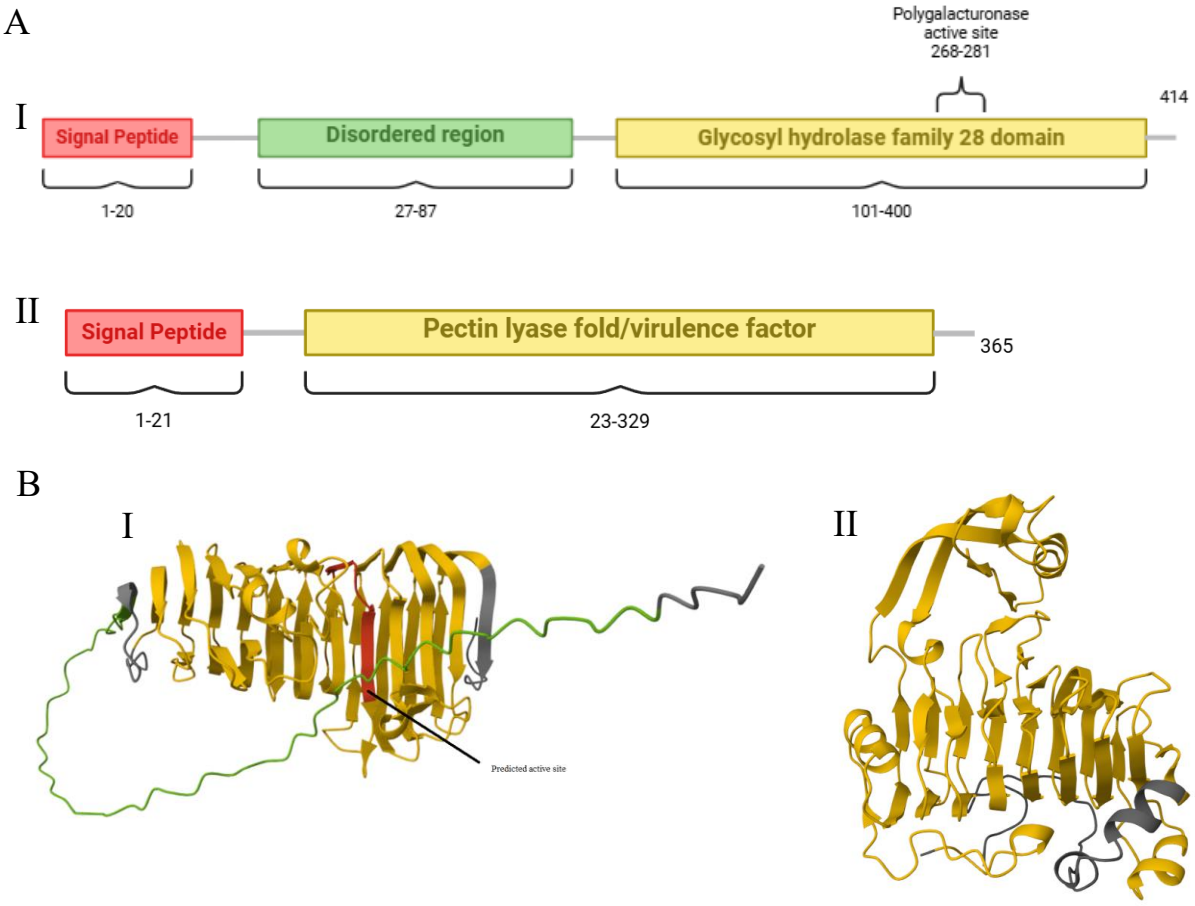

Figure 10: Structure of the Pc_PG and Pc_Pel proteins. A: Schematic representation of the conserved domains and other features of the amino acid sequences of Pc_PG (I) and Pc_Pel (II), predicted by InterPro's domain search tool. Made in BioRender. Red: signal peptide; Green: intrinsically disordered regions (IDRs); Yellow: Glycosyl hydrolase family 28 and Pectin lyase fold/virulence factor domains. B: AlphaFold Server 3.0 tridimensional structure prediction for Pc_PG (I) and Pc_Pe (II), with the predicted domains and important sites highlighted. Pc_PG's active site is highlighted in red.

As for Pc_Pel, no specific prediction for the active site was obtained. According to the literature, there are some residues that play an important role in substrate binding in pectin lyases. D154, R176, R236 and K239 are important for the activity of Pectin Lyase A in *A. niger* (Sánchez-Torres et al., 2003). In pectate lyases, those residues are more variable, depending on the protein family (Zheng et al., 2021). By comparing Pc_Pel with representatives from each family, the closest one was the PL1 family, although with a low score (Supplementary Fig. S18). When comparing it with pectate lyases and pectin lyases from other *Phytophtora* species and *A. niger*, the % identity values are similar for both pectinases from *Phytophthora* species, although slightly higher for the pectate lyase (Supplementary Fig. S19). But when compared to the pectinases from *A. niger*, it was closer to a pectin lyase. Furthermore, Pc_Pel also has 2 out of 4 of the conserved residues in pectin lyases (Supplementary Fig. S20) So, while it seems likely that Pc_Pel is a pectin lyase, functional studies are necessary to confirm its activity.

These results seem to reinforce the idea that Pc_PG and Pc_Pel are involved in cell wall degradation. Still, to fully understand *P. cinnamomi* hyphae propagation within the host, other CDWEs would need to be analyzed, as well as factors related to hyphal growth and survivability. Studying the effect of the IDR region in Pc_PG would also be of interest. Additionally, an analysis of multiple pectate lyases from *Phytophthora capsici* Leonian showed that some of them may have the potential to induce cell death when overexpressed (Fu et al., 2015). So, given the similarities with

pectin lyases, further analysis of the potential of Pc_Pel to induce cell death could reveal an additional function for this protein during chestnut interactions.

3.3.5. Pc_KatG may play a role in *P. cinnamomi* pathogenicity

InterPro's domain search classified Pc_KatG as part of the "Catalase-peroxidase haem" family (Fig. 11). Furthermore, the domain prediction for Pc_KatG also shows two separate heme peroxidase domains, aligning with its proposed family and fitting the initial annotation. The peptide sequences of KatGs are more similar to the sequences of heme peroxidases than to those of true catalases (Zámocký & Koller, 1999). These proteins are also, as the name implies, able to perform both peroxidase and catalase activity, important abilities for the defense against oxidative stress (Ighodaro & Akinloye, 2018; Smulevich et al., 2006). This means Pc_KatG may play a role in the *P. cinnamomi* stress response, and its expression could indicate how much stress is being induced by the host's defenses. Typically, in *Phytophthora* species, KatG enzymes are secreted, similarly to the fungal counterparts to those enzymes, therefore, the signal peptide prediction results of Pc_KatG (Table 6) also align well with published research (Blackman & Hardham, 2008; Zámocký et al., 2012). Host plants can increase ROS concentration as a response to pathogen detection, resulting in the induction of localized cell death and directly harming the pathogen (Lamb & Dixon, 1997). Many phytopathogens counter that mechanism by overexpressing KatGs, especially in the early stages of infection (Tanabe et al., 2011; T. Wang et al., 2023). So, besides increasing survivability, the expression and secretion of Pc_KatG may also influence pathogenicity.

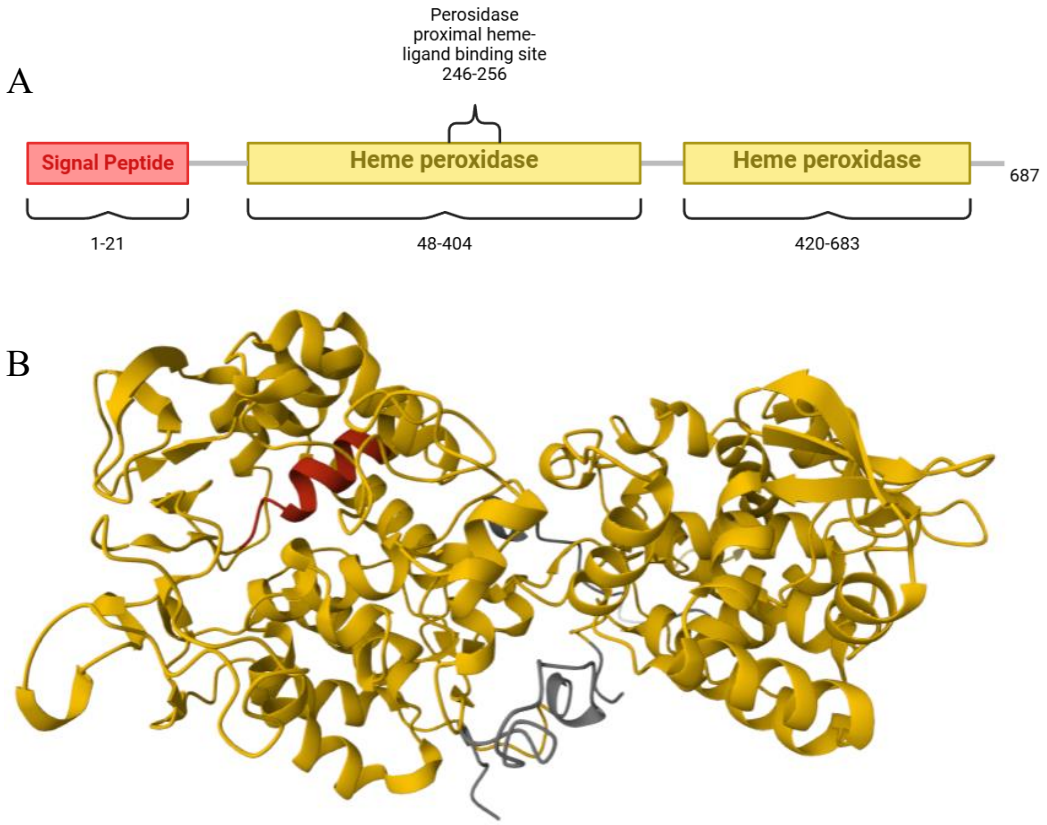

Figure 11: Structure of the Pc_KatG protein. A: Schematic representation of the conserved domains and other features of the amino acid sequence predicted by InterPro's domain search tool. Made in BioRender. Red: signal peptide Yellow: Heme peroxidase domains. B: AlphaFold Server 3.0 tridimensional structure prediction for Pc_KatG, with the predicted domains and important sites highlighted. The binding site is highlighted in red.

Additionally, results from Euk-mPLoc 2.0 indicated that Pc_KatG could be located in the cytoplasm as well (Supplementary Table S3). Given it might have peroxidase activity, it is possible for it to have a dual location and be present inside peroxisomes as well. However, in oomycetes, unlike fungi, KatGs tend to lack peroxisome targeting signal (PTS) of both existing types, reinforcing the idea that this catalase is secreted (T. Wang et al., 2023). The DeepLoc 2.1 predictions support this, since Pc_KatG is not directed into the peroxisome according to its probability value (less than 0,003) (Supplementary Table S7). There are two types of PTSs: PTS1, defined by a Serine-Lysine-Leucine tripeptide in the C-terminal, and PTS2, which consists of a more loose and variable consensus sequence ([R/K]-[L/V/I]-[X]5-[H/Q]-[L/A]), and is usually located closer to the N-terminus (Brocard & Hartig, 2006; Kunze, 2020). Pc_KatG lacks the PTS1 tripeptide (Supplementary Fig. S21) and, although DeepLoc 2.1 analysis shows a sequence between amino acids 240 and 250 may have an influence in its location signaling (Supplementary Fig. S22), it is unclear if it corresponds to a PTS2 consensus motif. Therefore, it seems likely that Pc_KatG is secreted to the extracellular environment, similar to other oomycete KatGs (Blackman & Hardham, 2008; Zámocký et al., 2012), and may have an influence on oxidative stress resistance and pathogenicity of *P. cinnamomi*. Further studies are needed to confirm these predictions.

3.3.6. Pc_GST contains an additional C-terminal domain

GSTs can be divided into 4 different types: cytosolic, mitochondrial (both soluble), microsomal (associated with the membrane) and a specific bacterial type which consists of fosfomycin resistance proteins (Hayes et al., 2005). Given the absence of a signal peptide (Fig. 12) and predicted subcellular location (Supplementary Tables S6 & S7), it seems that Pc_GST is cytosolic. However, looking at the results from DeepLoc 2.1, besides a prediction of a nuclear location signal, Pc_GST had a relatively high score for mitochondrial location (0,16820000). It is possible for a GST to be targeted both to the cytosol and the mitochondria, through phosphorylation of certain residues, but this has not been studied in fungi nor oomycetes (Raza, 2011).

The overall GST structure consists of a N-terminal domain (also referred to as Domain I), consisting of a thioredoxin superfamily fold, that binds to glutathione, and a C-terminal domain (also referred to as Domain II), comprised mostly of α-helices, whose function is the recognition of xenobiotic substrates (exogenous compounds) (Armstrong, 1997; Vaish et al., 2020). Pc_GST was predicted to include two C-terminal domains, one of which is closer to the N terminus of the protein than the N-terminal domain (it will be referred to as “C-terminal-like domain” from now on). However, the NCBI CD database search tool did not predict this domain. Since we did not find any reported cases of domain duplication in GSTs, it is unclear how this apparent domain duplication could affect Pc_GST, but since the C-terminal domain is involved in the binding of GSTs to xenobiotic compounds (Armstrong, 1997), it could probably influence their recognition by the protein.

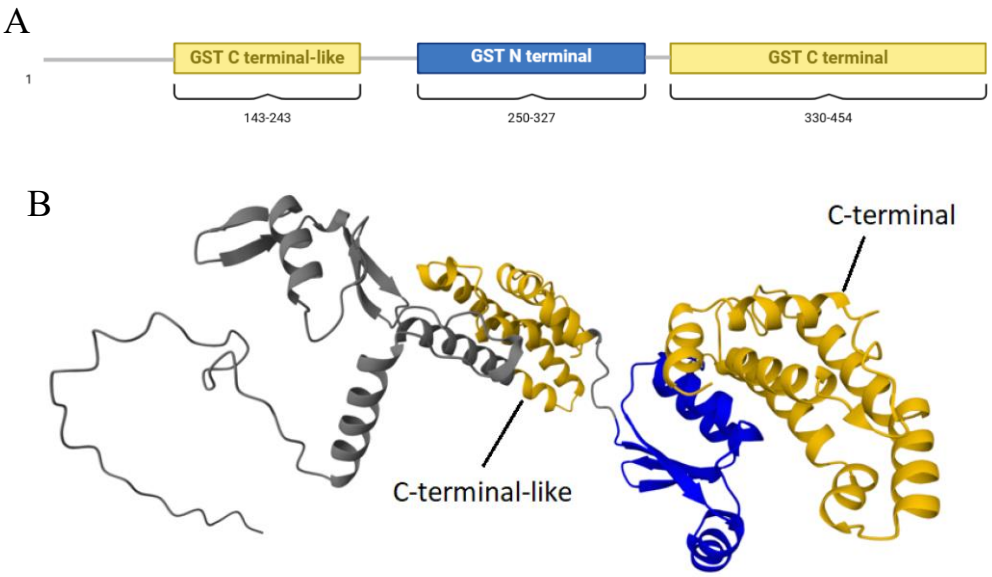

Figure 12: Structure of the Pc_GST protein. A: Schematic representation of the conserved domains of the amino acid sequence predicted by InterPro's domain search tool. Made in BioRender. Yellow: Different C terminal GST domains; Blue: N terminal GST domain. B: AlphaFold Server 3.0 tridimensional structure prediction for Pc_GST, with the predicted domains highlighted in the same colors as in A.

Also, since GSTs work in dimers (Armstrong, 1997), we tested if AlphaFold would predict a similar structure for Pc_GST. Indeed, both subunits seemed to form a dimer with the N-terminal domain of one protein interacting with the C-terminal domain of the other one (Supplementary Fig. S23), as expected for a GST dimer (Armstrong, 1997). The C-terminal-like domain showed a similar interaction with the uncharacterized N-terminal region of the other subunit, maintaining the overall organization of the dimer. This suggests that the presence of C-terminal-like domain may be compatible with protein function, and perhaps it could even play a role in binding to certain substrates. However, protein function studies with altered Pc_GSTs would be necessary to understand the role of the C-terminal-like domain in Pc_GST function and *P. cinnamomi* stress response.

3.4. Concluding remarks

Overall, these results are a positive contribution to the effort against the impact of *P. cinnamomi* on chestnuts and other woody plant species. The selected *C. sativa* transformants, the lines CL-9-GIN-1, CL-3-GIN-1, and CL-9-GIN-11, will be used in future research, contributing to increase our understanding of the *Cast_Gnk2-like* gene and ultimately to the protection of European chestnut production from the effects of *P. cinnamomi*. The *C. dentata* inoculation assay results, although inconclusive due to low amounts of root tissue collected and low RNA yield, allowed us to better prepare future inoculation assays. The in silico analysis of the selected *P. cinnamomi* proteins resulted in many insights regarding the putative function of each protein in the infection process, including the possible interaction between elicitins and Cast_Gnk2-like, the presence of the C-terminal-like domain in Pc_GST, the lack of the RxLR motif in Pc_Avr1b-1, and the classification of Pc_NPP1 as a type 1a NLP. This information will be useful for analyzing future inoculation assays and opens the possibility for more in-depth research on each protein.

4. References

Abramson, J., Adler, J., Dunger, J., Evans, R., Green, T., Pritzel, A., Ronneberger, O., Willmore, L., Ballard, A. J., Bambrick, J., Bodenstein, S. W., Evans, D. A., Hung, C.-C., O'Neill, M., Reiman, D., Tunyasuvunakool, K., Wu, Z., Žemgulytė, A., Arvaniti, E., … Jumper, J. M. (2024). Accurate structure prediction of biomolecular interactions with AlphaFold 3. *Nature*, *630*(8016), 493–500. https://doi.org/10.1038/s41586-024-07487-w

Ali, M., Cheng, Z., Ahmad, H., & Hayat, S. (2018). Reactive oxygen species (ROS) as defenses against a broad range of plant fungal infections and case study on ROS employed by crops against *Verticillium dahliae* wilts. *Journal of Plant Interactions*, *13*(1), 353–363. https://doi.org/10.1080/17429145.2018.1484188

Amack, S. C., & Antunes, M. S. (2020). CaMV35S promoter – A plant biology and biotechnology workhorse in the era of synthetic biology. *Current Plant Biology*, *24*, 100179. https://doi.org/10.1016/j.cpb.2020.100179

Anagnostakis, S. L. (1987). Chestnut Blight: The Classical Problem of an Introduced Pathogen. *Mycologia*, *79*(1), 23–37. https://doi.org/10.1080/00275514.1987.12025367

Anagnostakis, S. L. (2012). Chestnut Breeding in the United States for Disease and Insect Resistance. *Plant Disease*, *96*(10), 1392–1403. https://doi.org/10.1094/PDIS-04-12-0350-FE

Armstrong, R. N. (1997). Structure, Catalytic Mechanism, and Evolution of the Glutathione Transferases. *Chemical Research in Toxicology*, *10*(1), 2–18. https://doi.org/10.1021/tx960072x

Babu, M. M. (2016). The contribution of intrinsically disordered regions to protein function, cellular complexity, and human disease. *Biochemical Society Transactions*, *44*(5), 1185–1200. https://doi.org/10.1042/BST20160172

Backer, R., Engelbrecht, J., & Van Den Berg, N. (2022). Differing Responses to *Phytophthora cinnamomi* Infection in Susceptible and Partially Resistant *Persea americana* (Mill.) Rootstocks: A Case for the Role of Receptor-Like Kinases and Apoplastic Proteases. *Frontiers in Plant Science*, *13*, 928176. https://doi.org/10.3389/fpls.2022.928176

Badri, D. V., & Vivanco, J. M. (2009). Regulation and function of root exudates. *Plant, Cell & Environment*, *32*(6), 666–681. https://doi.org/10.1111/j.1365-3040.2009.01926.x

Bairrão, M., Trindade, M., Valdiviesso, T., Silva, M., Trindade, C. S., Ferreira, R. B., Cordovil, C., & Machado, H. (2021). Comparing Intraspecific Aggressiveness in *Phytophthora cinnamomi* Isolates. *Silva Lusitana*, *29*(2), 115–131. https://doi.org/10.1051/silu/20212902115

Bartnicki-Garcia, S. (1966). Chemistry of Hyphal Walls of Phytophthora. *Journal of General Microbiology*, *42*(1), 57–69. https://doi.org/10.1099/00221287-42-1-57

Benen, J. A. E., Kester, H. C. M., Pařenicová, L., & Visser, J. (2000). Characterization of *Aspergillus niger* Pectate Lyase A,. *Biochemistry*, *39*(50), 15563–15569. https://doi.org/10.1021/bi000693w

Bhatia, S., & Dahiya, R. (2015). Concepts and Techniques of Plant Tissue Culture Science. Em *Modern Applications of Plant Biotechnology in Pharmaceutical Sciences* (pp. 121–156). Elsevier. https://doi.org/10.1016/B978-0-12-802221-4.00004-2

Bhatt, B., & Sharma, G. (2020). Metalaxyl resistance in *Phytophthora infestans*: An overview. *International Journal of Chemical Studies*, *8*(4), 3047–3054. https://doi.org/10.22271/chemi.2020.v8.i4ak.10114

Blackman, L. M., & Hardham, A. R. (2008). Regulation of catalase activity and gene expression during Phytophthora nicotianae development and infection of tobacco. *Molecular Plant Pathology*, *9*(4), 495–510. https://doi.org/10.1111/j.1364-3703.2008.00478.x

Blom, N., Gammeltoft, S., & Brunak, S. (1999). Sequence and structure-based prediction of eukaryotic protein phosphorylation sites. *Journal of Molecular Biology*, *294*(5), 1351–1362. https://doi.org/10.1006/jmbi.1999.3310

Bojarová-Fialová, P., & Křen, V. (2007). Enzymatic Approaches to O-Glycoside Introduction: Glycosidases. Em *Comprehensive Glycoscience* (pp. 453–487). Elsevier. https://doi.org/10.1016/B978-044451967-2/00013-1
Bos, J. I. B., Kanneganti, T., Young, C., Cakir, C., Huitema, E., Win, J., Armstrong, M. R., Birch, P. R. J., & Kamoun, S. (2006). The C-terminal half of *Phytophthora infestans* RXLR effector AVR3a is sufficient to trigger R3a-mediated hypersensitivity and suppress INF1-induced cell death in *Nicotiana benthamiana*. *The Plant Journal*, *48*(2), 165–176. https://doi.org/10.1111/j.1365-313X.2006.02866.x
Bosso, L., Scelza, R., Varlese, R., Meca, G., Testa, A., Rao, M. A., & Cristinzio, G. (2016). Assessing the effectiveness of *Byssochlamys nivea* and *Scopulariopsis brumptii* in pentachlorophenol removal and biological control of two *Phytophthora* species. *Fungal Biology*, *120*(4), 645–653. https://doi.org/10.1016/j.funbio.2016.01.004
Bourne, Y., & Henrissat, B. (2001). Glycoside hydrolases and glycosyltransferases: Families and functional modules. *Current Opinion in Structural Biology*, *11*(5), 593–600. https://doi.org/10.1016/S0959-440X(00)00253-0
Brocard, C., & Hartig, A. (2006). Peroxisome targeting signal 1: Is it really a simple tripeptide? *Biochimica et Biophysica Acta (BBA) - Molecular Cell Research*, *1763*(12), 1565–1573. https://doi.org/10.1016/j.bbamcr.2006.08.022
Bryant, D., Cummins, I., Dixon, D. P., & Edwards, R. (2006). Cloning and characterization of a theta class glutathione transferase from the potato pathogen *Phytophthora infestans*. *Phytochemistry*, *67*(14), 1427–1434. https://doi.org/10.1016/j.phytochem.2006.05.012
Burgess, R. R. (2009). Chapter 20 Protein Precipitation Techniques. Em *Methods in Enzymology* (Vol. 463, pp. 331–342). Elsevier. https://doi.org/10.1016/S0076-6879(09)63020-2
Burgess, T. I., Scott, J. K., Mcdougall, K. L., Stukely, M. J. C., Crane, C., Dunstan, W. A., Brigg, F., Andjic, V., White, D., Rudman, T., Arentz, F., Ota, N., & Hardy, G. E. St. J. (2017). Current and projected global distribution of Phytophthora cinnamomi, one of the world's worst plant pathogens. *Global Change Biology*, *23*(4), 1661–1674. https://doi.org/10.1111/gcb.13492
Bustin, S. A. (2010). Why the need for qPCR publication guidelines?—The case for MIQE. *Methods*, *50*(4), 217–226. https://doi.org/10.1016/j.ymeth.2009.12.006
Cabral, A., Oome, S., Sander, N., Küfner, I., Nürnberger, T., & Van Den Ackerveken, G. (2012). Nontoxic Nep1-Like Proteins of the Downy Mildew Pathogen *Hyaloperonospora arabidopsidis*: Repression of Necrosis-Inducing Activity by a Surface-Exposed Region. *Molecular Plant-Microbe Interactions®*, *25*(5), 697–708. https://doi.org/10.1094/MPMI-10-11-0269
Cahill, D. M. (1994). Exploitation of Zoospore Taxis in the Development of a Novel Dipstick Immunoassay for the Specific Detection of *Phytophthora cinnamomi*. *Phytopathology*, *84*(2), 193. https://doi.org/10.1094/Phyto-84-193
Catanzariti, A.-M., Dodds, P. N., & Ellis, J. G. (2007). Avirulence proteins from haustoria-forming pathogens. *FEMS Microbiology Letters*, *269*(2), 181–188. https://doi.org/10.1111/j.1574-6968.2007.00684.x
Chandani Kamble, Rohankumar Chavan, & Vikas Kamble. (2021). A Review on Amino Acids. *Research & Reviews: A Journal of Drug Design & Discovery*, *8*(3), 19–27.
Chang, S., Puryear, J., & Cairney, J. (1993). A simple and efficient method for isolating RNA from pine trees. *Plant Molecular Biology Reporter*, *11*(2), 113–116. https://doi.org/10.1007/BF02670468
Chou, K.-C., & Shen, H.-B. (2007). Euk-mPLoc: A Fusion Classifier for Large-Scale Eukaryotic Protein Subcellular Location Prediction by Incorporating Multiple Sites. *Journal of Proteome Research*, *6*(5), 1728–1734. https://doi.org/10.1021/pr060635i
Chou, K.-C., & Shen, H.-B. (2008). Cell-PLoc: A package of Web servers for predicting subcellular localization of proteins in various organisms. *Nature Protocols*, *3*(2), 153–162. https://doi.org/10.1038/nprot.2007.494

Chou, K.-C., & Shen, H.-B. (2010). A New Method for Predicting the Subcellular Localization of Eukaryotic Proteins with Both Single and Multiple Sites: Euk-mPLoc 2.0. *PLoS ONE*, *5*(4), e9931. https://doi.org/10.1371/journal.pone.0009931
Colas, V., Conrod, S., Venard, P., Keller, H., Ricci, P., & Panabières, F. (2001). Elicitin Genes Expressed In Vitro by Certain Tobacco Isolates of *Phytophthora parasitica* Are Down Regulated During Compatible Interactions. *Molecular Plant-Microbe Interactions®*, *14*(3), 326–335. https://doi.org/10.1094/MPMI.2001.14.3.326
Colavolpe, M. B., Vaz Dias, F., Serrazina, S., Malhó, R., & Lourenço Costa, R. (2023). Castanea crenata Ginkbilobin-2-like Recombinant Protein Reveals Potential as an Antimicrobial against *Phytophthora cinnamomi*, the Causal Agent of Ink Disease in European Chestnut. *Forests*, *14*(4), 785. https://doi.org/10.3390/f14040785
Crone, M., McComb, J. A., O'Brien, P. A., & Hardy, G. E. S. J. (2013). Survival of *Phytophthora cinnamomi* as oospores, stromata, and thick-walled chlamydospores in roots of symptomatic and asymptomatic annual and herbaceous perennial plant species. *Fungal Biology*, *117*(2), 112–123. https://doi.org/10.1016/j.funbio.2012.12.004
de Sampaio e Paiva Camilo-Alves, C., Da Clara, M. I. E., & De Almeida Ribeiro, N. M. C. (2013). Decline of Mediterranean oak trees and its association with *Phytophthora cinnamomi*: A review. *European Journal of Forest Research*, *132*(3), 411–432. https://doi.org/10.1007/s10342-013-0688-z
Del Castillo-González, L., Soudani, S., De La Cruz-Gómez, N., Manzanera, J. A., & Berrocal-Lobo, M. (2024). An improved method to study *Phytophthora cinnamomi* Rands zoospores interactions with host. *BMC Plant Biology*, *24*(1), 508. https://doi.org/10.1186/s12870-024-05205-2
DellaPenna, D., & Bennett, A. B. (1988). *In Vitro* Synthesis and Processing of Tomato Fruit Polygalacturonase. *Plant Physiology*, *86*(4), 1057–1063. https://doi.org/10.1104/pp.86.4.1057
Dou, D., Kale, S. D., Wang, X., Jiang, R. H. Y., Bruce, N. A., Arredondo, F. D., Zhang, X., & Tyler, B. M. (2008). RXLR-mediated entry of *Phytophthora sojae* effector Avr1b into soybean cells does not require pathogen-encoded machinery. *The Plant Cell*, *20*(7), 1930–1947. https://doi.org/10.1105/tpc.107.056093
D'Ovidio, R., Mattei, B., Roberti, S., & Bellincampi, D. (2004). Polygalacturonases, polygalacturonase-inhibiting proteins and pectic oligomers in plant–pathogen interactions. *Biochimica et Biophysica Acta (BBA) - Proteins and Proteomics*, *1696*(2), 237–244. https://doi.org/10.1016/j.bbapap.2003.08.012
Downer, A. J., Menge, J. A., & Pond, E. (2001). Association of Cellulytic Enzyme Activities in Eucalyptus Mulches with Biological Control of *Phytophthora cinnamomi*. *Phytopathology®*, *91*(9), 847–855. https://doi.org/10.1094/PHYTO.2001.91.9.847
Du, J., Verzaux, E., Chaparro-Garcia, A., Bijsterbosch, G., Keizer, L. C. P., Zhou, J., Liebrand, T. W. H., Xie, C., Govers, F., Robatzek, S., Van Der Vossen, E. A. G., Jacobsen, E., Visser, R. G. F., Kamoun, S., & Vleeshouwers, V. G. A. A. (2015). Elicitin recognition confers enhanced resistance to Phytophthora infestans in potato. *Nature Plants*, *1*(4), 15034. https://doi.org/10.1038/nplants.2015.34
Dunker, A. K., Bondos, S. E., Huang, F., & Oldfield, C. J. (2015). Intrinsically disordered proteins and multicellular organisms. *Seminars in Cell & Developmental Biology*, *37*, 44–55. https://doi.org/10.1016/j.semcdb.2014.09.025
Engelbrecht, J., Duong, T. A., Prabhu, S. A., Seedat, M., & Van Den Berg, N. (2021). Genome of the destructive oomycete *Phytophthora cinnamomi* provides insights into its pathogenicity and adaptive potential. *BMC Genomics*, *22*(1), 302. https://doi.org/10.1186/s12864-021-07552-y
FAOSTAT. (2024). https://www.fao.org/faostat/en/#data/QCL/visualize
Fernandes, P., Colavolpe, M. B., Serrazina, S., & Costa, R. L. (2022). European and American chestnuts: An overview of the main threats and control efforts. *Frontiers in Plant Science*, *13*, 951844. https://doi.org/10.3389/fpls.2022.951844

Fernandes, P., Pimentel, D., Ramiro, R. S., Silva, M. do C., Fevereiro, P., & Costa, R. L. (2024). Dual transcriptomic analysis reveals early induced *Castanea* defense-related genes and *Phytophthora cinnamomi* effectors. *Frontiers in Plant Science*, *15*. https://doi.org/10.3389/fpls.2024.1439380
Frova, C. (2006). Glutathione transferases in the genomics era: New insights and perspectives. *Biomolecular Engineering*, *23*(4), 149–169. https://doi.org/10.1016/j.bioeng.2006.05.020
Fu, L., Zhu, C., Ding, X., Yang, X., Morris, P. F., Tyler, B. M., & Zhang, X. (2015). Characterization of Cell-Death-Inducing Members of the Pectate Lyase Gene Family in *Phytophthora capsici* and Their Contributions to Infection of Pepper. *Molecular Plant-Microbe Interactions®*, *28*(7), 766–775. https://doi.org/10.1094/MPMI-11-14-0352-R
Gambino, G., Perrone, I., & Gribaudo, I. (2008). A Rapid and effective method for RNA extraction from different tissues of grapevine and other woody plants. *Phytochemical Analysis*, *19*(6), 520–525. https://doi.org/10.1002/pca.1078
Gasteiger, E. (2003). ExPASy: The proteomics server for in-depth protein knowledge and analysis. *Nucleic Acids Research*, *31*(13), 3784–3788. https://doi.org/10.1093/nar/gkg563
Gelvin, S. B. (2003). *Agrobacterium* -Mediated Plant Transformation: The Biology behind the "Gene-Jockeying" Tool. *Microbiology and Molecular Biology Reviews*, *67*(1), 16–37. https://doi.org/10.1128/MMBR.67.1.16-37.2003
Gijzen, M., & Nürnberger, T. (2006). Nep1-like proteins from plant pathogens: Recruitment and diversification of the NPP1 domain across taxa. *Phytochemistry*, *67*(16), 1800–1807. https://doi.org/10.1016/j.phytochem.2005.12.008
Gonçalo Candeias. (2024). Functional Analysis of Chestnut *Ginkbilobin2-like* Gene, a candidate to *Phytophthora cinnamomi* resistance. [Universidade de Coimbra]. https://estudogeral.uc.pt/retrieve/277573/Disserta%C3%A7%C3%A3o%20Corrigida%20-%20Gon%C3%A7alo%20Calmeiro%20Candeias%20-%20MBBV.pdf
Götesson, A., Marshall, J. S., Jones, D. A., & Hardham, A. R. (2002). Characterization and Evolutionary Analysis of a Large Polygalacturonase Gene Family in the Oomycete Plant Pathogen *Phytophthora cinnamomi*. *Molecular Plant-Microbe Interactions®*, *15*(9), 907–921. https://doi.org/10.1094/MPMI.2002.15.9.907
Goto, M. (2007). Protein *O* -Glycosylation in Fungi: Diverse Structures and Multiple Functions. *Bioscience, Biotechnology, and Biochemistry*, *71*(6), 1415–1427. https://doi.org/10.1271/bbb.70080
Grams, N., Komar, H., Jainchill, D., & Ospina-Giraldo, M. (2019). Comparative expression analysis of *Phytophthora sojae* polysaccharide lyase family 3 (pectate lyase) genes during infection of the soybean Glycine max. *Phytopathology Research*, *1*(1), 15. https://doi.org/10.1186/s42483-019-0020-z
Gupta, R., & Brunak, S. (2002). Prediction of glycosylation across the human proteome and the correlation to protein function. *Pacific Symposium on Biocomputing. Pacific Symposium on Biocomputing*, 310–322.
Gupta, R., Jung, E., Gooley, A. A., Williams, K. L., Brunak, S., & Hansen, J. (1999). Scanning the available *Dictyostelium discoideum* proteome for O-linked GlcNAc glycosylation sites using neural networks. *Glycobiology*, *9*(10), 1009–1022. https://doi.org/10.1093/glycob/9.10.1009
Gyeltshen, J., Dunstan, W. A., Grigg, A. H., Burgess, T. I., & St. J. Hardy, G. E. (2021). The influence of time, soil moisture and exogenous factors on the survival potential of oospores and chlamydospores of *Phytophthora cinnamomi*. *Forest Pathology*, *51*(1), e12637. https://doi.org/10.1111/efp.12637
Han, G. (2019). Origin and evolution of the plant immune system. *New Phytologist*, *222*(1), 70–83. https://doi.org/10.1111/nph.15596
Hardham, A. R., & Blackman, L. M. (2018). *Phytophthora cinnamomi*. *Molecular Plant Pathology*, *19*(2), 260–285. https://doi.org/10.1111/mpp.12568

Hart, R. P., Freebury, G., & Barrett, S. (2024). *Phytophthora cinnamomi*: Extent and impact in Two Peoples Bay Nature Reserve, Western Australia (1983–2024). *Pacific Conservation Biology*, *30*(4). https://doi.org/10.1071/PC24028
Hayes, J. D., Flanagan, J. U., & Jowsey, I. R. (2005). GLUTATHIONE TRANSFERASES. *Annual Review of Pharmacology and Toxicology*, *45*(1), 51–88. https://doi.org/10.1146/annurev.pharmtox.45.120403.095857
Hellemans, J., Mortier, G., De Paepe, A., Speleman, F., & Vandesompele, J. (2007). qBase relative quantification framework and software for management and automated analysis of real-time quantitative PCR data. *Genome Biology*, *8*(2), R19. https://doi.org/10.1186/gb-2007-8-2-r19
Horta, M., Caetano, P., Medeira, C., Maia, I., & Cravador, A. (2010). Involvement of the β-cinnamomin elicitin in infection and colonisation of cork oak roots by *Phytophthora cinnamomi*. *European Journal of Plant Pathology*, *127*(3), 427–436. https://doi.org/10.1007/s10658-010-9609-x
Horta, M., Sousa, N., Coelho, A. C., Neves, D., & Cravador, A. (2008). *In vitro* and *in vivo* quantification of elicitin expression in *Phytophthora cinnamomi*. *Physiological and Molecular Plant Pathology*, *73*(1), 48–57. https://doi.org/10.1016/j.pmpp.2009.02.003
Hugouvieux-Cotte-Pattat, N. (2016). Metabolism and Virulence Strategies in Dickeya–Host Interactions. Em *Progress in Molecular Biology and Translational Science* (Vol. 142, pp. 93–129). Elsevier. https://doi.org/10.1016/bs.pmbts.2016.05.006
Ighodaro, O. M., & Akinloye, O. A. (2018). First line defence antioxidants-superoxide dismutase (SOD), catalase (CAT) and glutathione peroxidase (GPX): Their fundamental role in the entire antioxidant defence grid. *Alexandria Journal of Medicine*, *54*(4), 287–293. https://doi.org/10.1016/j.ajme.2017.09.001
Jeffers, S. N. (1986). Comparison of Two Media Selective for *Phytophthora* and *Pythium* Species. *Plant Disease*, *70*(11), 1038. https://doi.org/10.1094/PD-70-1038
Jia, Y. J., Feng, B. Z., Sun, W. X., & Zhang, X. G. (2009). Polygalacturonase, Pectate Lyase and Pectin Methylesterase Activity in Pathogenic Strains of *Phytophthora capsici* Incubated under Different Conditions. *Journal of Phytopathology*, *157*(10), 585–591. https://doi.org/10.1111/j.1439-0434.2008.01533.x
Jiang, R. H. Y., Tyler, B. M., Whisson, S. C., Hardham, A. R., & Govers, F. (2006). Ancient Origin of Elicitin Gene Clusters in *Phytophthora* Genomes. *Molecular Biology and Evolution*, *23*(2), 338–351. https://doi.org/10.1093/molbev/msj039
Jing, M., Guo, B., Li, H., Yang, B., Wang, H., Kong, G., Zhao, Y., Xu, H., Wang, Y., Ye, W., Dong, S., Qiao, Y., Tyler, B. M., Ma, W., & Wang, Y. (2016). A *Phytophthora sojae* effector suppresses endoplasmic reticulum stress-mediated immunity by stabilizing plant Binding immunoglobulin Proteins. *Nature Communications*, *7*(1), 11685. https://doi.org/10.1038/ncomms11685
Jones, P., Binns, D., Chang, H.-Y., Fraser, M., Li, W., McAnulla, C., McWilliam, H., Maslen, J., Mitchell, A., Nuka, G., Pesseat, S., Quinn, A. F., Sangrador-Vegas, A., Scheremetjew, M., Yong, S.-Y., Lopez, R., & Hunter, S. (2014). InterProScan 5: Genome-scale protein function classification. *Bioinformatics*, *30*(9), 1236–1240. https://doi.org/10.1093/bioinformatics/btu031
Joubert, M., Backer, R., Engelbrecht, J., & Van Den Berg, N. (2021). Expression of several *Phytophthora cinnamomi* putative RxLRs provides evidence for virulence roles in avocado. *PLOS ONE*, *16*(7), e0254645. https://doi.org/10.1371/journal.pone.0254645
Judelson, H. S., & Ah-Fong, A. M. V. (2019). Exchanges at the Plant-Oomycete Interface That Influence Disease. *Plant Physiology*, *179*(4), 1198–1211. https://doi.org/10.1104/pp.18.00979
Jung, T., Colquhoun, I. J., & Hardy, G. E. St. J. (2013). New insights into the survival strategy of the invasive soilborne pathogen *P hytophthora cinnamomi* in different natural ecosystems in W estern A ustralia. *Forest Pathology*, *43*(4), 266–288. https://doi.org/10.1111/efp.12025

Kasteel, M., Ketelaar, T., & Govers, F. (2023). Fatal attraction: How *Phytophthora* zoospores find their host. *Seminars in Cell & Developmental Biology*, *148–149*, 13–21. https://doi.org/10.1016/j.semcdb.2023.01.014
Kongtragoul, P., Ishikawa, K., & Ishii, H. (2021). Metalaxyl Resistance of *Phytophthora palmivora* Causing Durian Diseases in Thailand. *Horticulturae*, *7*(10), Artigo 10. https://doi.org/10.3390/horticulturae7100375
Koornneef, A., & Pieterse, C. M. J. (2008). Cross Talk in Defense Signaling. *Plant Physiology*, *146*(3), 839–844. https://doi.org/10.1104/pp.107.112029
Krishna, H., Alizadeh, M., Singh, D., Singh, U., Chauhan, N., Eftekhari, M., & Sadh, R. K. (2016). Somaclonal variations and their applications in horticultural crops improvement. *3 Biotech*, *6*(1), 54. https://doi.org/10.1007/s13205-016-0389-7
Kunze, M. (2020). The type-2 peroxisomal targeting signal. *Biochimica et Biophysica Acta (BBA) - Molecular Cell Research*, *1867*(2), 118609. https://doi.org/10.1016/j.bbamcr.2019.118609
Lamb, C., & Dixon, R. A. (1997). THE OXIDATIVE BURST IN PLANT DISEASE RESISTANCE. *Annual Review of Plant Biology*, *48*(Volume 48, 1997), 251–275. https://doi.org/10.1146/annurev.arplant.48.1.251
Le Provost, G., Herrera, R., Paiva, J. A., Chaumeil, P., Salin, F., & Plomion, C. (2007). A micromethod for high throughput RNA extraction in forest trees. *Biological Research*, *40*(3). https://doi.org/10.4067/S0716-97602007000400003
Liao, C.-J., Hailemariam, S., Sharon, A., & Mengiste, T. (2022). Pathogenic strategies and immune mechanisms to necrotrophs: Differences and similarities to biotrophs and hemibiotrophs. *Current Opinion in Plant Biology*, *69*, 102291. https://doi.org/10.1016/j.pbi.2022.102291
Lin, B., Qing, X., Liao, J., & Zhuo, K. (2020). Role of Protein Glycosylation in Host-Pathogen Interaction. *Cells*, *9*(4), 1022. https://doi.org/10.3390/cells9041022
Liu, J., Perumal, N. B., Oldfield, C. J., Su, E. W., Uversky, V. N., & Dunker, A. K. (2006). Intrinsic Disorder in Transcription Factors. *Biochemistry*, *45*(22), 6873–6888. https://doi.org/10.1021/bi0602718
Lo Presti, L., Lanver, D., Schweizer, G., Tanaka, S., Liang, L., Tollot, M., Zuccaro, A., Reissmann, S., & Kahmann, R. (2015). Fungal Effectors and Plant Susceptibility. *Annual Review of Plant Biology*, *66*(1), 513–545. https://doi.org/10.1146/annurev-arplant-043014-114623
Lv, P., Wan, J., Zhang, C., Hina, A., Al Amin, G. M., Begum, N., & Zhao, T. (2023). Unraveling the Diverse Roles of Neglected Genes Containing Domains of Unknown Function (DUFs): Progress and Perspective. *International Journal of Molecular Sciences*, *24*(4), 4187. https://doi.org/10.3390/ijms24044187
Marchler-Bauer, A., & Bryant, S. H. (2004). CD-Search: Protein domain annotations on the fly. *Nucleic Acids Research*, *32*(Web Server issue), W327-331. https://doi.org/10.1093/nar/gkh454
Marchler-Bauer, A., Lu, S., Anderson, J. B., Chitsaz, F., Derbyshire, M. K., DeWeese-Scott, C., Fong, J. H., Geer, L. Y., Geer, R. C., Gonzales, N. R., Gwadz, M., Hurwitz, D. I., Jackson, J. D., Ke, Z., Lanczycki, C. J., Lu, F., Marchler, G. H., Mullokandov, M., Omelchenko, M. V., … Bryant, S. H. (2011). CDD: A Conserved Domain Database for the functional annotation of proteins. *Nucleic Acids Research*, *39*(Database issue), D225-229. https://doi.org/10.1093/nar/gkq1189
Marrs, K. A. (1996). THE FUNCTIONS AND REGULATION OF GLUTATHIONE S-TRANSFERASES IN PLANTS. *Annual Review of Plant Biology*, *47*(Volume 47, 1996), 127–158. https://doi.org/10.1146/annurev.arplant.47.1.127
Martins, I. M., Meirinho, S., Costa, R., Cravador, A., & Choupina, A. (2019). Cloning, characterization, in vitro and in planta expression of a necrosis-inducing *Phytophthora* protein 1 gene npp1 from *Phytophthora cinnamomi. Molecular Biology Reports*, *46*(6), 6453–6462. https://doi.org/10.1007/s11033-019-05091-0

Mayans, O., Scott, M., Connerton, I., Gravesen, T., Benen, J., Visser, J., Pickersgill, R., & Jenkins, J. (1997). Two crystal structures of pectin lyase A from *Aspergillus* reveal a pH driven conformational change and striking divergence in the substrate-binding clefts of pectin and pectate lyases. *Structure*, *5*(5), 677–689. https://doi.org/10.1016/S0969-2126(97)00222-0
McConnell, M. E., & Balci, Y. (2015). Fine root dynamics of oak saplings in response to *Phytophthora cinnamomi* infection under different temperatures and durations. *Forest Pathology*, *45*(2), 155–164. https://doi.org/10.1111/efp.12150
McGuigan, L., Fernandes, P., Oakes, A., Stewart, K., & Powell, W. (2020). Transformation of American Chestnut (*Castanea dentata* (Marsh.) Borkh) Using RITA® Temporary Immersion Bioreactors and We Vitro Containers. *Forests*, *11*(11), 1196. https://doi.org/10.3390/f11111196
Mellano, M. G., Beccaro, G. L., Donno, D., Marinoni, D. T., Boccacci, P., Canterino, S., Cerutti, A. K., & Bounous, G. (2012). *Castanea* spp. biodiversity conservation: Collection and characterization of the genetic diversity of an endangered species. *Genetic Resources and Crop Evolution*, *59*(8), 1727–1741. https://doi.org/10.1007/s10722-012-9794-x
Midgley, K. A., Van Den Berg, N., Backer, R., & Swart, V. (2024). Identification of *Phytophthora cinnamomi* CRN effectors and their roles in manipulating cell death during *Persea americana* infection. *BMC Genomics*, *25*(1), 435. https://doi.org/10.1186/s12864-024-10358-3
Midgley, K. A., Van Den Berg, N., & Swart, V. (2022). Unraveling Plant Cell Death during *Phytophthora* Infection. *Microorganisms*, *10*(6), 1139. https://doi.org/10.3390/microorganisms10061139
Miyakawa, T., Hatano, K., Miyauchi, Y., Suwa, Y., Sawano, Y., & Tanokura, M. (2014). A Secreted Protein with Plant-Specific Cysteine-Rich Motif Functions as a Mannose-Binding Lectin That Exhibits Antifungal Activity. *Plant Physiology*, *166*(2), 766–778. https://doi.org/10.1104/pp.114.242636
Miyakawa, T., Sawano, Y., Miyazono, K., Hatano, K., & Tanokura, M. (2007). Crystallization and preliminary X-ray analysis of ginkbilobin-2 from *Ginkgo biloba* seeds: A novel antifungal protein with homology to the extracellular domain of plant cysteine-rich receptor-like kinases. *Acta Crystallographica Section F Structural Biology and Crystallization Communications*, *63*(9), 737–739. https://doi.org/10.1107/S1744309107034793
Morel, M., Ngadin, A. A., Droux, M., Jacquot, J.-P., & Gelhaye, E. (2009). The fungal glutathione S-transferase system. Evidence of new classes in the wood-degrading basidiomycete *Phanerochaete chrysosporium*. *Cellular and Molecular Life Sciences*, *66*(23), 3711–3725. https://doi.org/10.1007/s00018-009-0104-5
Nakamura, M., & Iwai, H. (2019). Functions and mechanisms: Polygalacturonases from plant pathogenic fungi as pathogenicity and virulence factors. *Journal of General Plant Pathology*, *85*(4), 243–250. https://doi.org/10.1007/s10327-019-00856-8
National Cancer Institute. (2011, fevereiro 2). *Definition of molecular weight—NCI Dictionary of Cancer Terms—NCI* (nciglobal,ncienterprise) [nciAppModulePage]. https://www.cancer.gov/publications/dictionaries/cancer-terms/def/molecular-weight
Nespoulous, C., Huet, J.-C., & Pernollet, J.-C. (1992). Structure-function relationships of α and β elicitins, signal proteins involved in the plant-*Phytophthora* interaction. *Planta*, *186*(4). https://doi.org/10.1007/BF00198035
Ngou, B. P. M., Ahn, H.-K., Ding, P., & Jones, J. D. G. (2021). Mutual potentiation of plant immunity by cell-surface and intracellular receptors. *Nature*, *592*(7852), 110–115. https://doi.org/10.1038/s41586-021-03315-7
Ngou, B. P. M., Jones, J. D. G., & Ding, P. (2022). Plant immune networks. *Trends in Plant Science*, *27*(3), 255–273. https://doi.org/10.1016/j.tplants.2021.08.012

Ødum, M. T., Teufel, F., Thumuluri, V., Almagro Armenteros, J. J., Johansen, A. R., Winther, O., & Nielsen, H. (2024). DeepLoc 2.1: Multi-label membrane protein type prediction using protein language models. *Nucleic Acids Research*, *52*(W1), W215–W220. https://doi.org/10.1093/nar/gkae237
Oome, S., & Van Den Ackerveken, G. (2014). Comparative and Functional Analysis of the Widely Occurring Family of Nep1-Like Proteins. *Molecular Plant-Microbe Interactions®*, *27*(10), 1081–1094. https://doi.org/10.1094/MPMI-04-14-0118-R
Oßwald, W., Fleischmann, F., Rigling, D., Coelho, A. C., Cravador, A., Diez, J., Dalio, R. J., Horta Jung, M., Pfanz, H., Robin, C., Sipos, G., Solla, A., Cech, T., Chambery, A., Diamandis, S., Hansen, E., Jung, T., Orlikowski, L. B., Parke, J., … Werres, S. (2014). Strategies of attack and defence in woody plant– *Phytophthora* interactions. *Forest Pathology*, *44*(3), 169–190. https://doi.org/10.1111/efp.12096
Ottmann, C., Luberacki, B., Küfner, I., Koch, W., Brunner, F., Weyand, M., Mattinen, L., Pirhonen, M., Anderluh, G., Seitz, H. U., Nürnberger, T., & Oecking, C. (2009). A common toxin fold mediates microbial attack and plant defense. *Proceedings of the National Academy of Sciences*, *106*(25), 10359–10364. https://doi.org/10.1073/pnas.0902362106
Pagès, S., Heijne, W. H. M., Kester, H. C. M., Visser, J., & Benen, J. A. E. (2000). Subsite Mapping of *Aspergillus niger* Endopolygalacturonase II by Site-directed Mutagenesis. *Journal of Biological Chemistry*, *275*(38), 29348–29353. https://doi.org/10.1074/jbc.M910112199
Payne, C. M., Resch, M. G., Chen, L., Crowley, M. F., Himmel, M. E., Taylor, L. E., Sandgren, M., Ståhlberg, J., Stals, I., Tan, Z., & Beckham, G. T. (2013). Glycosylated linkers in multimodular lignocellulose-degrading enzymes dynamically bind to cellulose. *Proceedings of the National Academy of Sciences*, *110*(36), 14646–14651. https://doi.org/10.1073/pnas.1309106110
Pimentel, A. A. L. (1947). *A Phytophthora cinnamomi rando: Um outro agente, extremamente virulento, da" doença da tinta" do Castanheiro.*
Plešková, V., Kašparovský, T., Obořil, M., Ptáčková, N., Chaloupková, R., Ladislav, D., Damborský, J., & Lochman, J. (2011). Elicitin–membrane interaction is driven by a positive charge on the protein surface: Role of Lys13 residue in lipids loading and resistance induction. *Plant Physiology and Biochemistry*, *49*(3), 321–328. https://doi.org/10.1016/j.plaphy.2011.01.008
Rayon, C., Lerouge, P., & Faye, L. (1998). The protein N-glycosylation in plants. *Journal of Experimental Botany*, *49*(326), 1463–1472. https://doi.org/10.1093/jxb/49.326.1463
Raza, H. (2011). Dual localization of glutathione *S* -transferase in the cytosol and mitochondria: Implications in oxidative stress, toxicity and disease. *The FEBS Journal*, *278*(22), 4243–4251. https://doi.org/10.1111/j.1742-4658.2011.08358.x
Redondo, M. Á., Pérez-Sierra, A., Abad-Campos, P., Torres, L., Solla, A., Reig-Armiñana, J., & García-Breijo, F. (2015). Histology of *Quercus ilex* roots during infection by *Phytophthora cinnamomi*. *Trees*, *29*(6), 1943–1957. https://doi.org/10.1007/s00468-015-1275-3
Reeksting, B. J., Coetzer, N., Mahomed, W., Engelbrecht, J., & Van Den Berg, N. (2014). De Novo Sequencing, Assembly, and Analysis of the Root Transcriptome of *Persea americana* (Mill.) in Response to *Phytophthora cinnamomi* and Flooding. *PLoS ONE*, *9*(2), e86399. https://doi.org/10.1371/journal.pone.0086399
Richter, B. S., Ivors, K., Shi, W., & Benson, D. M. (2011). Cellulase Activity as a Mechanism for Suppression of *Phytophthora* Root Rot in Mulches. *Phytopathology®*, *101*(2), 223–230. https://doi.org/10.1094/PHYTO-04-10-0125
Robin, C., Morel, O., Vettraino, A.-M., Perlerou, C., Diamandis, S., & Vannini, A. (2006). Genetic variation in susceptibility to *Phytophthora Cambivora* in European chestnut (*Castanea sativa*). *Forest Ecology and Management*, *226*(1), 199–207. https://doi.org/10.1016/j.foreco.2006.01.035

Rocafort, M., Fudal, I., & Mesarich, C. H. (2020). Apoplastic effector proteins of plant-associated fungi and oomycetes. *Current Opinion in Plant Biology*, *56*, 9–19. https://doi.org/10.1016/j.pbi.2020.02.004
Ruiz Gómez, F. J., Navarro-Cerrillo, R. M., Sánchez-Cuesta, R., & Pérez-de-Luque, A. (2015). Histopathology of infection and colonization of *Quercus ilex* fine roots by *Phytophthora cinnamomi*. *Plant Pathology*, *64*(3), 605–616. https://doi.org/10.1111/ppa.12310
Sabnam, N., Hussain, A., & Saha, P. (2023). The secret password: Cell death-inducing proteins in filamentous phytopathogens - As versatile tools to develop disease-resistant crops. *Microbial Pathogenesis*, *183*, 106276. https://doi.org/10.1016/j.micpath.2023.106276
Sánchez-Torres, P., Visser, J., & Benen, J. A. E. (2003). Identification of amino acid residues critical for catalysis and stability in *Aspergillus niger* family 1 pectin lyase A. *Biochemical Journal*, *370*(1), 331–337. https://doi.org/10.1042/bj20021071
Santos, C., Duarte, S., Tedesco, S., Fevereiro, P., & Costa, R. L. (2017). Expression Profiling of *Castanea* Genes during Resistant and Susceptible Interactions with the Oomycete Pathogen *Phytophthora cinnamomi* Reveal Possible Mechanisms of Immunity. *Frontiers in Plant Science*, *8*. https://doi.org/10.3389/fpls.2017.00515
Sarmast, M. K. (2016). Genetic transformation and somaclonal variation in conifers. *Plant Biotechnology Reports*, *10*(6), 309–325. https://doi.org/10.1007/s11816-016-0416-5
Sato, M., Hosokawa, M., & Doi, M. (2011). Somaclonal Variation Is Induced De Novo via the Tissue Culture Process: A Study Quantifying Mutated Cells in Saintpaulia. *PLoS ONE*, *6*(8), e23541. https://doi.org/10.1371/journal.pone.0023541
Sehnal, D., Bittrich, S., Deshpande, M., Svobodová, R., Berka, K., Bazgier, V., Velankar, S., Burley, S. K., Koča, J., & Rose, A. S. (2021). Mol* Viewer: Modern web app for 3D visualization and analysis of large biomolecular structures. *Nucleic Acids Research*, *49*(W1), W431–W437. https://doi.org/10.1093/nar/gkab314
Seok, S.-H. (2021). Structural Insights into Protein Regulation by Phosphorylation and Substrate Recognition of Protein Kinases/Phosphatases. *Life*, *11*(9), 957. https://doi.org/10.3390/life11090957
Sepasi Tehrani, H., & Moosavi-Movahedi, A. A. (2018). Catalase and its mysteries. *Progress in Biophysics and Molecular Biology*, *140*, 5–12. https://doi.org/10.1016/j.pbiomolbio.2018.03.001
Serrazina, S., Martínez, M., Soudani, S., Candeias, G., Berrocal-Lobo, M., Piñeiro, P., Malhó, R., Costa, R. L., & Corredoira, E. (2024a). Overexpression of Ginkbilobin-2 homologous domain gene improves tolerance to *Phytophthora cinnamomi* in somatic embryos of *Quercus suber*. *Scientific Reports*, *14*(1), 19357. https://doi.org/10.1038/s41598-024-70272-2
Serrazina, S., Martínez, M. T., Cano, V., Malhó, R., Costa, R. L., & Corredoira, E. (2022). Genetic Transformation of *Quercus ilex* Somatic Embryos with a Gnk2-like Protein That Reveals a Putative Anti-Oomycete Action. *Plants*, *11*(3), 304. https://doi.org/10.3390/plants11030304
Serrazina, S., Martínez, M. T., Fernandes, P., Colavolpe, B., Dias, F., Conde, P., Malhó, R., Corredoira, E., & Lourenço Costa, R. (2024b). *Castanea crenata* Ginkbilobin2-like as a resistance gene to *Phytophthora cinnamomi* infection. *Acta Horticulturae*, *1400*, 77–88. https://doi.org/10.17660/ActaHortic.2024.1400.9
Serrazina, S., Martínez, M. T., Valladares, S., Castillo, L. D., Francisco, M., Berrocal-Lobo, M., Piñas, E., Piñeiro, P., Malhó, R., Costa, R., & Corredoira, E. (2025). *Overexpression of Ginkbilobin-2 homologous domain gene to enhance the tolerance to Phytophthora cinnamomi in plants of European chestnut*. In Review. https://doi.org/10.21203/rs.3.rs-7973831/v1
Serrazina, S., Santos, C., Machado, H., Pesquita, C., Vicentini, R., Pais, M. S., Sebastiana, M., & Costa, R. (2015). *Castanea* root transcriptome in response to *Phytophthora cinnamomi* challenge. *Tree Genetics & Genomes*, *11*(1), 6. https://doi.org/10.1007/s11295-014-0829-7

Shands, A. C., Xu, G., Belisle, R. J., Seifbarghi, S., Jackson, N., Bombarely, A., Cano, L. M., & Manosalva, P. M. (2024). Genomic and transcriptomic analyses of *Phytophthora cinnamomi* reveal complex genome architecture, expansion of pathogenicity factors, and host-dependent gene expression profiles. *Frontiers in Microbiology*, *15*, 1341803. https://doi.org/10.3389/fmicb.2024.1341803
Shen, H.-B., & Chou, K.-C. (2006). Ensemble classifier for protein fold pattern recognition. *Bioinformatics*, *22*(14), 1717–1722. https://doi.org/10.1093/bioinformatics/btl170
Sievers, F., & Higgins, D. G. (2021). The Clustal Omega Multiple Alignment Package. Em K. Katoh (Ed.), *Multiple Sequence Alignment* (Vol. 2231, pp. 3–16). Springer US. https://doi.org/10.1007/978-1-0716-1036-7_1
Smigielski, L., Aguilar, G. B., Kwaaitaal, M., Zhang, W., & Thordal-Christensen, H. (2019). The isoelectric point of proteins influences their translocation to the extrahaustorial matrix of the barley powdery mildew fungus. *Cellular Microbiology*, *21*(12). https://doi.org/10.1111/cmi.13091
Smulevich, G., Jakopitsch, C., Droghetti, E., & Obinger, C. (2006). Probing the structure and bifunctionality of catalase-peroxidase (KatG). *Journal of Inorganic Biochemistry*, *100*(4), 568–585. https://doi.org/10.1016/j.jinorgbio.2006.01.033
Strange, R. C., Spiteri, M. A., Ramachandran, S., & Fryer, A. A. (2001). Glutathione-S-transferase family of enzymes. *Mutation Research/Fundamental and Molecular Mechanisms of Mutagenesis*, *482*(1–2), 21–26. https://doi.org/10.1016/S0027-5107(01)00206-8
Strasser, R., Seifert, G., Doblin, M. S., Johnson, K. L., Ruprecht, C., Pfrengle, F., Bacic, A., & Estevez, J. M. (2021). Cracking the "Sugar Code": A Snapshot of N- and O-Glycosylation Pathways and Functions in Plants Cells. *Frontiers in Plant Science*, *12*, 640919. https://doi.org/10.3389/fpls.2021.640919
Tahir, J., Rashid, M., & Afzal, A. J. (2019). Post-translational modifications in effectors and plant proteins involved in host–pathogen conflicts. *Plant Pathology*, *68*(4), 628–644. https://doi.org/10.1111/ppa.12983
Tanabe, S., Ishii-Minami, N., Saitoh, K.-I., Otake, Y., Kaku, H., Shibuya, N., Nishizawa, Y., & Minami, E. (2011). The Role of Catalase-Peroxidase Secreted by *Magnaporthe oryzae* During Early Infection of Rice Cells. *Molecular Plant-Microbe Interactions®*, *24*(2), 163–171. https://doi.org/10.1094/MPMI-07-10-0175
Teufel, F., Almagro Armenteros, J. J., Johansen, A. R., Gíslason, M. H., Pihl, S. I., Tsirigos, K. D., Winther, O., Brunak, S., Von Heijne, G., & Nielsen, H. (2022). SignalP 6.0 predicts all five types of signal peptides using protein language models. *Nature Biotechnology*, *40*(7), 1023–1025. https://doi.org/10.1038/s41587-021-01156-3
Vaattovaara, A., Brandt, B., Rajaraman, S., Safronov, O., Veidenberg, A., Luklová, M., Kangasjärvi, J., Löytynoja, A., Hothorn, M., Salojärvi, J., & Wrzaczek, M. (2019). Mechanistic insights into the evolution of DUF26-containing proteins in land plants. *Communications Biology*, *2*(1). https://doi.org/10.1038/s42003-019-0306-9
Vaish, S., Gupta, D., Mehrotra, R., Mehrotra, S., & Basantani, M. K. (2020). Glutathione S-transferase: A versatile protein family. *3 Biotech*, *10*(7), 321. https://doi.org/10.1007/s13205-020-02312-3
Van Alebeek, G.-J. W. M., Christensen, T. M. I. E., Schols, H. A., Mikkelsen, J. D., & Voragen, A. G. J. (2002). Mode of Action of Pectin Lyase A of *Aspergillus niger* on Differently C6-substituted Oligogalacturonides. *Journal of Biological Chemistry*, *277*(29), 25929–25936. https://doi.org/10.1074/jbc.M202250200
Vitali, J., Schick, B., Kester, H. C. M., Visser, J., & Jurnak, F. (1998). The Three-Dimensional Structure of *Aspergillus niger* Pectin Lyase B at 1.7-Å Resolution1. *Plant Physiology*, *116*(1), 69–80. https://doi.org/10.1104/pp.116.1.69

Wang, H., Fu, L., & Zhang, X. (2011). Comparison of expression, purification and characterization of a new pectate lyase from *Phytophthora capsici* using two different methods. *BMC Biotechnology*, *11*(1), 32. https://doi.org/10.1186/1472-6750-11-32
Wang, S., McLellan, H., Boevink, P. C., & Birch, P. R. J. (2023). RxLR Effectors: Master Modulators, Modifiers and Manipulators. *Molecular Plant-Microbe Interactions®*, *36*(12), 754–763. https://doi.org/10.1094/MPMI-05-23-0054-CR
Wang, T., Lv, J., Xu, J., Wang, X., Zhu, X., & Guo, L. (2023). The catalase-peroxidase PiCP1 plays a critical role in abiotic stress resistance, pathogenicity and asexual structure development in *Phytophthora infestans*. *Environmental Microbiology*, *25*(2), 532–547. https://doi.org/10.1111/1462-2920.16305
Welinder, K. G. (1992). Superfamily of plant, fungal and bacterial peroxidases. *Current Opinion in Structural Biology*, *2*(3), 388–393. https://doi.org/10.1016/0959-440X(92)90230-5
West, C. M., & Kim, H. W. (2019). Nucleocytoplasmic O-glycosylation in protists. *Current Opinion in Structural Biology*, *56*, 204–212. https://doi.org/10.1016/j.sbi.2019.03.031
Yadav, S., Yadav, P. K., Yadav, D., & Yadav, K. D. S. (2009). Pectin lyase: A review. *Process Biochemistry*, *44*(1), 1–10. https://doi.org/10.1016/j.procbio.2008.09.012
Ye, J., Coulouris, G., Zaretskaya, I., Cutcutache, I., Rozen, S., & Madden, T. L. (2012). Primer-BLAST: A tool to design target-specific primers for polymerase chain reaction. *BMC Bioinformatics*, *13*(1), 134. https://doi.org/10.1186/1471-2105-13-134
Yin, X., Fu, Q., Shang, B., Wang, Y., Liu, R., Chen, T., Xiang, G., Dou, M., Liu, G., & Xu, Y. (2022). An RxLR effector from *Plasmopara viticola* suppresses plant immunity in grapevine by targeting and stabilizing VpBPA1. *The Plant Journal*, *112*(1), 104–114. https://doi.org/10.1111/tpj.15933
Yu, L. M. (1995). Elicitins from *Phytophthora* and basic resistance in tobacco. *Proceedings of the National Academy of Sciences*, *92*(10), 4088–4094. https://doi.org/10.1073/pnas.92.10.4088
Yu, X., Niu, H., Liu, C., Wang, H., Yin, W., & Xia, X. (2024). PTI-ETI synergistic signal mechanisms in plant immunity. *Plant Biotechnology Journal*, *22*(8), 2113–2128. https://doi.org/10.1111/pbi.14332
Zamocky, M., Furtmüller, P. G., Bellei, M., Battistuzzi, G., Stadlmann, J., Vlasits, J., & Obinger, C. (2009). Intracellular catalase/peroxidase from the phytopathogenic rice blast fungus *Magnaporthe grisea*: Expression analysis and biochemical characterization of the recombinant protein. *Biochemical Journal*, *418*(2), 443–451. https://doi.org/10.1042/BJ20081478
Zámocký, M., Gasselhuber, B., Furtmüller, P. G., & Obinger, C. (2012). Molecular evolution of hydrogen peroxide degrading enzymes. *Archives of Biochemistry and Biophysics*, *525*(2), 131–144. https://doi.org/10.1016/j.abb.2012.01.017
Zámocký, M., & Koller, F. (1999). Understanding the structure and function of catalases: Clues from molecular evolution and in vitro mutagenesis. *Progress in Biophysics and Molecular Biology*, *72*(1), 19–66. https://doi.org/10.1016/S0079-6107(98)00058-3
Zheng, L., Xu, Y., Li, Q., & Zhu, B. (2021). Pectinolytic lyases: A comprehensive review of sources, category, property, structure, and catalytic mechanism of pectate lyases and pectin lyases. *Bioresources and Bioprocessing*, *8*(1), 79. https://doi.org/10.1186/s40643-021-00432-z

5. Supplementary material

5.1. Supplementary Figures

Supplementary Figure S1: Representative image of the *C. sativa* somatic embryo clumps delivered from Misión Biológica de Galicia.

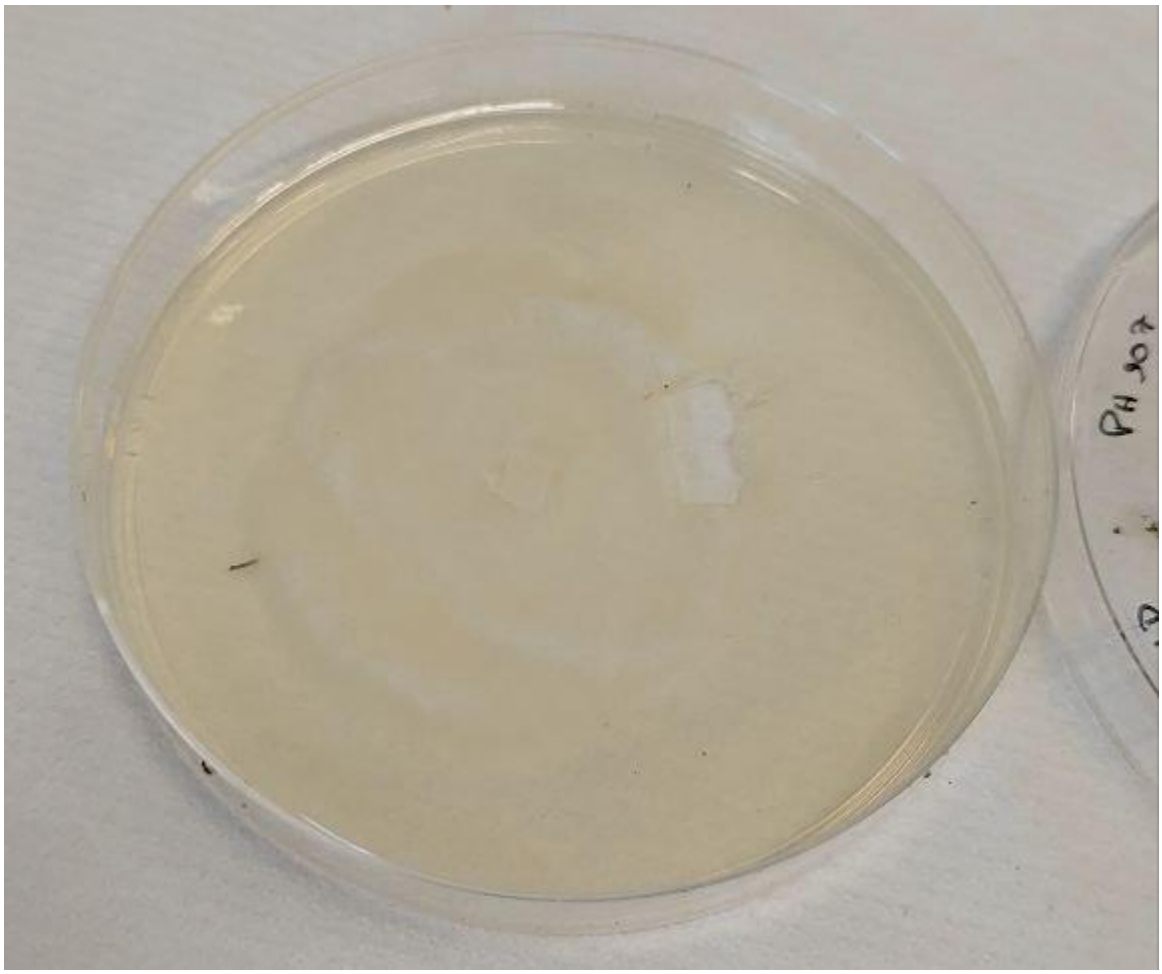

Supplementary Figure S2: Representative image of the *P. cinnamomi* mycelium used for the inoculation assays, grown in a petri dish.

Supplementary Figure S3: Representative close-up image of a *C. dentata* plantlet in a paper pot used in the inoculation assay, with an agar block pinned onto one of the roots.

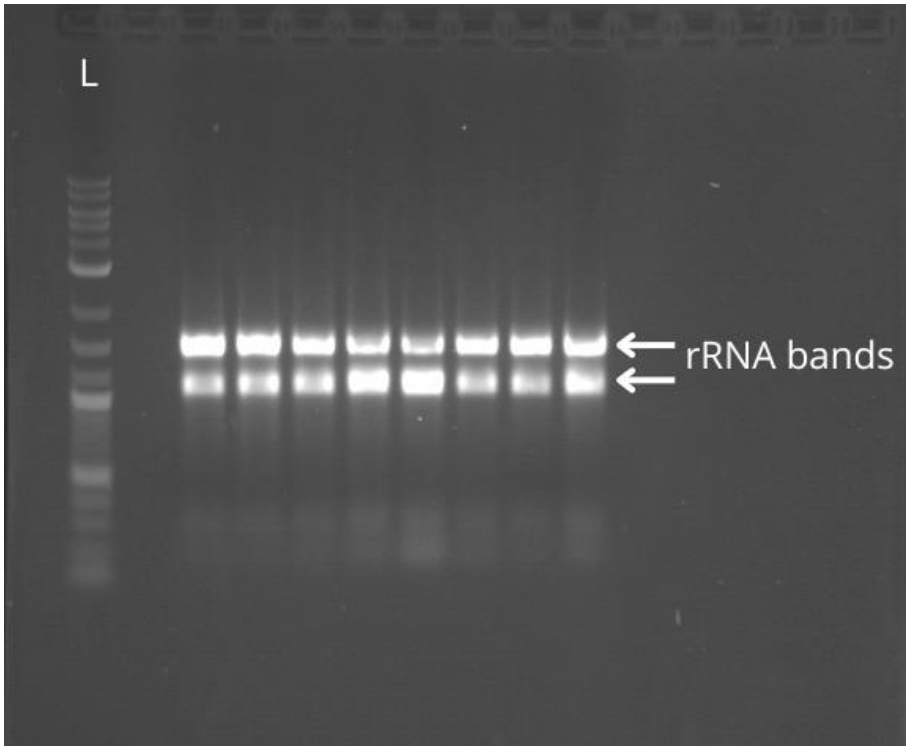

Supplementary Figure S4: Representative image of gel electrophoresis using the extracted *C. sativa* RNA. The visible RNA bands correspond to ribosomal RNA and can be used to infer overall RNA integrity. L- DNA molecular size marker.

A

Nonparametric Tests

Notes

Output Created		30-SEP-2025 00:36:36
Comments		
Input	Data	C:\Users\Utilizador\Desktop\tese mestrado\C sativa\qPCR\testes significância\c sativa with excluded values.sav
	Active Dataset	DataSet2
	Filter	<none>
	Weight	<none>
	Split File	<none>
	N of Rows in Working Data File	59
Syntax		NPTESTS /INDEPENDENT TEST (VAR00003) GROUP (VAR00002) KRUSKAL_WALLIS(COMPARE=PAIRWISE) /MISSING SCOPE=ANALYSIS USERMISSING=EXCLUDE /CRITERIA ALPHA=0.05 CILEVEL=95.
Resources	Processor Time	00:00:00,61
	Elapsed Time	00:00:00,69

Hypothesis Test Summary

	Null Hypothesis	Test	Sig.[a,b]
1	The distribution of VAR00003 is the same across categories of VAR00002.	Independent-Samples Kruskal-Wallis Test	,002

Hypothesis Test Summary

	Decision
1	Reject the null hypothesis.

a. The significance level is ,050.
b. Asymptotic significance is displayed.

Independent-Samples Kruskal-Wallis Test Summary

Total N	24
Test Statistic	12,620[a]
Degree Of Freedom	2
Asymptotic Sig.(2-sided test)	,002

a. The test statistic is adjusted for ties.

Pairwise Comparisons of VAR00002

Sample 1-Sample 2	Test Statistic	Std. Error	Std. Test Statistic	Sig.	Adj. Sig.[a]
2,00-3,00	-10,111	3,944	-2,564	,010	,031
2,00-1,00	13,700	3,873	3,537	<,001	,001
3,00-1,00	3,589	3,249	1,105	,269	,808

Each row tests the null hypothesis that the Sample 1 and Sample 2 distributions are the same.
Asymptotic significances (2-sided tests) are displayed. The significance level is ,050.
a. Significance values have been adjusted by the Bonferroni correction for multiple tests.

B

Nonparametric Tests

Notes

Output Created		30-SEP-2025 00:37:26
Comments		
Input	Data	C:\Users\Utilizador\Desktop\tese mestrado\C sativa\qPCR\testes significância\c sativa with excluded values.sav
	Active Dataset	DataSet2
	Filter	<none>
	Weight	<none>
	Split File	<none>
	N of Rows in Working Data File	59
Syntax		NPTESTS /INDEPENDENT TEST (VAR00006) GROUP (VAR00005) KRUSKAL_WALLIS(COMPARE=PAIRWISE) /MISSING SCOPE=ANALYSIS USERMISSING=EXCLUDE /CRITERIA ALPHA=0.05 CILEVEL=95.
Resources	Processor Time	00:00:00,66
	Elapsed Time	00:00:00,67

Hypothesis Test Summary

	Null Hypothesis	Test	Sig.[a,b]
1	The distribution of VAR00006 is the same across categories of VAR00005.	Independent-Samples Kruskal-Wallis Test	<,001

Hypothesis Test Summary

	Decision
1	Reject the null hypothesis.

a. The significance level is ,050.
b. Asymptotic significance is displayed.

Independent-Samples Kruskal-Wallis Test Summary

Total N	54
Test Statistic	38,692[a]
Degree Of Freedom	4
Asymptotic Sig.(2-sided test)	<,001

a. The test statistic is adjusted for ties.

Pairwise Comparisons of VAR00005

Sample 1-Sample 2	Test Statistic	Std. Error	Std. Test Statistic	Sig.	Adj. Sig.[a]
2,00-4,00	-8,367	6,736	-1,242	,214	1,000
2,00-5,00	-21,800	7,035	-3,099	,002	,019
2,00-3,00	-23,550	7,035	-3,347	<,001	,008
2,00-1,00	37,992	6,736	5,640	<,001	,000
4,00-5,00	-13,433	6,736	-1,994	,046	,461
4,00-3,00	15,183	6,736	2,254	,024	,242
4,00-1,00	29,625	6,422	4,613	<,001	,000
5,00-3,00	1,750	7,035	,249	,804	1,000
5,00-1,00	16,192	6,736	2,404	,016	,162
3,00-1,00	14,442	6,736	2,144	,032	,320

Each row tests the null hypothesis that the Sample 1 and Sample 2 distributions are the same.
Asymptotic significances (2-sided tests) are displayed. The significance level is ,050.
a. Significance values have been adjusted by the Bonferroni correction for multiple tests.

Supplementary Figure S5: Kruskal-Wallis test results of the C. sativa lines tested. A: results relative to CL-3 lines. 1,00 = CL-3-WT; 2,00 = CL-3-GIN-1; 3,00 = CL-3-GIN-3 B: results relative to CL-9 lines. 1,00 = CL-9-WT; 2,00 = CL-9-GIN-1; 3,00 = CL-9-GIN-4; 4,00 = CL-9-GIN-11; 5,00 = CL-9-GIN-12.

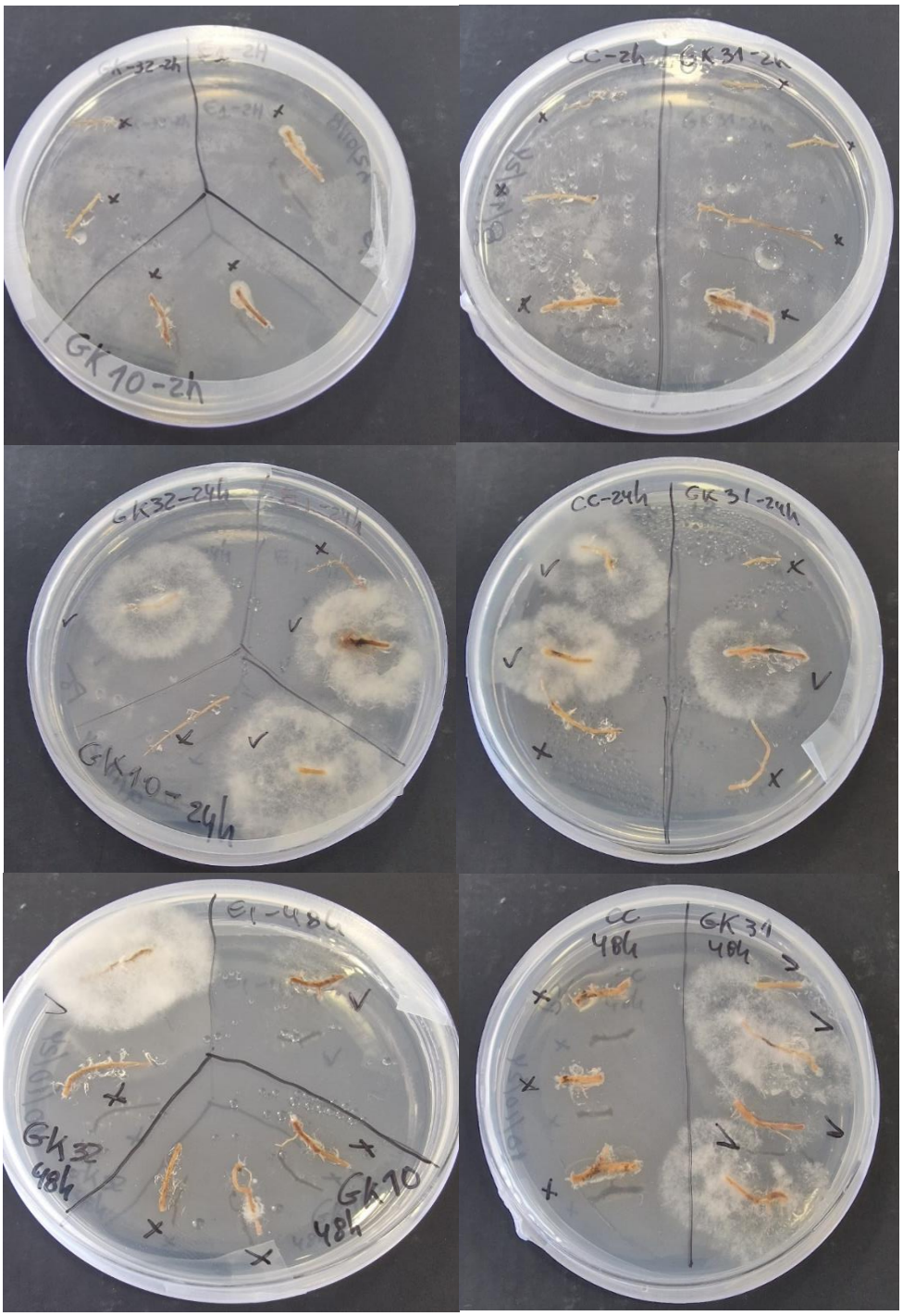

Supplementary Figure S6: P. *cinnamomi* reisolation assay results. X- no noticeable *P. cinnamomi* growth in the root segment; V - *P. cinnamomi* growth detected in the root segment

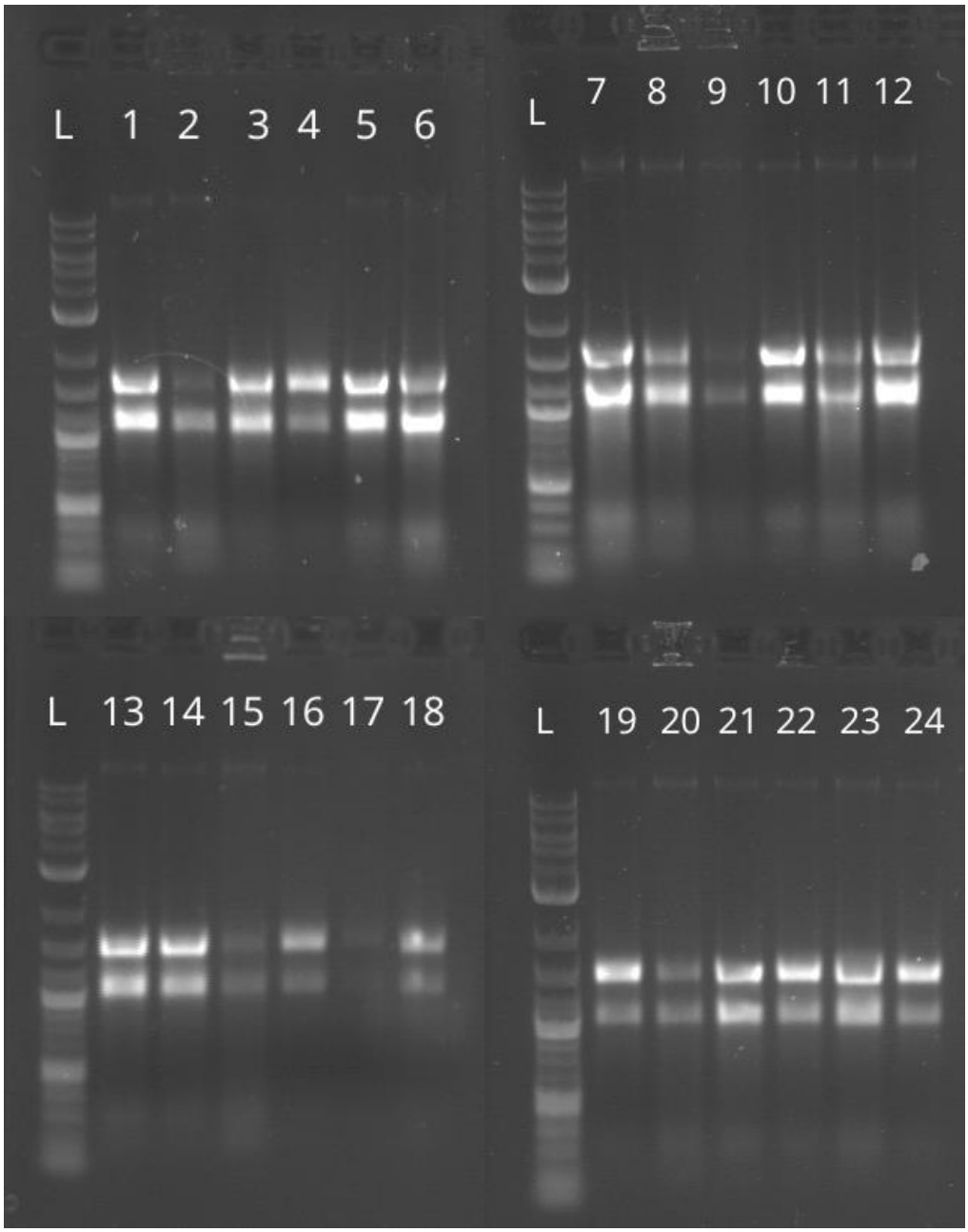

Supplementary Figure S7: images of gel electrophoresis using the extracted RNA from the inoculation assay. The visible RNA bands correspond to ribosomal RNA and can be used to infer overall RNA integrity. L- DNA molecular size marker. 1-6: RNA extracted from CC14 roots. 7-12: RNA extracted from PF-B4GK31 roots. 13-18: RNA extracted from PF-B4GK32 roots. 19-24: RNA extracted from Ellis #1 roots.

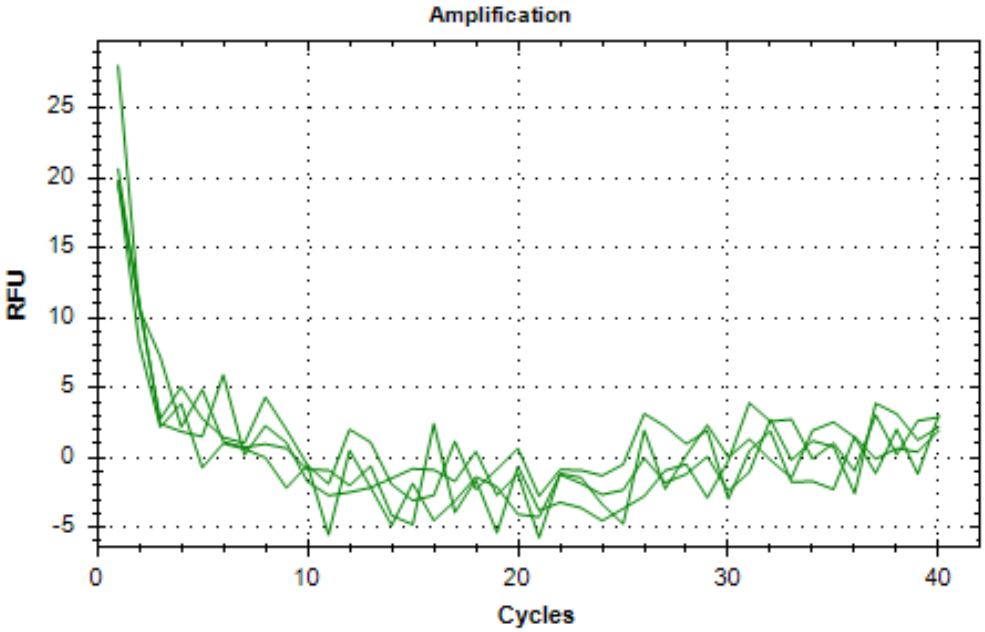

Supplementary Figure S8: Amplification plot of the qPCR reaction done using three RNA samples subjected to the gDNA buffer used in the reverse transcription reaction. The primers for *Cast_Gnk2-like* were used for this test. The amplification plots of the samples used cannot be distinguished from the negative control, strongly suggesting that all genomic DNA has been eliminated.

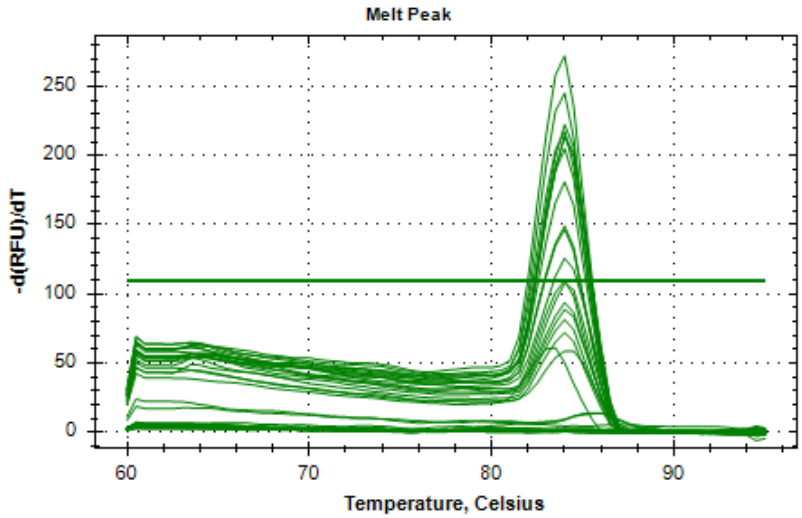

Supplementary Figure S9: melting curve data of the *40S ribosomal protein S3a* gene qPCR plate.

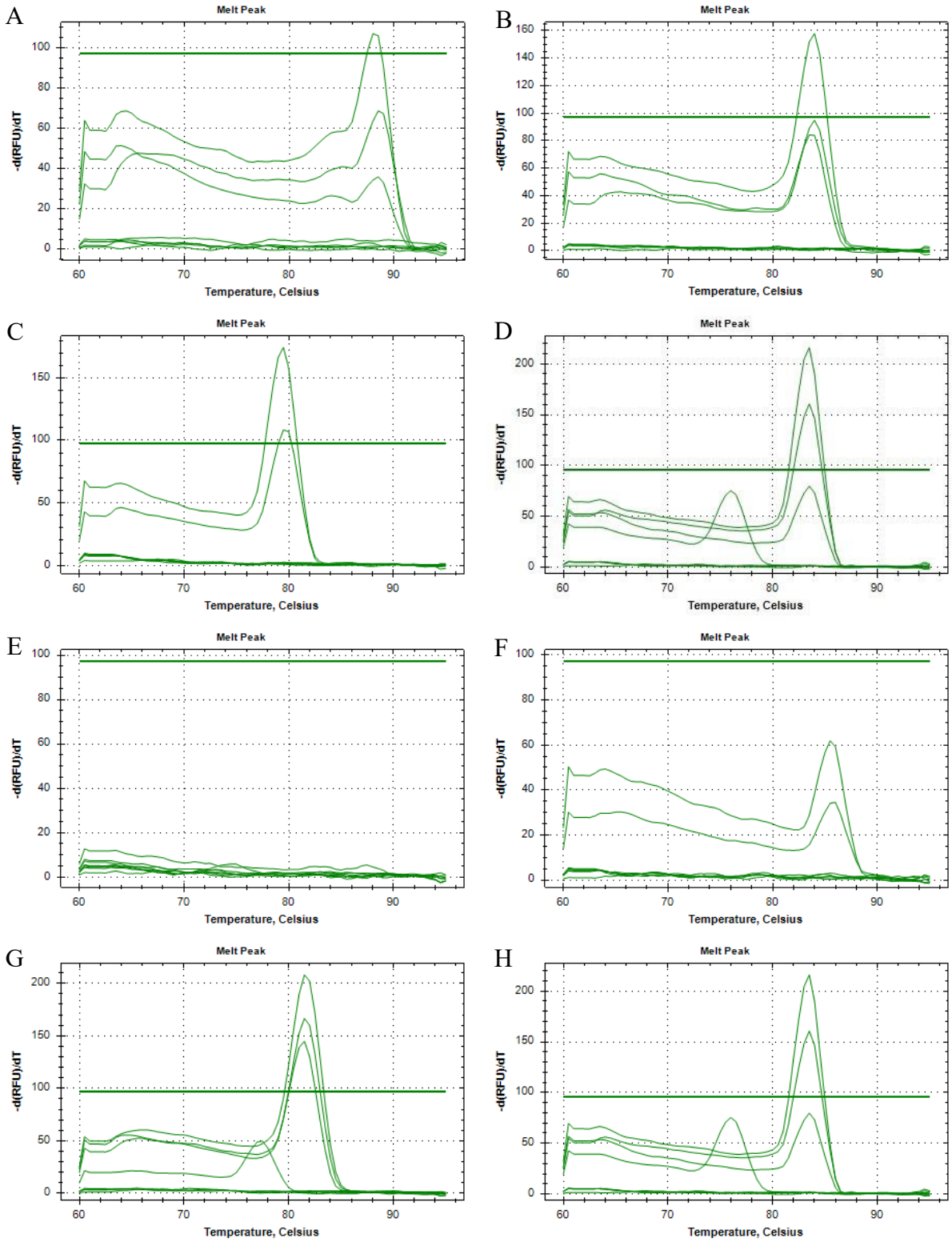

Supplementary Figure S10: melting curve of the *P. cinnamomi* gene amplification tests. A: Pc_ELI-1B; B: Pc_ELL; C: Pc_NPP1; D: Pc_Avr1b-1; E: Pc_Pel; F: Pc_PG; G: Pc_KatG; H: Pc_GST.

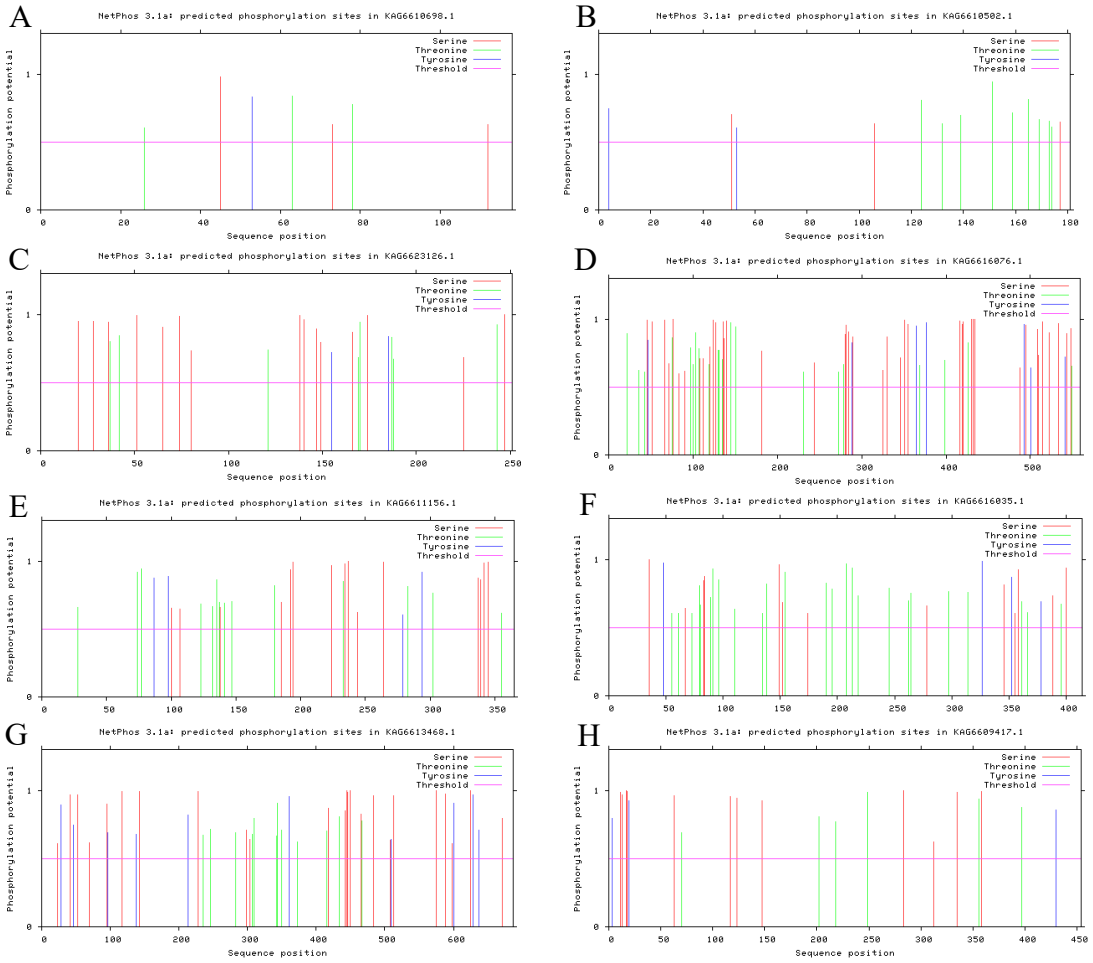

Supplementary Figure S11: NetPhos 3.1 predictions of the phosphorylation profile of *P. cinnamomi* proteins, with a graphical summary. Every predicted site includes the position (#) and corresponding amino acid (x). The "context" column shows the surrounding amino acids. In the graphs, the pink horizontal line represents the default phosphorylation threshold, which is set to a score of 0,5, and vertical line represents a potential phosphorylation site along the amino acid sequence, with the height corresponding to the score (only scores of 0,6 or above are shown in the lists and the graphs). A: Pc_ELI-1B; B: Pc_ELL; C: Pc_NPP1; D: Pc_Avr1b-1; E: Pc_Pel; F: Pc_PG; G: Pc_KatG; H: Pc_GST. Signal peptides were included in the input sequences.

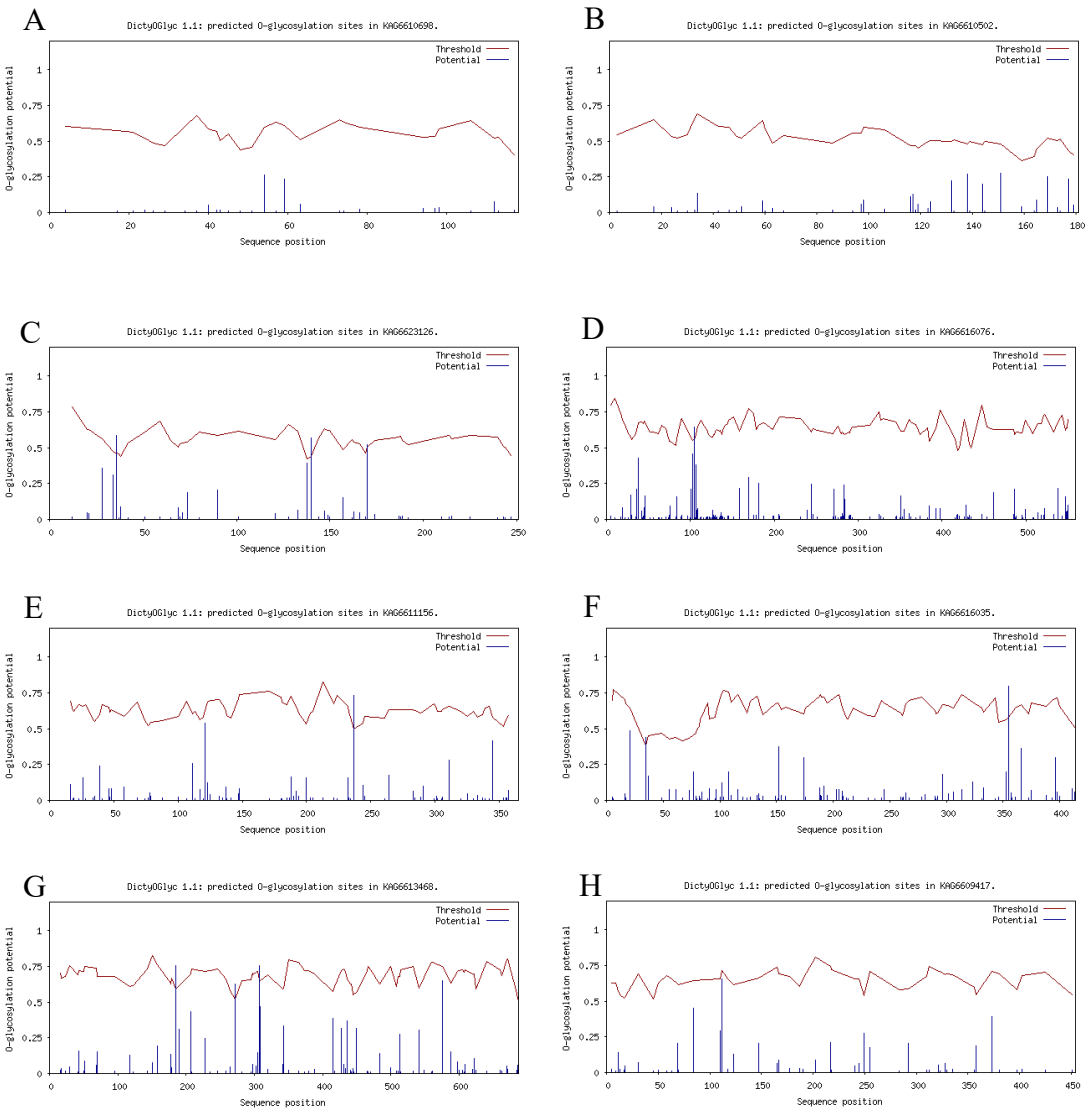

Supplementary Figure S12: DictyOGlyc 1.1 predictions of potential O-glycosylation sites. Default parameters were used. The vertical blue lines represent potential O-glycosylation sites, and their height corresponds to the score. The fluctuating red line represents the minimum glycosylation threshold A: Pc_ELI-1B; B: Pc_ELL; C: Pc_NPP1; D: Pc_Avr1b-1; E: Pc_Pel; F: Pc_PG; G: Pc_KatG; H: Pc_GST.

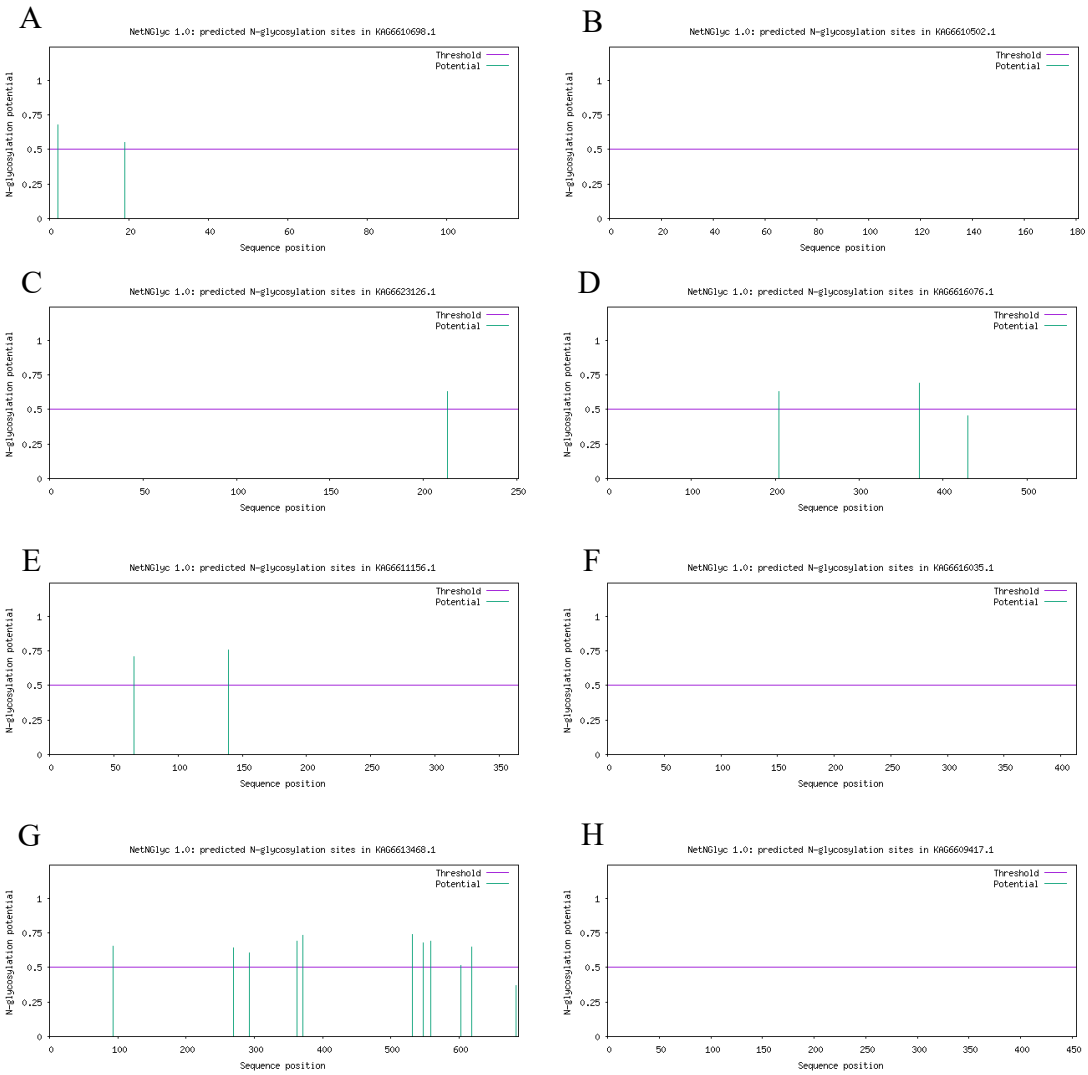

Supplementary Figure S13: NetNGlyc 1.0 predictions of potential N-glycosylation sites. Asn-Xaa-Ser/Thr sequons in the sequence output are highlighted in blue. Asparagines predicted to be N-glycosylated are highlighted in red. In the graphs, the vertical lines represent potential N-glycosylation sites, and their height represents the corresponding score. The horizontal line represents the glycosylation threshold, set to 0,5 by default. A: Pc_ELI-1B; B: Pc_ELL; C: Pc_NPP1; D: Pc_Avr1b-1; E: Pc_Pel; F: Pc_PG; G: Pc_KatG; H: Pc_GST.

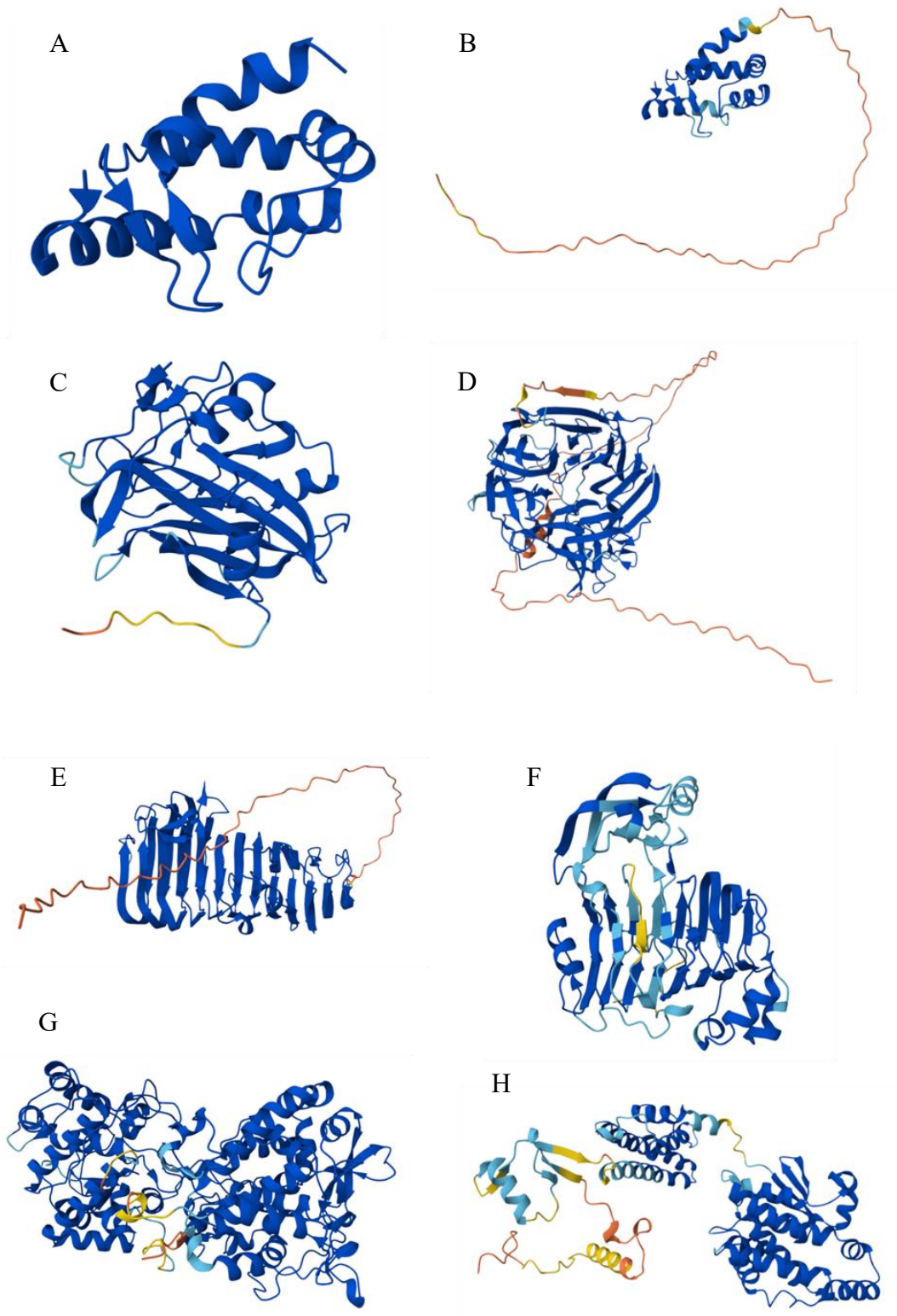

Supplementary Figure S14: AlphaFold Server 3.0 tridimensional structure prediction for P. cinnamomi proteins. A: Pc_ELI-1B; B: Pc_ELL; C: Pc_NPP1; D: Pc_Avr1b-1; E: Pc_PG; F: Pc_Pel; G: Pc_KatG; H: Pc_GST. Colors represent the predicted local distance difference test (pLDDT), which is the confidence level of the predicted structure per-residue on a scale of 0 to 100. Dark blue: Very high (pLDDT > 90); Light Blue: High (90 > pLDDT > 70); Yellow: Low (70 > pLDDT > 50); Orange: Very low (pLDDT < 50).

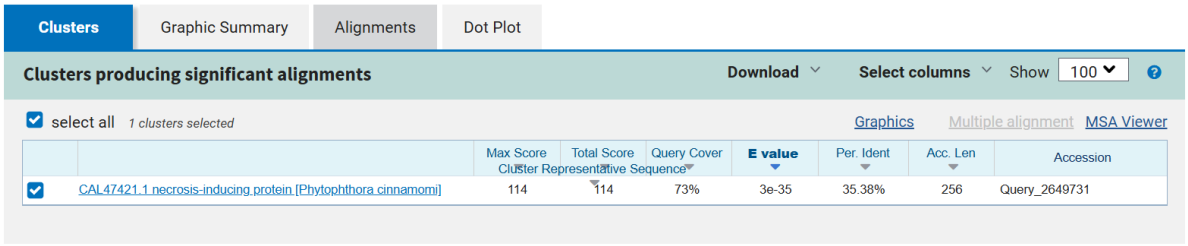

Supplementary Figure S15: Summary of NCBI BLASTp results of Pc_NPP1 and the NPP1 protein described in Martins et al (2019) (CAL47421.1).

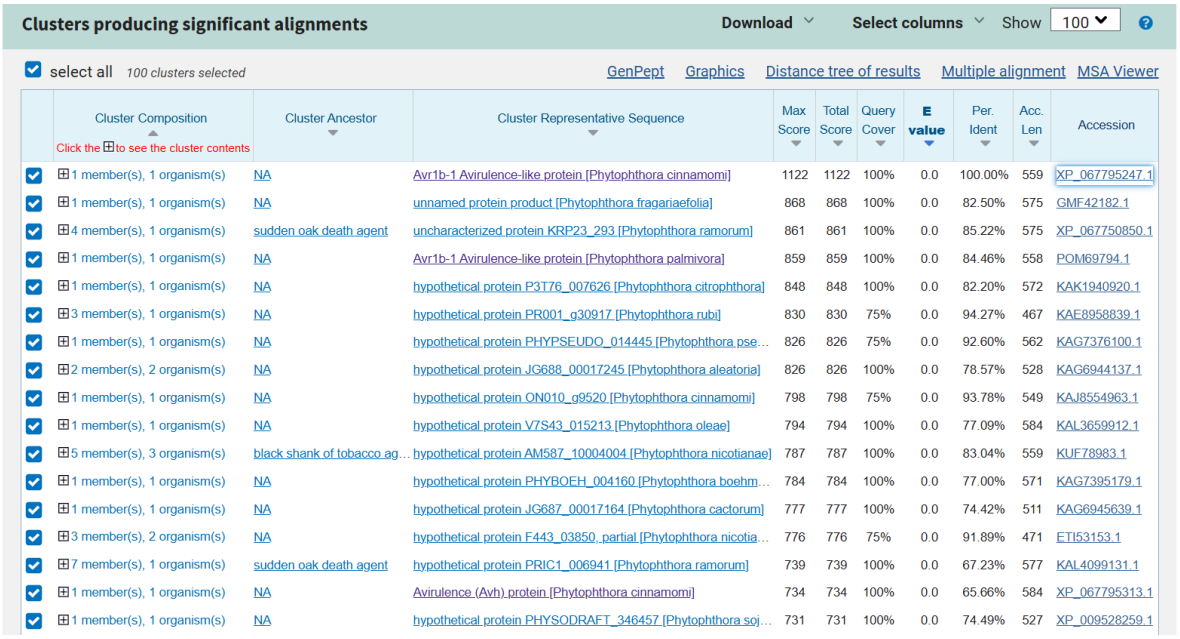

Supplementary Figure S16: Summary of the NCBI BLASTp results using Pc:Avr1b-1 as query, showing the sequences with higher similarity.

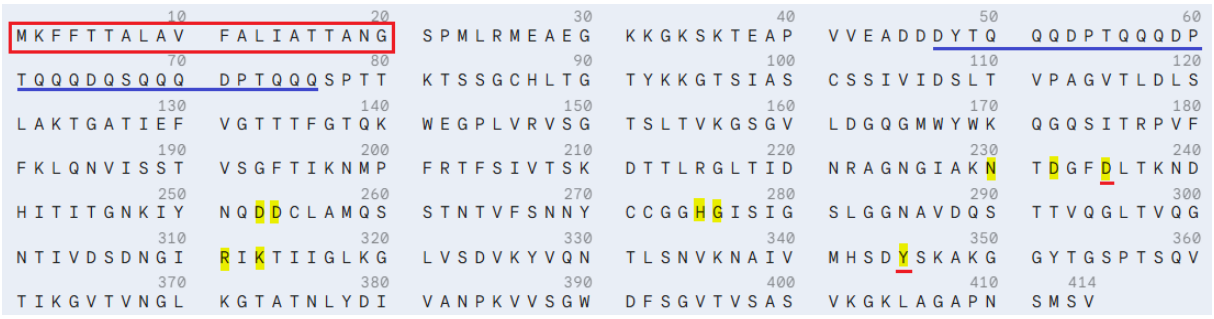

Supplementary Figure S17: Conserved residues in the protein sequence of Pc_PG, highlighted in yellow. Residues adjacent to the active site are underlined in red. The repeat D(P/Q)TQQQ region is underlined in blue. The signal peptide is marked by the red box.

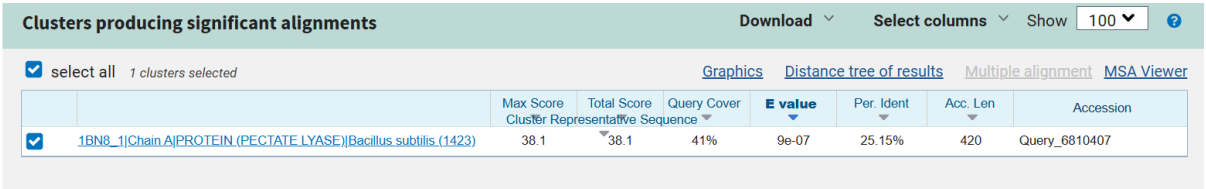

Clusters producing significant alignments Download Select columns Show 100

select all *1 clusters selected* Graphics Distance tree of results Multiple alignment MSA Viewer

	Cluster Representative Sequence	Max Score	Total Score	Query Cover	E value	Per. Ident	Acc. Len	Accession
☑	1BN8_1|Chain A|PROTEIN (PECTATE LYASE)|Bacillus subtilis (1423)	38.1	38.1	41%	9e-07	25.15%	420	Query_6810407

Supplementary Figure S18: NCBI BLASTp results between Pc_Pel and representative proteins from the different pectate lyase families described in Zheng et al. (2021). Only the PL1 family pectate lyase from Bacillus subtilis had significant similarity according to NCBI.

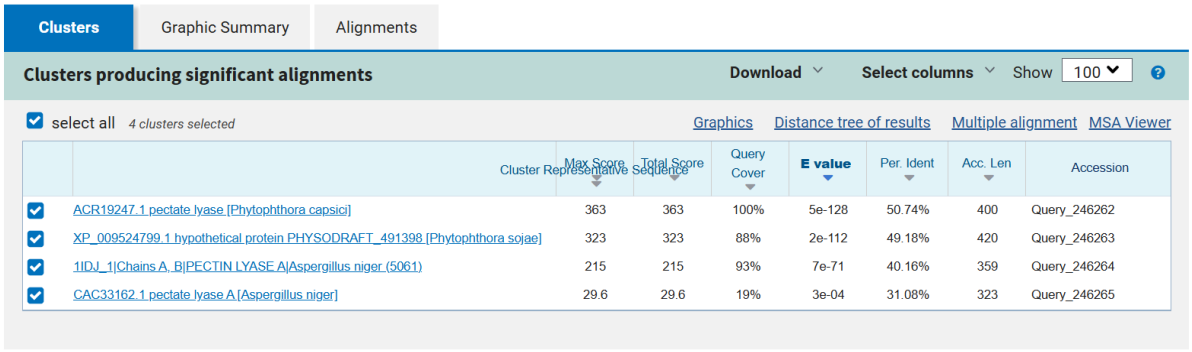

Clusters | Graphic Summary | Alignments

Clusters producing significant alignments Download Select columns Show 100

select all *4 clusters selected* Graphics Distance tree of results Multiple alignment MSA Viewer

	Cluster Representative Sequence	Max Score	Total Score	Query Cover	E value	Per. Ident	Acc. Len	Accession
☑	ACR19247.1 pectate lyase [Phytophthora capsici]	363	363	100%	5e-128	50.74%	400	Query_246262
☑	XP_009524799.1 hypothetical protein PHYSODRAFT_491398 [Phytophthora sojae]	323	323	88%	2e-112	49.18%	420	Query_246263
☑	1IDJ_1|Chains A, B|PECTIN LYASE A|Aspergillus niger (5061)	215	215	93%	7e-71	40.16%	359	Query_246264
☑	CAC33162.1 pectate lyase A [Aspergillus niger]	29.6	29.6	19%	3e-04	31.08%	323	Query_246265

Supplementary Figure S19: Summary of the NCBI BLASTp results between Pc_Pel and other pectinases. ACR19247.1: Pectate lyase from *Phytophthora capsici* (H. Wang et al., 2011). XP_009524799.1: Pectin lyase from *P. sojae* (Grams et al., 2019). 1IDJ_1: Pectin lyase A from *A. niger* (Sánchez-Torres et al., 2003). CAC33162.1: Pectate lyase A from *A. niger* (Benen et al., 2000).

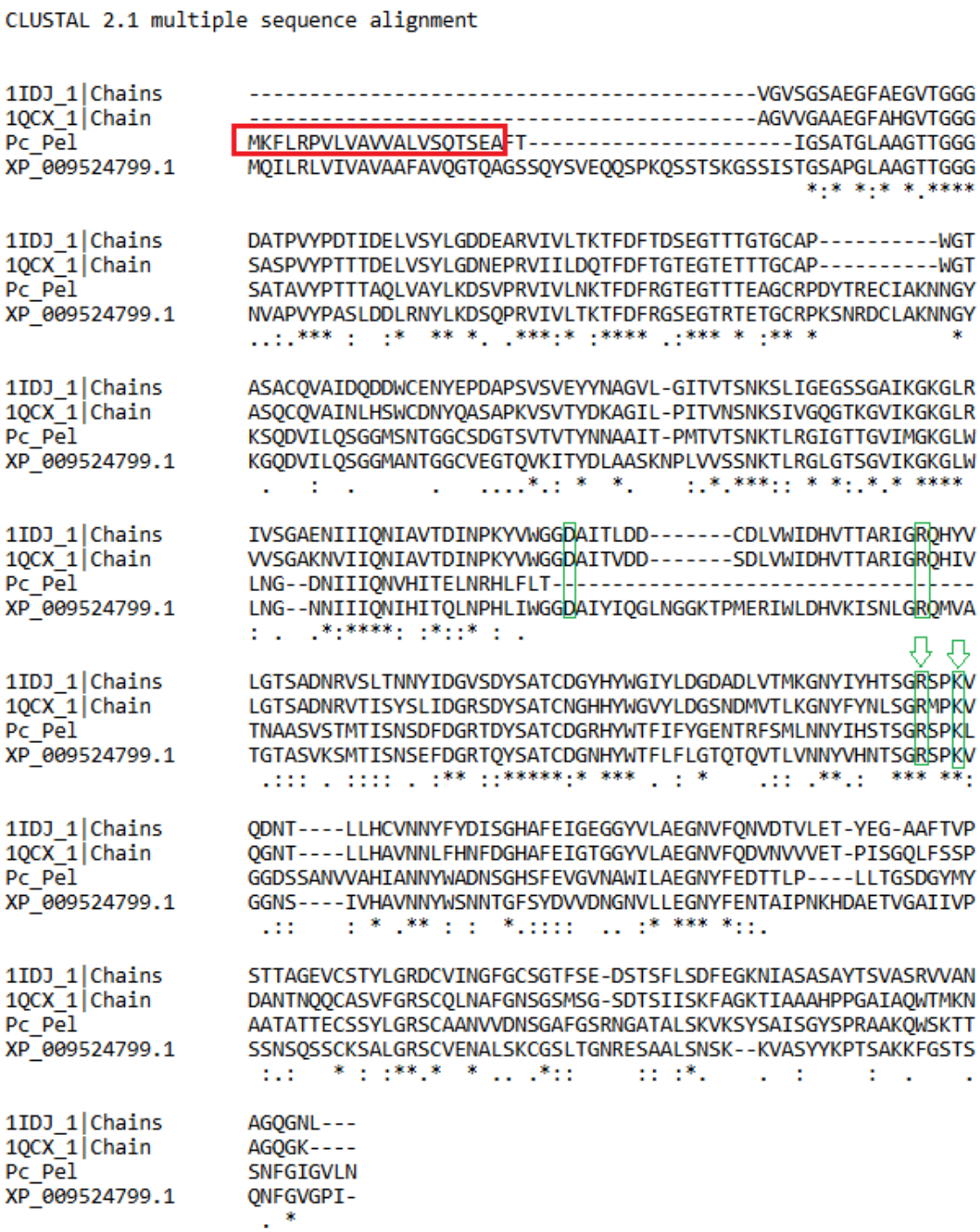

Supplementary Figure S20: Alignment of Pc_Pel with other pectin lyases. The signal peptide of Pc_Pel is marked by the red box. The green boxes indicate the typical conserved residues in pectin lyases, and the green arrows point to the ones present in Pc_Pel. 1IDJ: Pectin lyase A from *A. niger* (Sánchez-Torres et al., 2003). 1QCX: Pectin lyase B from *A. niger* (Vitali et al., 1998). XP_009524799.1: Pectin lyase from *P. sojae* (Grams et al., 2019).

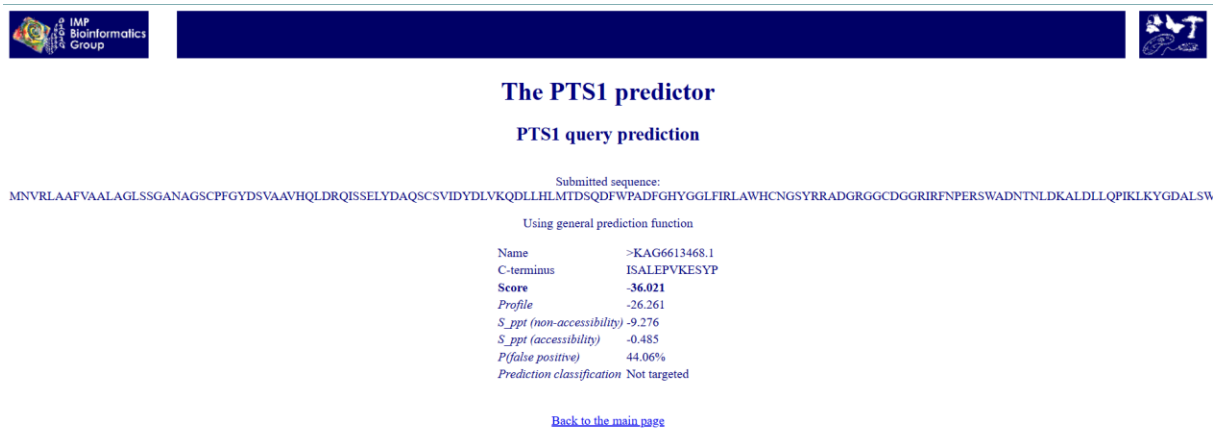

Supplementary Figure S21: PTS1 sequence prediction of localization using the amino acid sequence of Pc_KatG as the input.

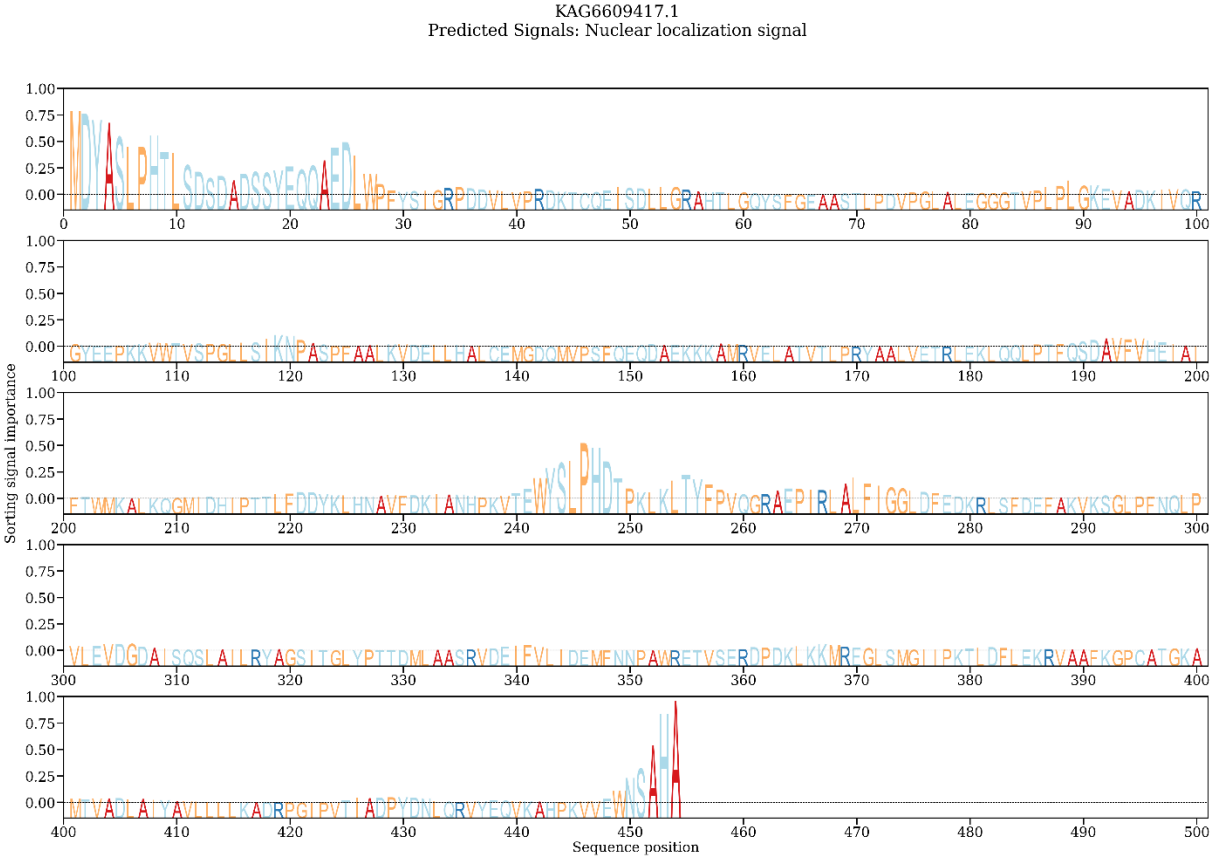

Supplementary Figure S22: DeepLoc 2.1 graphical representation of residue influence in Pc_KatG location.

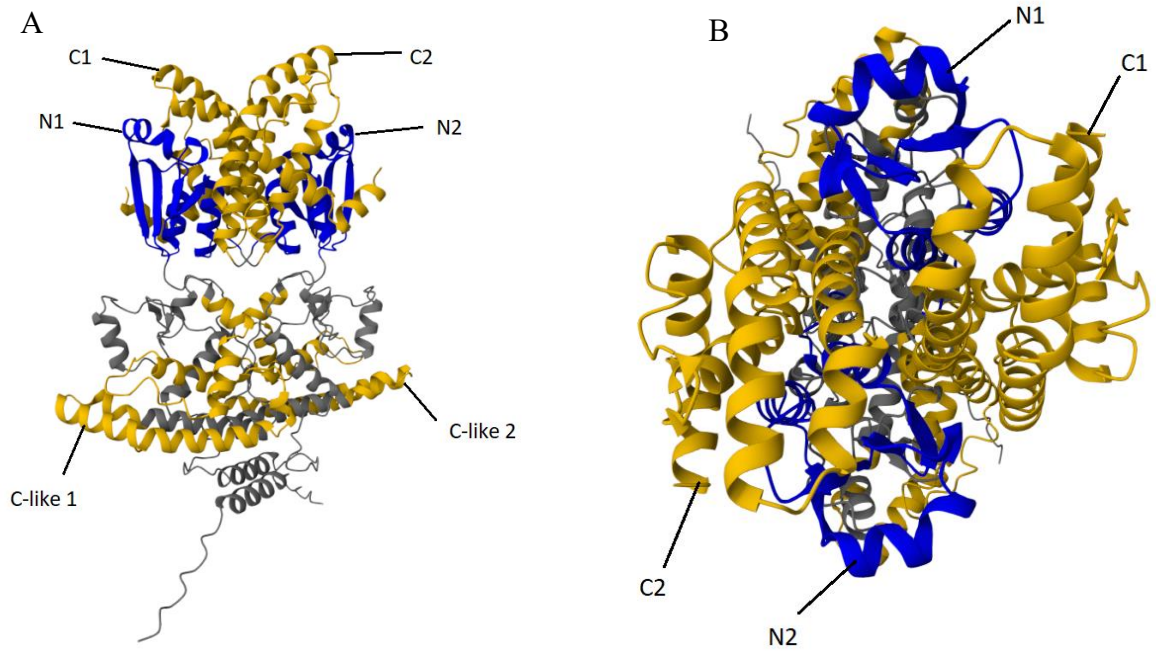

Supplementary Figure S23: A: AlphaFold predicted dimer structure of Pc_GST. Yellow: Different C terminal GST domains (C: C-terminal domain C-like: C-terminal like domain); Blue: N terminal GST domain. B: View of the Pc_GST dimer down the twofold axis relating the two subunits. The domains of each dimer are differentiated as “1” and “2”.

5.2. Supplementary Tables

Supplementary Table S1: RNA concentration of the *C. sativa* somatic embryos' samples. The sample column shows the biological replicates of each genotype. For each biological replicate there is the total fresh weight of the embryo clumps used, the RNA yield after extraction and the remaining RNA after the DNAse reaction.

Genotype	Sample	Fresh weight (mg)	RNA Concentration (ng/µL)	Post-DNAse RNA Concentration (ng/µL)
Cl-3-WT	Cl3W-1	122,3	260,708	135,328
	Cl3W-2	101,3	424,805	151,980
	Cl3W-3	121,5	959,229	256,872
Cl-3-GIN1	Cl3G1-2	113,1	772,742	272,906
	Cl3G1-3	101,2	972,180	297,733
	Cl3G1-4	137,0	1020,748	343,744
Cl-3-GIN3	Cl3G3-1	110,5	226,653	159,888
	Cl3G3-2	112,4	935,676	293,443
	Cl3G3-3	100,0	840,520	294,764
Cl-9-WT	Cl9W-2	105,8	316,493	113,337
	Cl9W-3	114,6	735,942	264,029
	Cl9W-4	147,0	1238,111	215,989
Cl-9-GIN1	Cl9G1-2	122,0	410,768	281,418
	Cl9G1-3	134,5	519,407	354,177
	Cl9G1-4	102,2	941,636	284,875
Cl-9-GIN4	Cl9G4-1	101,7	552,133	277,048
	Cl9G4-2	101,6	616,241	227,629
	Cl9G4-3	102,1	912,248	315,326
Cl-9-GIN11	Cl9G11-1	104,9	222,867	174,651
	Cl9G11-3	137,8	499,522	338,478
	Cl9G11-4	122,0	590,089	222,339
Cl-9-GIN12	Cl9G12-1	123,6	203,244	151,950
	Cl9G12-2	107,3	475,800	313,624
	Cl9G12-3	122,9	391,590	215,639

Supplementary Table S2: Ct values obtained from the *40S ribosomal protein S3a plate*, which was prepared as established in Materials and Methods. N/A- no amplification.

Target	Content	Sample	Ct	Target	Content	Sample	Ct
S3a	Standard	Pool -1	24,4	*S3a*	Unknown	GK31 2h inoc	N/A
S3a	Standard	Pool -1	24,36	*S3a*	Unknown	GK31 2h inoc	N/A
S3a	Standard	Pool -1	24,38	*S3a*	Unknown	GK31 24h inoc	N/A
S3a	Standard	Pool -2	28,7	*S3a*	Unknown	GK31 24h inoc	N/A
S3a	Standard	Pool -2	29,1	*S3a*	Unknown	GK31 48h inoc	N/A
S3a	Standard	Pool -2	29,33	*S3a*	Unknown	GK31 48h inoc	N/A
S3a	Standard	Pool -3	35,39	*S3a*	Unknown	GK32 2h mock	N/A
S3a	Standard	Pool -3	36,59	*S3a*	Unknown	GK32 2h mock	N/A
S3a	Standard	Pool -3	36,87	*S3a*	Unknown	GK32 24h mock	N/A
S3a	Standard	Pool -4	36,53	*S3a*	Unknown	GK32 24h mock	N/A
S3a	Standard	Pool -4	35,8	*S3a*	Unknown	GK32 48h mock	N/A
S3a	Standard	Pool -4	N/A	*S3a*	Unknown	GK32 48h mock	N/A
S3a	Unknown	CC14 2h mock	N/A	*S3a*	Unknown	GK32 2h inoc	36,29
S3a	Unknown	CC14 2h mock	N/A	*S3a*	Unknown	GK32 2h inoc	37,01
S3a	Unknown	CC14 24h mock	N/A	*S3a*	Unknown	GK32 48h inoc	N/A
S3a	Unknown	CC14 24h mock	N/A	*S3a*	Unknown	GK32 48h inoc	N/A
S3a	Unknown	CC14 48h mock	39,45	*S3a*	Unknown	Ellis 2h mock	N/A
S3a	Unknown	CC14 48h mock	39,33	*S3a*	Unknown	Ellis 2h mock	N/A
S3a	Unknown	CC14 2h inoc	35,67	*S3a*	Unknown	Ellis 24h mock	N/A
S3a	Unknown	CC14 2h inoc	34,6	*S3a*	Unknown	Ellis 24h mock	N/A
S3a	Unknown	CC14 24h inoc	33,54	*S3a*	Unknown	Ellis 48h mock	N/A
S3a	Unknown	CC14 24h inoc	33,7	*S3a*	Unknown	Ellis 48h mock	N/A
S3a	Unknown	CC14 48h inoc	N/A	*S3a*	Unknown	Ellis 2h inoc	N/A
S3a	Unknown	CC14 48h inoc	N/A	*S3a*	Unknown	Ellis 2h inoc	N/A
S3a	Unknown	GK31 2h mock	N/A	*S3a*	Unknown	Ellis 24h inoc	N/A
S3a	Unknown	GK31 2h mock	N/A	*S3a*	Unknown	Ellis 24h inoc	N/A
S3a	Unknown	GK31 24h mock	N/A	*S3a*	Unknown	Ellis 48h inoc	N/A
S3a	Unknown	GK31 24h mock	N/A	*S3a*	Unknown	Ellis 48h inoc	N/A
S3a	Unknown	GK31 48h mock	N/A	*S3a*	Unknown	Mycelium	20,35
S3a	Unknown	GK31 48h mock	N/A	*S3a*	Unknown	Mycelium	20,48
				S3a	NTC		N/A

Supplementary Table S3: Ct values obtained from the *Actin* plate, which was prepared as established in Materials and Methods. Samples that were not detected are highlighted in bold. N/A- no amplification.

Target	Content	Sample	Ct	Target	Content	Sample	Ct
Actin	Standard	Pool -2	29,24	*Actin*	Unknown	GK31 24h inoc	35,11
Actin	Standard	Pool -2	29,18	*Actin*	Unknown	GK31 24h inoc	36,24
Actin	Standard	Pool -2	29,45	*Actin*	Unknown	**GK31 48h inoc**	**N/A**
Actin	Standard	Pool -3	33,21	*Actin*	Unknown	GK31 48h inoc	35,12
Actin	Standard	Pool -3	33,4	*Actin*	Unknown	GK32 2h mock	34,75
Actin	Standard	Pool -4	37,14	*Actin*	Unknown	GK32 2h mock	35,05
Actin	Standard	Pool -4	N/A	*Actin*	Unknown	GK32 24h mock	34,81
Actin	Standard	Pool -4	N/A	*Actin*	Unknown	GK32 24h mock	37,38
Actin	Unknown	CC14 2h mock	26,23	*Actin*	Unknown	**GK32 48h mock**	**N/A**
Actin	Unknown	CC14 2h mock	26,43	*Actin*	Unknown	**GK32 48h mock**	**N/A**
Actin	Unknown	**CC14 24h mock**	**N/A**	*Actin*	Unknown	GK32 2h inoc	22,16
Actin	Unknown	**CC14 24h mock**	**N/A**	*Actin*	Unknown	GK32 2h inoc	22,26
Actin	Unknown	CC14 48h mock	28,04	*Actin*	Unknown	GK32 48h inoc	31,05
Actin	Unknown	CC14 48h mock	27,75	*Actin*	Unknown	GK32 48h inoc	31,5
Actin	Unknown	CC14 2h inoc	22,46	*Actin*	Unknown	Ellis 2h mock	35,31
Actin	Unknown	CC14 2h inoc	22,49	*Actin*	Unknown	Ellis 2h mock	37,84
Actin	Unknown	CC14 24h inoc	23,62	*Actin*	Unknown	**Ellis 24h mock**	**N/A**
Actin	Unknown	CC14 24h inoc	23,76	*Actin*	Unknown	**Ellis 24h mock**	**N/A**
Actin	Unknown	**CC14 48h inoc**	**N/A**	*Actin*	Unknown	Ellis 48h mock	33,31
Actin	Unknown	**CC14 48h inoc**	**N/A**	*Actin*	Unknown	Ellis 48h mock	32,27
Actin	Unknown	GK31 2h mock	25,05	*Actin*	Unknown	Ellis 2h inoc	32,71
Actin	Unknown	GK31 2h mock	24,73	*Actin*	Unknown	Ellis 2h inoc	32,7
Actin	Unknown	GK31 24h mock	27,29	*Actin*	Unknown	**Ellis 24h inoc**	**N/A**
Actin	Unknown	GK31 24h mock	27,24	*Actin*	Unknown	Ellis 24h inoc	35,41
Actin	Unknown	GK31 48h mock	32,45	*Actin*	Unknown	**Ellis 48h inoc**	**N/A**
Actin	Unknown	GK31 48h mock	32,15	*Actin*	Unknown	Ellis 48h inoc	35,09
Actin	Unknown	GK31 2h inoc	28,36	*Actin*	Unknown	Mycelium	N/A
Actin	Unknown	GK31 2h inoc	27,18	*Actin*	Unknown	Mycelium	N/A
				Actin	NTC		N/A

Supplementary Table S4: Ct values obtained from the *Actin* plate using selected samples after the preparation of new dilutions. N/A- no amplification.

Target	Content	Sample	Ct	Target	Content	Sample	Ct
Actin	Standard	Pool -1	23,86	*Actin*	Unknown	GK31 24h inoc	36,78
Actin	Standard	Pool -1	23,6	*Actin*	Unknown	GK31 24h inoc	36,1
Actin	Standard	Pool -1	23,83	*Actin*	Unknown	GK31 48h inoc	N/A
Actin	Standard	Pool -2	29,67	*Actin*	Unknown	GK31 48h inoc	35,35
Actin	Standard	Pool -2	29,5	*Actin*	Unknown	GK32 24h mock	34,93
Actin	Standard	Pool -2	29,65	*Actin*	Unknown	GK32 24h mock	36,81
Actin	Standard	Pool -3	31,46	*Actin*	Unknown	GK32 48h mock	N/A
Actin	Standard	Pool -3	32,03	*Actin*	Unknown	GK32 48h mock	N/A
Actin	Standard	Pool -3	32,14	*Actin*	Unknown	Ellis 2h mock	N/A
Actin	NTC		N/A	*Actin*	Unknown	Ellis 2h mock	N/A
Actin	Unknown	CC14 2h mock	25,15	*Actin*	Unknown	Ellis 24h mock	N/A
Actin	Unknown	CC14 2h mock	25,17	*Actin*	Unknown	Ellis 24h mock	39,64
Actin	Unknown	CC14 24h mock	N/A	*Actin*	Unknown	Ellis 24h inoc	36,04
Actin	Unknown	CC14 24h mock	34,86	*Actin*	Unknown	Ellis 24h inoc	36,01
Actin	Unknown	CC14 2h inoc	22,08	*Actin*	Unknown	Ellis 48h inoc	N/A
Actin	Unknown	CC14 2h inoc	22,15	*Actin*	Unknown	Ellis 48h inoc	N/A
Actin	Unknown	CC14 48h inoc	36,77	*Actin*	Unknown	Mycelium	N/A
Actin	Unknown	CC14 48h inoc	N/A	*Actin*	Unknown	Mycelium	N/A

Supplementary Table S5: Ct values obtained from the *Cast_Gnk2-like plate*, which was prepared as established in Materials and Methods. N/A- no amplification.

Target	Content	Sample	Ct	Target	Content	Sample	Ct
Cast_Gnk2-like	Standard	Pool -1	22	*Cast_Gnk2-like*	Unknown	GK31 2h inoc	23,51
Cast_Gnk2-like	Standard	Pool -1	21,79	*Cast_Gnk2-like*	Unknown	GK31 24h inoc	30,76
Cast_Gnk2-like	Standard	Pool -1	21,87	*Cast_Gnk2-like*	Unknown	GK31 24h inoc	30,43
Cast_Gnk2-like	Standard	Pool -2	25,59	*Cast_Gnk2-like*	Unknown	GK31 48h inoc	31,19
Cast_Gnk2-like	Standard	Pool -2	25,69	*Cast_Gnk2-like*	Unknown	GK31 48h inoc	31,75
Cast_Gnk2-like	Standard	Pool -3	29,82	*Cast_Gnk2-like*	Unknown	GK32 2h mock	27,66
Cast_Gnk2-like	Standard	Pool -3	29,47	*Cast_Gnk2-like*	Unknown	GK32 2h mock	27,46
Cast_Gnk2-like	Standard	Pool -4	32,65	*Cast_Gnk2-like*	Unknown	GK32 24h mock	28,57
Cast_Gnk2-like	Standard	Pool -4	33,06	*Cast_Gnk2-like*	Unknown	GK32 24h mock	28,6
Cast_Gnk2-like	Standard	Pool -4	33,48	*Cast_Gnk2-like*	Unknown	GK32 48h mock	31,06
Cast_Gnk2-like	Unknown	CC14 2h mock	35,15	*Cast_Gnk2-like*	Unknown	GK32 48h mock	31,18
Cast_Gnk2-like	Unknown	CC14 2h mock	34,36	*Cast_Gnk2-like*	Unknown	GK32 2h inoc	19,45
Cast_Gnk2-like	Unknown	CC14 24h mock	29,52	*Cast_Gnk2-like*	Unknown	GK32 2h inoc	19,28
Cast_Gnk2-like	Unknown	CC14 24h mock	30,02	*Cast_Gnk2-like*	Unknown	GK32 48h inoc	24,84
Cast_Gnk2-like	Unknown	CC14 48h mock	27,82	*Cast_Gnk2-like*	Unknown	GK32 48h inoc	24,73
Cast_Gnk2-like	Unknown	CC14 48h mock	28	*Cast_Gnk2-like*	Unknown	Ellis 2h mock	35,87
Cast_Gnk2-like	Unknown	CC14 2h inoc	32,26	*Cast_Gnk2-like*	Unknown	Ellis 2h mock	36,25
Cast_Gnk2-like	Unknown	CC14 2h inoc	31,81	*Cast_Gnk2-like*	Unknown	Ellis 24h mock	35,88
Cast_Gnk2-like	Unknown	CC14 24h inoc	24,49	*Cast_Gnk2-like*	Unknown	Ellis 24h mock	37,02
Cast_Gnk2-like	Unknown	CC14 24h inoc	24,5	*Cast_Gnk2-like*	Unknown	Ellis 48h mock	30,01
Cast_Gnk2-like	Unknown	CC14 48h inoc	32,8	*Cast_Gnk2-like*	Unknown	Ellis 48h mock	30,01
Cast_Gnk2-like	Unknown	CC14 48h inoc	33,68	*Cast_Gnk2-like*	Unknown	Ellis 2h inoc	35,4
Cast_Gnk2-like	Unknown	GK31 2h mock	22,29	*Cast_Gnk2-like*	Unknown	Ellis 2h inoc	35,79
Cast_Gnk2-like	Unknown	GK31 2h mock	22,22	*Cast_Gnk2-like*	Unknown	Ellis 24h inoc	33,82
Cast_Gnk2-like	Unknown	GK31 24h mock	23,85	*Cast_Gnk2-like*	Unknown	Ellis 24h inoc	34,08
Cast_Gnk2-like	Unknown	GK31 24h mock	23,94	*Cast_Gnk2-like*	Unknown	Ellis 48h inoc	34,17
Cast_Gnk2-like	Unknown	GK31 48h mock	26,94	*Cast_Gnk2-like*	Unknown	Ellis 48h inoc	33,5
Cast_Gnk2-like	Unknown	GK31 48h mock	26,79	*Cast_Gnk2-like*	Unknown	Mycelium	N/A
Cast_Gnk2-like	Unknown	GK31 2h inoc	23,57	*Cast_Gnk2-like*	Unknown	Mycelium	N/A
				Cast_Gnk2-like	NTC		N/A

Supplementary Table S6: Euk-Mloc predictions for protein location. Extracell.- the protein is predicted to be secreted.

Query protein	Predicted location(s)
Pc_ELI-1B	Extracell.
Pc_ELL	Extracell.
Pc_NPP1	Extracell.
Pc_Avr1b-1	Extracell.
Pc_Pel	Extracell.
Pc_PG	Extracell.
Pc_KatG	Cytoplasm. Extracell.
Pc_GST	Cytoplasm.

Supplementary Table S7: Deeploc 2.1 protein localization predictions NLS- nuclear localizaton signal; L/V-lysosome/vacuole. The numeric values represent the probability assigned by the model to each of the subcellular localizations.

Protein	Pc_ELI-1B	Pc_ELL	Pc_NPP1	Pc_Avr1b-1	Pc_Pel	Pc_PG	Pc_KatG	Pc_GST
Protein_ID	KAG6610698.1	KAG6610502.1	KAG6623126.1	KAG6616076.1	KAG6611156.1	KAG6616035.1	KAG6613468.1	KAG6609417.1
Localizations	Extracellular	Extracellular	Extracellular	Extracellular	Extracellular	Extracellular	Extracellular	Cytoplasm
Signals	Signal peptide	Signal peptide	Signal peptide	Signal peptide	Signal peptide	Signal peptide	Signal peptide	Nuclear localization signal
Membrane types	Soluble	Soluble	Soluble	Soluble	Soluble	Soluble	Soluble	Soluble
Cytoplasm	0.08110000193119049	0.18209999799728394	0.16820000112056732	0.22220000624656677	0.13420000672340393	0.17239999771118164	0.2962000072002411	0.751800000667572
Nucleus	0.05739999935030937	0.04479999840259552	0.039400000125169754	0.03200000151991844	0.08470000326633453	0.06580000037074089	0.031700000166893005	0.2703999876976013
Extracellular	0.9703000187873840	0.9605000019073486	0.9746999740600586	0.9503999948501587	0.9731000065803528	0.9663000106811523	0.6370000243186951	0.19339999556541443
Cell membrane	0.09989999979734421	0.2799000144004822	0.06140000000596046	0.19269999861717224	0.07760000228881836	0.11089999973773956	0.17499999701976776	0.18580000102519990
Mitochondrion	0.07240000367164612	0.04560000076889992	0.0340999998152256	0.017500000074505806	0.043699998408555984	0.05469999834895134	0.09880000352859497	0.16820000112056732
Plastid	0.010200000368058681	0.014999999664723873	0.0041000000020116568	0.024299999698996544	0.00930000003427267	0.019300000742077827	0.03280000016093254	0.010900000110268593
Endoplasmic reticulum	0.06549999862909317	0.065700002014637	0.1808999925851822	0.2354000061750412	0.1784999966621399	0.13279999792575836	0.3921999931335449	0.19179999828338623
Lysosome/Vacuole	0.29789999127388	0.35519999265670776	0.22990000247955322	0.3197999894618988	0.11379999667406082	0.09839999675750732	0.5076000094413757	0.33869999647140503
Golgi apparatus	0.055700000375509260	0.06520000100135803	0.20170000195503235	0.35539999604225160	0.10809999704360962	0.11050000041723251	0.17399999499320984	0.31209999322891235
Peroxisome	0.002199999988079071	0.0005000000237487257	0.0015999999595806003	0.002400000113993883	0.0013000000035390258	0.0019000000320374966	0.002099999925121665	0.008200000040233135
Peripheral	0.48359999606063080	0.37749999761581420	0.19939999282360077	0.37310001254081726	0.31619998812675476	0.26129999756813050	0.48399999737739563	0.44429999589920044
Transmembrane	0.010499999858438969	0.010099999606609344	0.018899999558925630	0.059599999338388440	0.026300000026822090	0.019700000062584877	0.026300000026822090	0.12330000102519989
Lipid anchor	0.39120000600814820	0.67599999904632570	0.44429999589920044	0.54149997234344480	0.19650000333786010	0.34439998865127563	0.11599999666213989	0.10499999672174454
Soluble	0.88059997558593750	0.91229999065399170	0.92900002002716060	0.82730001211166380	0.88270002603530880	0.91109997034072880	0.86440002918243410	0.74849998950958250